Title

Regulation of Budding Yeast γ-Tubulin Ring Complex Assembly by Spc110p

Permalink

https://escholarship.org/uc/item/3zh1f1rm

Author

Lyon, Andrew S.

Publication Date

2017

Peer reviewed|Thesis/dissertation

Regulation of Budding Yeast γ-Tubulin Ring Complex Assembly by
Spc110p

by

Andrew S. Lyon

DISSERTATION

Submitted in partial satisfaction of the requirements for the degree of

DOCTOR OF PHILOSOPHY

in

Biochemistry and Molecular Biology

in the

GRADUATE DIVISION

of the

UNIVERSITY OF CALIFORNIA, SAN FRANCISCO

Abstract

The microtubule (MT) cytoskeleton is a dynamic, micrometer-scale network of polymeric

filaments composed of αβ-tubulin heterodimers. The MT cytoskeleton dramatically reorganizes

in response to cell cycle state, developmental transitions, and signaling events. This requires

the coordinated activity of a variety of regulatory molecules. These processes ultimately

depend on the creation of new MTs, which is regulated by molecules known as MT nucleators.

The γ-tubulin ring complex (γTuRC), an approximately 2.1 megadalton protein complex, is one

such nucleator that plays important roles in regulating the MT cytoskeleton in organisms

ranging from unicellular fungi to humans. γTuRC contains multiple γ-tubulin molecules arranged

in a helix which acts as a template from which αβ-tubulin may polymerize. In the budding yeast

S. cerevisiae, γTuRC lacks several components present in metazoans which are thought to

stabilize γTuRC assembly. Previous work indicates that the subcomplex that comprises γTuRC, γ-

tubulin small complex (γTuSC), fail to form helical assemblies in isolation. However, the

presence of the coiled-coil protein Spc110, characterized as receptor for γTuSC at the nuclear

face of the spindle pole body (SPB), induces formation of helical γTuSC assemblies which are

the *S. cerevisiae* counterpart of metazoan γTuRCs. This work aims to characterize in molecular

detail the mechanisms underlying assembly of budding yeast γTuRC. I show through

biochemical and live-cell imaging approaches that γTuRC assembly critically depends on the

oligomerization state of Spc110, as γTuSCs self-interact weakly and must be stabilized by high-

order oligomers of Spc110. By a variety of structural approaches, I show that the 44-residue N-

terminal coiled-coil domain forms ordered contacts with γTuSC. The disordered N-terminal

domain, which stabilizes γTuRC and is required in vivo, was not observed in previously

determined cryo-electron microscopy reconstructions. Cross-linking mass spectrometry and biochemical experiments suggests that one N-terminal domain within an Spc110 dimer interacts with the same γTuSC bound by the dimer's N-terminal coiled-coil domain, while the other N-terminal domain stabilizes contacts with an adjacent γTuSC. Together, this work provides a framework for understanding the spatial specificity of MT nucleation by coupling γTuRC assembly to its localization via dependence on Spc110.

Table of Contents

List of Tables

Chapter 1

Appendix

List of Figures

Chapter 1

Chapter 2

Chapter 3

Appendix

Chapter 1

Introduction

Microtubules are hollow, cylindrical polymers composed of αβ-tubulin heterodimers. The interface between α- and β-tubulin contains a non-hydrolyzable GTP, while β-tubulin can also bind GTP (Figure 1A). Once β-tubulin binds GTP, αβ-tubulin polymerizes via head-to-tail longitudinal contacts to form protofilaments (Figure 1B). Protofilaments make lateral contacts that make up the cylindrical wall of the MT (Figure 2C). Under appropriate conditions in vitro, purified αβ-tubulin (typically from bovine or porcine brain) assembles spontaneously into MTs (Olmsted & Borisy, 1975). However, the curve relating fraction of polymerized αβ-tubulin to time is sigmoidal with a lag phase due to slow nucleation kinetics (Voter & Erickson, 1984). Classical models of MT assembly include thermodynamically unstable intermediates on the pathway to a nucleus, defined as point on the pathway to MT assembly after which addition of further αβ-tubulin subunits is thermodynamically favorable (Flyvbjerg, et al., 1996).

As MTs polymerize, GTP hydrolysis is stimulated by contacts between α-tubulin of the newly added subunit and β-tubulin of the existing MT end. When the rate of hydrolysis is slower than the rate of new αβ-tubulin addition, the MT elongates with a region at its tip enriched in GTP-bound subunits called the GTP cap. If GTP within this cap is hydrolyzed, MTs rapidly depolymerize in a process known as catastrophe. MTs can recover from catastrophe, which is termed rescue. These three types of MT behavior are collectively known as dynamic instability (Mitchison & Kirschner, 1984). Numerous factors, including both proteins and small-molecule natural products, have evolved to modulate the intrinsic activities of αβ-tubulin in MT assembly and dynamics, as reviewed in (Akhmanova & Steinmetz, 2015).

1
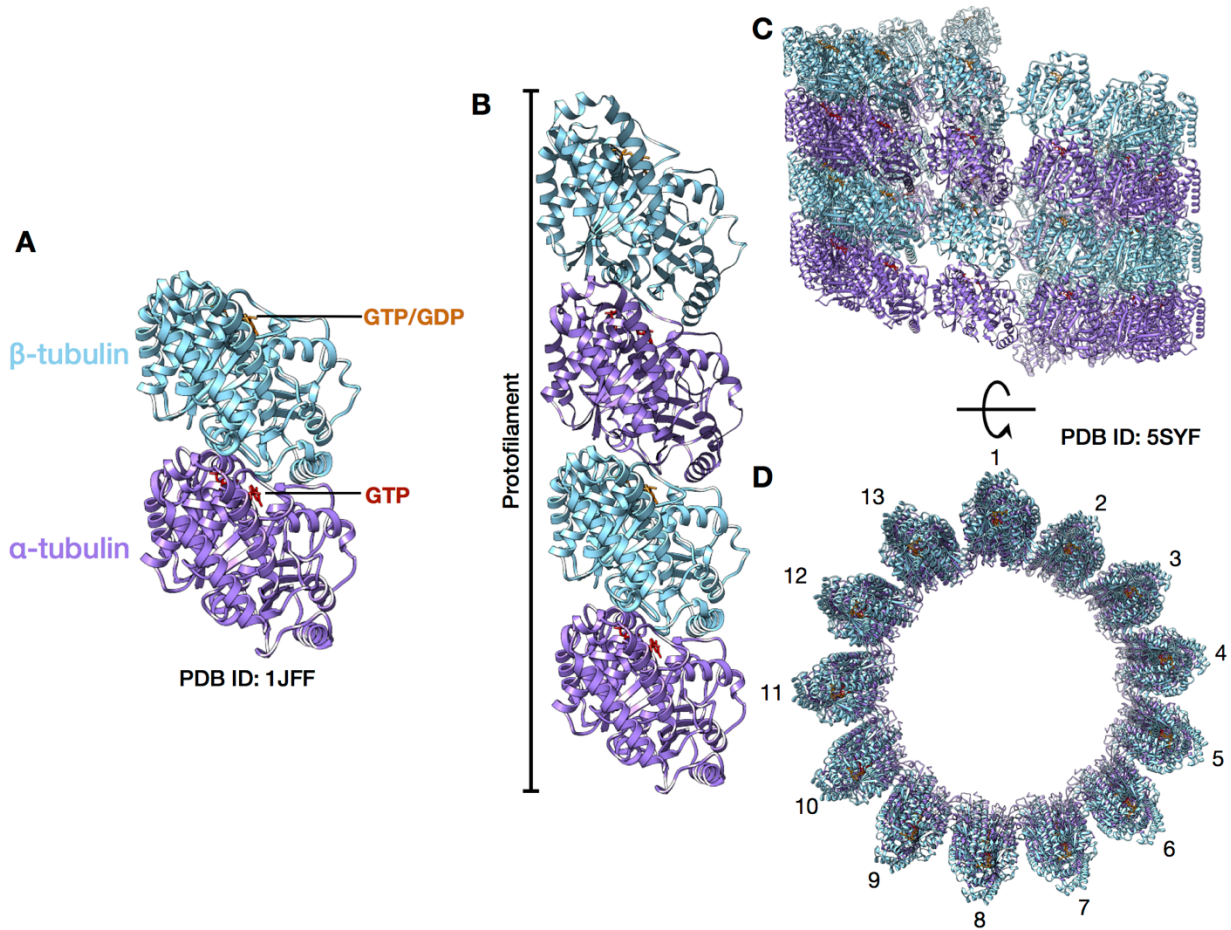
Figure 1. MT assembly interactions. A. αβ-tubulin heterodimer. **B**. αβ-tubulins assemble in a GTP-dependent manner, forming a protofilament via longitudinal contacts. **C.** Lateral contacts between protofilaments form the wall of the cylindrical MT. **D.** In most organisms MTs have 13 protofilaments, though in vitro polymerized MTs from with a distribution of protofilament counts ranging from 12-16.

The collective result of the activities of αβ-tubulin and its many regulatory molecules is to create the micron-scale MT cytoskeleton, which differs dramatically across species, among cell types of multicellular organisms, and cell-cycle states of individual cells. Despite differing in many crucial regards, the MT cytoskeleton of the budding yeast *Saccharomyces cerevisiae* has served as an invaluable model for understanding homologous structures and processes in metaozoa. *S. cerevisiae* has an extremely minimal MT cytoskeleton compared with metazoans.

While metazoan kinetochores bind many microtubules, forming MT bundles known as K-fibers, the point centromeres of budding yeast recruit a single site of MT attachment. The mitotic spindle thus consists of just 32 kinetochore microtubules, with an additional 10 or so forming interpolar MTs. Three to five additional microtubules are nucleated into the cytoplasm. The microtubule organizing center (MTOC) in budding yeast is also strikingly divergent in structure compared with the metazoan centrosome, the primary MTOC in most eukaryotes (Carvalho-Santos, et al., 2011). Centrosomes are organized around a MT-based structure known as the centriole. In a cell-cycle dependent manner, the centriole recruits a variety of proteins to form the pericentriolar material (PCM), an amorphous assembly that recruits microtubule nucleation machinery, among other regulatory components. Some PCM components are organized in a toroidal manner around the centriole, while others form a less-ordered matrix-like network (Mennella, et al., 2012). The yeasts and many other fungi have lost the centriole over the course of evolution and instead form an MTOC called the spindle pole body (SPB), a dramatically different structure that serves the same purpose as the centrosome in organizing the MT cytoskeleton. Consistent with the lack of nuclear envelope breakdown in yeasts, the SPB is embedded in the nuclear envelope, leading to an asymmetry in SPB structure. One face of the SPB nucleates the microtubules that comprise the mitotic spindle within the nucleus, while the other nucleates microtubules into the cytoplasm. The organizational principle of the SPB is plaque-like rather than toroidal or matrix-like as in the centrosome. The details of SPB structure and assembly are critical to the arguments made in this work and are thus discussed in detail.

SPB Structure and Biogenesis

SPBs are roughly cylindrical, with the circular faces of the cylinder oriented toward the nucleus or cytoplasm. SPBs are approximately 150 nm thick measured between the nuclear and cytoplasmic faces. The diameter of SPBs changes throughout the cell cycle, from approximately 80 nm in G1 to 110 nm in mitosis in haploid cells, with diploid SPBs still larger at 160 nm (Cavanaugh & Jaspersen, 2017). The organizational principle of the SPB is layer-like rather than toroidal or matrix-like as in the centrosome, with five major layers visible by electron microscopy termed the inner plaque, central plaque, intermediate layers 1 and 2, and outer plaque. The central plaque is composed of Spc42, Spc29, Cmd1 (calmodulin), and the carboxy (C)-terminal domain of Spc110. Spc42 is a coiled-coil protein that self-assembles into a two-dimensional, hexagonal crystalline lattice (Bullitt, et al., 1997). At its amino (N)-terminus, Spc42 binds Spc29 and the C-terminal domain of Spc110. Spc110 is bound by Cmd1 in a calcium-independent manner, increasing the resistance of the SPB to force applied by MTs (Fong, et al., 2017). The inner plaque is composed of the N-terminal region of Spc110 and Spc97, Spc98, and Tub4 (γ-tubulin), which compose the MT-nucleating γ-tubulin small complex (γTuSC). The outer plaque is located in the cytoplasm and also contains γTuSC, which is bound by the N-terminal domain of Spc72 rather than Spc110 as at the inner plaque. Spc72 interacts at its C-terminus with Nud1 in intermediate layer 1. Nud1 is attached to intermediate layer 2 via the N-terminal region of Cnm67, which binds via its C-terminal globular domain to the C-terminal domain of Spc42. The genetic, biochemical, structural, and imaging data that led to this understanding of SPB structure is reviewed in (Cavanaugh & Jaspersen, 2017). An integrated structural model
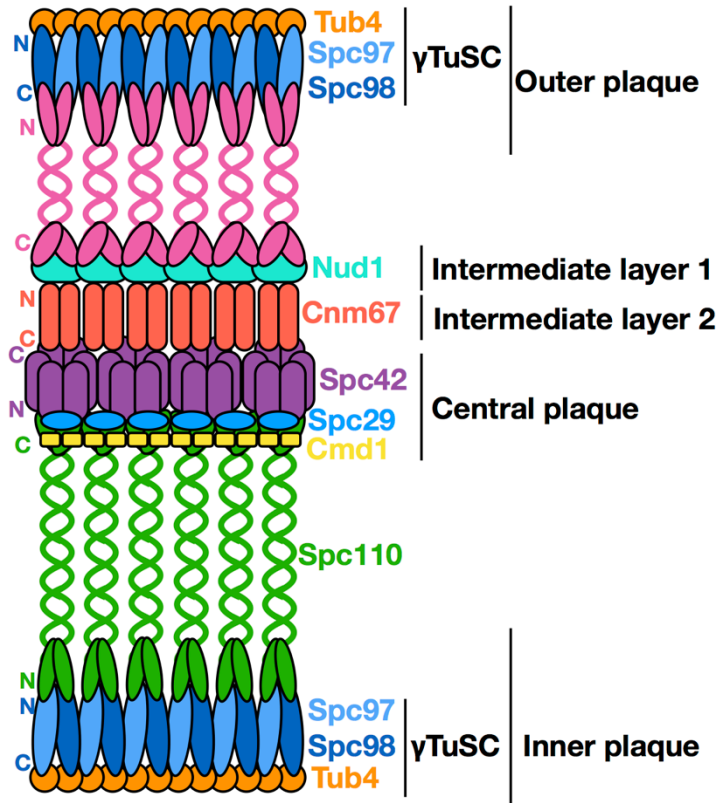
Figure 2. Schematic of the SPB core of S. cerevisiae. N- and C- termini of proteins are indicated where the orientations are known.

taking into account all these data was constructed by Viswanath and colleagues (Viswanath, et al., 2017).

Like chromosomal DNA, the SPB duplicates once per cell cycle with daughter SPBs "born" from mothers. A structure known as the half-bridge, composed of the filamentous protein Sfi1, is attached to the SPB core on the cytoplasmic side of the nuclear envelope. In mitosis, the C-terminal domain of Sfi1, located distal to the core SPB, is phosphorylated by cyclin B-Cdk1 (Avena, et al., 2014). Downregulation of cyclin B-Cdk1 activity in late anaphase leads to Sfi1 dephosphorylation by Cdc14. This licensing event permits "tail-to-tail" interaction between C-termini of Sfi1, which leads to elongation of the half bridge. The free Sfi1 N-terminal domain then accumulates proteins that form the satellite, a precursor to the SPB core. The first

SPB core protein to arrive at the satellite is Spc42, followed by Spc29, Nud1, and Cnm67 (Burns, et al., 2015).

The first stages of daughter SPB assembly occur in the cytoplasm, and none of the core SPB components contain transmembrane domains. Thus, additional factors must create a pore across the nuclear envelope through which the new SPB is inserted. As the nuclear envelope is a double-membrane structure, this involves the creation of a highly curved membrane domain linking the inner and outer nuclear membranes. As the satellite assembles, Mps2, a membrane protein, and Bbp1, a soluble protein that connects Spc29 with Mps2 (Schramm, et al., 2000), also accumulate at the distal end of the elongated half bridge (Burns, et al., 2015). Then membrane protein Ndc1 then accumulates at the daughter SPB, followed by the membrane protein Nbp1. However, it is not clear which component is responsible for opening a pore, though Mps2, Ndc1, and Nbp1 are the best candidates, being membrane proteins. Nbp1 in particular contains an amphipathic helix that is thought to insert into the outer leaflet of the inner nuclear membrane, similar to the membrane-bound components of the nuclear pore complex (NPC). The connection with NPCs may be even more direct, as Ndc1 is also present in NPCs and SPBs are frequently observed in proximity to NPCs. NPC depletion delays SPB duplication, as does tethering NPCs into clusters, presumably preventing close apposition with SPBs (Rüthnick, et al., 2017). However the SPB is inserted into the nuclear envelope, Spc110 recruitment to the central plaque is concomitant with SPB insertion. It is possible that Spc110 assists with SPB nuclear envelope insertion, as an Spc110 mutant with compromised Cmd1 binding shows defects in SPB insertion (Rüthnick, et al., 2017). It is unclear if additional events are required to permit binding of Spc110 to Spc42 and Spc29 part from physical accessibility in

the nucleus. As Spc110 contains a nuclear localization signal (Adams & Kilmartin, 1999), the simplest model is that Spc110 is depleted from the cytoplasm and is only able to associate with the central plaque once the daughter SPB is inserted into the cytoplasm. Once Spc110 is recruited to the SPB, γTuSC binds to the Spc110 N-terminal domain and MTs are nucleated into the cytoplasm.

Microtubule Nucleation by γ-Tubulin Complexes

The primary function of the SPB is to nucleate the MTs that form the mitotic spindle, as well as the cytoplasmic MTs responsible for directing the dividing nucleus into the bud. In both cases, MT nucleation is controlled by the conserved γTuSC. Following the identification of γ-tubulin in the filamentous fungus *Aspergillus nidulans* (Oakley & Oakley, 1989), it was found to have highly conserved MTOC localization (Oakley, et al., 1990; Stearns, et al., 1991; Zheng, et al., 1991; Sobel & Snyder, 1995). γ-tubulin exists in a conserved complex with homologues of budding yeast Spc97 and Spc98 (GCP2 and GCP3 in humans), the previously mentioned γTuSC (Kollman, et al., 2011). In metazoa, γ-tubulin also associates with the additional Spc97/98 homologues GCP4, -5, and -6. Known as γTuRC-specific components, GCP4-6 are thought to stabilize complexes that present γ-tubulins in a helical "lock washer" arrangement that matches the geometry of αβ-tubulins within the MT (Zheng, et al., 1995; Moritz, et al., 1995; Moritz, et al., 2000; Vérollet, et al., 2006). This complex is called the γ-tubulin ring complex (γTuRC). As described, formation of early MT assembly intermediates are thermodynamically unfavorable. In contrast, γTuRC is a stable complex whose structure organizes γ-tubulins in a geometry favorable for nucleating MTs, meaning MT nucleation in the cellular context bypasses the lag phase observed with spontaneously polymerizing αβ-tubulin in vitro. While genetic studies

have confirmed the central role of γTuRC in cellular MT nucleation, the extent to which additional factors play important roles is under active investigation (Wieczorek, et al., 2015; Roostalu & Surrey, 2017).

γTuRC and Spc110

The localization of γTuRC to MTOCs is mediated by a variety of attachment factors, including homologues of the budding yeast attachment factor Spc110 (Lin, et al., 2015). The *SPC110* gene was originally identified via expression cloning using antibodies prepared against nuclear extract or enriched SPBs (Rout & Kilmartin, 1990; Mirzayan, et al., 1992; Kilmartin, et al., 1993). The Spc110 protein was originally characterized as a spacer protein linking nuclear MTs and the central plaque, as deletions in its central coiled-coil domain decreased the distance between the ends of nuclear MTs and the central plaque (Kilmartin, et al., 1993). Following the identification of the components of the budding yeast γTuSC (Sobel & Snyder, 1995; Geissler, et al., 1996; Knop, et al., 1997), Spc110 was found to interact directly with Spc97 and Spc98 of γTuSC via its N-terminal domain (Knop & Schiebel, 1997; Sundberg & Davis, 1997; Knop & Schiebel, 1998).

Unlike metazoans and several fungi like *Schizosaccharomyces pombe*, the budding yeast genome does not encode homologues of GCP4-6. This raised questions about the nature of γTuRC in budding yeast. Recombinant expression of Tub4, Spc97, and Spc98 via baculovirus infection in insect cells yielded a complex consistent with γTuSC as assessed by gradient centrifugation and size exclusion chromatography (Vinh, et al., 2002). A similar complex was identified in yeast cell extracts prepared in a Tris buffer that does not support MT polymerization due to the presence of the magnesium cation chelator EDTA. However, extracts

prepared in a HEPES buffer that supports MT polymerization contained a γTuSC-based complex which migrated in gradient centrifugation experiments similarly to metazoan γTuRC. This complex contained neither Spc110 nor α-tubulin, though western blots for α-tubulin were not shown. The two buffer systems were identical in pH and salt concentration, though differing in buffer concentration, salt (sodium versus potassium chloride), and chelator (EDTA and EGTA) concentration. This study indicated that γTuRCs do assemble in budding yeast, though the mechanism by which assembly is regulated was not clear and is potentially obscured by the strong dependence on buffer composition.

A low-resolution negative stain electron microscopy structure of baculovirus-expressed γTuSC was subsequently determined (Kollman, et al., 2008). γTuSC was observed in a predominantly non-ring-like assembly state, though laterally associated γTuSCs were observed. Co-expression of Spc110 and γTuSC components led to appearance of large helical assemblies (Kollman, et al., 2010). This key observation led to the proposal that Spc110 is not simply a passive anchor for assembled γTuRCs, but is required to stabilize formation of γTuRCs in the first place.

This is the central question addressed in this work: What are the molecular details of the mechanism by which Spc110 stabilizes assembly of γTuRC, and what does that imply about MT organization in budding yeast? Chapter 2 describes how coiled-coil mediated oligomerization of Spc110 is a crucial determinant of γTuRC assembly. A version of this chapter was published in *Molecular Biology of the Cell* in May 2016 (Lyon, et al., 2016). Chapter 3 is a manuscript currently in preparation describing the role of the N-terminal disordered region of Spc110 in stabilizing γTuRC assembly.

References

Adams, I. & Kilmartin, J., 1999. Localization of core spindle pole body (SPB) components during SPB duplication in saccharomyces cerevisiae. *Journal of Cell Biology* **145**: 809-823.

Akhmanova, A. & Steinmetz, M., 2015. Control of microtubule organization and dynamics: two ends in the limelight. *Nature Reviews Molecular Cell Biology* **16:** 711-726.

Avena, J. S. et al., 2014. Licensing of Yeast Centrosome Duplication Requires Phosphoregulation of Sfi1. *PLOS Genetics* **10:** e1004666

Bullitt, E., Rout, M. P., Kilmartin, J. V. & Akey, C. W., 1997. The Yeast Spindle Pole Body Is Assembled around a Central Crystal of Spc42p. *Cell* **89**: 1077-1086.

Burns, S. et al., 2015. Structured illumination with particle averaging reveals novel roles for yeast centrosome components during duplication. *eLife* **4**: e08586.

Carvalho-Santos, Z., Azimzadeh, J., Pereira-Leal, J. B. & Bettencourt-Dias, M., 2011. Tracing the origins of centrioles, cilia, and flagella. *Journal of Cell Biology* **194**: 165-175.

Cavanaugh, A. M. & Jaspersen, S. L., 2017. Big Lessons from Little Yeast: Budding and Fission Yeast Centrosome Structure, Duplication, and Function. *Annual Review of Genetics* **51:** 361-383.

Flyvbjerg, H., Jobs, E. & Leibler, S., 1996. Kinetics of self-assembling microtubules: an "inverse problem" in biochemistry.. *Proceedings of the National Academy of Sciences of the United States of America* **93**: 5975-5979.

Fong, K. K. et al., 2017. Direct measurement of the strength of microtubule attachment to yeast centrosomes. *Molecular Biology of the Cell* **28**: 1853-1861.

Geissler, S. et al., 1996. The spindle pole body component Spc98p interacts with the gamma-tubulin-like Tub4p of Saccharomyces cerevisiae at the sites of microtubule attachment. *The EMBO Journal* **15**: 3899-3911.

Kilmartin, J. V., Dyos, S. L., Kershaw, D. & Finch, J. T., 1993. A spacer protein in the Saccharomyces cerevisiae spindle poly body whose transcript is cell cycle-regulated.. *Journal of Cell Biology* **123**: 1175-1184.

Knop, M. et al., 1997. The spindle pole body component Spc97p interacts with the gamma-tubulin of Saccharomyces cerevisiae and functions in microtubule organization and spindle pole body duplication.. *The EMBO Journal* **16**: 1550-1564.

Knop, M. & Schiebel, E., 1997. Spc98p and Spc97p of the yeast γ-tubulin complex mediate binding to the spindle pole body via their interaction with Spc110p.. *EMBO Journal* **16**: 6985-6995.

Knop, M. & Schiebel, E., 1998. Receptors determine the cellular localization of a γ-tubulin complex and thereby the site of microtubule formation. *The EMBO Journal* **17**: 3952-3967.

Kollman, J. M., Merdes, A., Mourey, L. & Agard, D. A., 2011. Microtubule nucleation by γ-tubulin complexes. *Nature Reviews Molecular Cell Biology* **12**: 709-721.

Kollman, J. M. et al., 2008. The Structure of the γ-Tubulin Small Complex: Implications of Its Architecture and Flexibility for Microtubule Nucleation. *Molecular Biology of the Cell* **19**: 207-215.

Kollman, J. et al., 2010. Microtubule nucleating gamma-TuSC assembles structures with 13-fold microtubule-like symmetry. *Nature* **466**: 879-882.

Lin, T.-c., Neuner, A. & Schiebel, E., 2015. Targeting of γ-tubulin complexes to microtubule organizing centers: conservation and divergence. *Trends in Cell Biology* **25**: 296-307.

Mennella, V. et al., 2012. Subdiffraction-resolution fluorescence microscopy reveals a domain of the centrosome critical for pericentriolar material organization. *Nature Cell Biology* **14**: 1159-1168.

Mirzayan, C., Copeland, C. & Snyder, M., 1992. The NUF1 Gene Encodes an Essential Coiled-Coil Related Protein That Is a Potential Component of the Yeast Nucleoskeleton. *Journal of Cell Biology* **116**: 1319-1332.

Mitchison, T. J. & Kirschner, M. W., 1984. Dynamic instability of microtubule growth. *Nature* **312**: 237-242.

Moritz, M. et al., 2000. Structure of the γ-tubulin ring complex : a template for microtubule nucleation. *Nature Cell Biology* **2**: 365-370.

Moritz, M. et al., 1995. Microtubule nucleation by γ-tubulin-containing rings in the centrosome. *Nature* **378**: 638-640.

Oakley, B. R., Oakley, C. E., Yoon, Y. & Jung, M. K., 1990. γ-tubulin is a component of the spindle pole body that is essential for microtubule function in Aspergillus nidulans. *Cell* **61**: 1289-1301.

Oakley, C. & Oakley, B., 1989. Identification of γ-tubulin, a new member of the tubulin superfamily encoded by mipA gene of Aspergillus nidulans. *Nature* **338**: 662-664.

Olmsted, J. B. & Borisy, G. G., 1975. Ionic and nucleotide requirements for microtubule polymerization in vitro. *Biochemistry* 14: 2996-3005.

Rüthnick, D. et al., 2017. Characterization of spindle pole body duplication reveals a regulatory role for nuclear pore complexes. *Journal of Cell Biology* **216**: 2425-2442.

Roostalu, J. & Surrey, T., 2017. Microtubule nucleation: beyond the template. *Nature Reviews Molecular Cell Biology* **18**: 702-720.

Rout, M. P. & Kilmartin, J. V., 1990. Components of the yeast spindle and spindle pole body.. *Journal of Cell Biology* **111**: 1913-1927.

Schramm, C. et al., 2000. The Bbp1p–Mps2p complex connects the SPB to the nuclear envelope and is essential for SPB duplication. *The EMBO Journal* **19**: 421-433.

Sobel, S. & Snyder, M., 1995. A highly divergent gamma-tubulin gene is essential for cell growth and proper microtubule organization in Saccharomyces cerevisiae. *Journal of Cell Biology* **131**: 1775-1788.

Stearns, T., Evans, L. & Kirschner, M. W., 1991. γ-Tubulin is a highly conserved component of the centrosome. *Cell* **65**: 825-836.

Sundberg, H. A. & Davis, T. N., 1997. A MUTATIONAL ANALYSIS IDENTIFIES THREE FUNCTIONAL REGIONS OF THE SPINDLE POLE COMPONENT SPC110P IN SACCHAROMYCES CEREVISIAE. *Molecular Biology of the Cell* **8**: 2575-2590.

Vérollet, C. et al., 2006. Drosophila melanogaster γ-TuRC is dispensable for targeting γ-tubulin to the centrosome and microtubule nucleation. *Journal of Cell Biology* **172**: 517-528.

Vinh, D. et al., 2002. Reconstitution and Characterization of Budding Yeast γ-Tubulin Complex. *Molecular Biology of the Cell* **13**: 1144-1157.

Viswanath, S. et al., 2017. The molecular architecture of the yeast spindle pole body core determined by Bayesian integrative modeling. *Molecular Biology of the Cell* **28**: 3298-3314.

Voter, W. & Erickson, H., 1984. The Kinetics of Microtubule Assembly. Evidence For a Two-Stage Nucleation Mechanism. *Journal of Biological Chemistry* **259**: 10430-10438.

Wieczorek, M., Bechstedt, S., Chaaban, S. & Brouhard, G. J., 2015. Microtubule-associated proteins control the kinetics of microtubule nucleation. *Nature Cell Biology* **17**: 907-916.

Zheng, Y., Jung, M. K. & Oakley, B. R., 1991. γ-Tubulin is present in Drosophila melanogaster and homo sapiens and is associated with the centrosome. *Cell* **65**: 817-823.

Zheng, Y., Wong, M., Alberts, B. & Mitchison, T., 1995. Nucleation of microtubule assembly by a γ-tubulin-containing ring complex. *Nature* **378**: 578-583.

Higher-order oligomerization of Spc110p drives γ-tubulin ring complex assembly

Contributing Authors

Geneviève Morin (University of Washington), Michelle Moritz (UCSF), King Clyde B. Yabut (University of Washington), Tamira Vojnar (University of Washington), Alex Zelter (University of Washington), Eric Muller (University of Washington), Trisha N. Davis (University of Washington), and David A. Agard (UCSF).

Preface

The bulk of this chapter appears as Lyon et al. (2016) *Mol Biol Cell* **27**: 2245-2258. The original observations that led to the manuscript, however, are unpublished and are presented here. Kollman and colleagues demonstrated that an Spc110 construct consisting of the N-terminal 401 residues with a C-terminal GST fusion expressed with γTuSC components assembles γTuRCs rather than the helical filaments observed with the Spc110$^{1-220}$ construct. We reasoned this construct would be ideal for dissecting γTuRC assembly in vitro as any confounding effects due to filament formation would be avoided.

Upon purifying Spc110$^{1-401}$-GST via anion exchange chromatography, I observed a complex elution profile with three overlapping peaks (Figure 1A). In the FRET assay for γTuRC assembly described in detail below, the three peaks had significantly different activity, with both apparent affinity and average assembly size (which is proportional
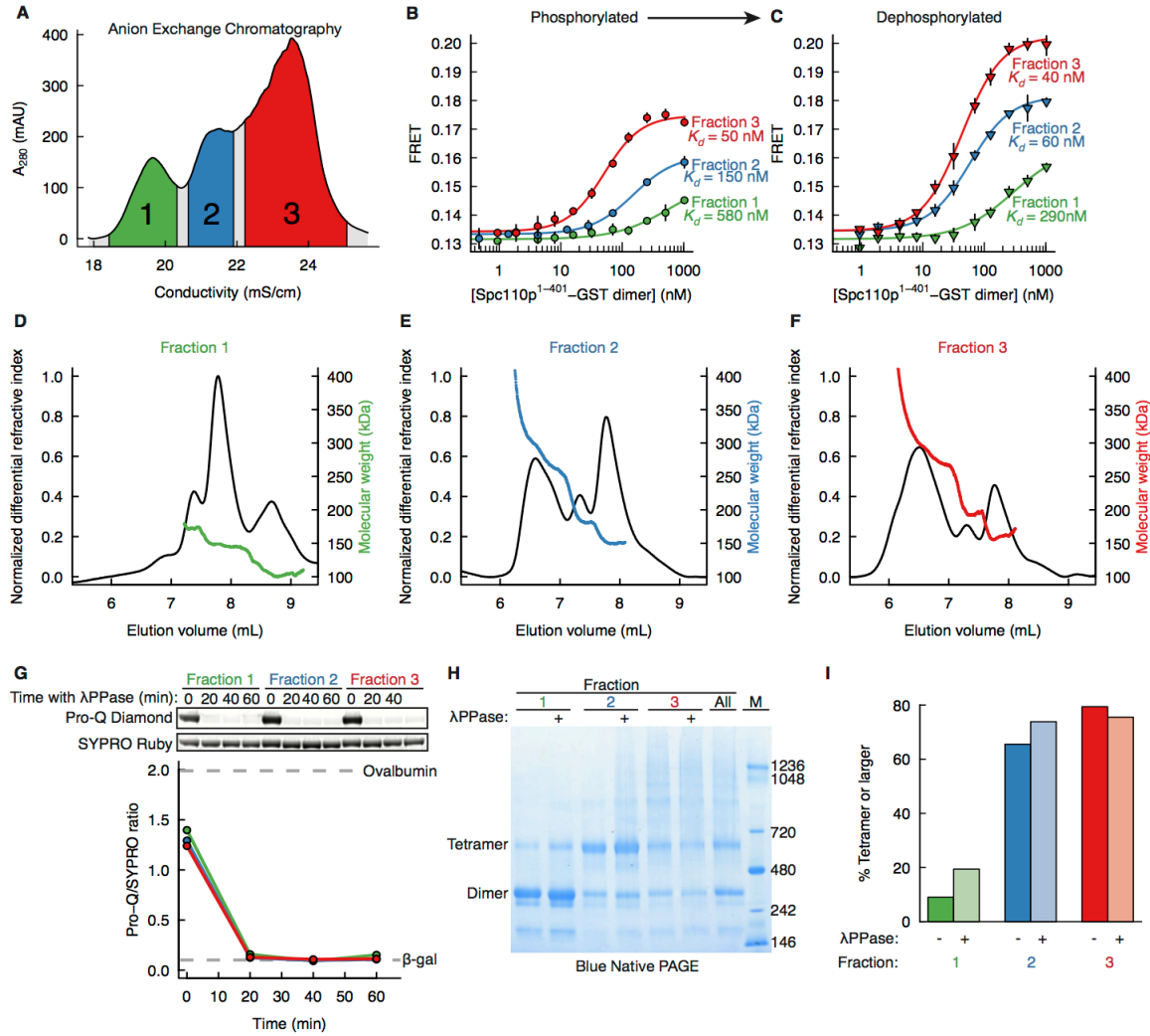
Figure 1. **Higher-order oligomers of Spc110 stabilize γTuRC assembly. A.** Anion exchange chromatogram of Spc110$^{1-401}$-GST expressed in baculovirus infected insect cells. The three fractions analyzed are indicated. **B.** FRET assay for γTuRC assembly in the presence of the three Spc110$^{1-401}$-GST fractions. **C.** As in **B**, but Spc110$^{1-401}$-GST was dephosphorylated with His-tagged bacteriophage λ protein phosphatase (λPPase). Spc110$^{1-401}$-GST was subtractively purified by removing λPPase with nickel-affinity chromatography and was then used in the FRET assay. **D-F.** SEC-MALS analysis of Spc110$^{1-401}$-GST shows later-eluting fractions contain a larger fraction of higher-order oligomers. **G.** Analysis of Spc110$^{1-401}$-GST dephosphorylation using bacteriophage λ protein phosphatase (λPPase). Spc110$^{1-401}$-GST was incubated with λPPase then reactions were quenched by boiling in SDS loading buffer. Gel was stained first with Pro-Q diamond to detect phosphoprotein, then SYPRO Ruby for total protein. Pro-Q/SYPRO ratio was then calculated from band intensities and compared with a control phosphoprotein (ovalbumin) and non-phosphoprotein (β-galactosidase). **H.** Blue native PAGE analysis of phosphorylated and dephosphorylated Spc110$^{1-401}$-GST. **I.** Quantification of oligomerization state from the gel in **H**.

FRET signal at saturating Spc110 concentration) increasing in the later-eluted fractions (Figure

1B). As phosphorylation is predicted to increase the net negative surface charge, more highly

phosphorylated species should elute later from the anion exchange column. Spc110 is known to

be phosphorylated (Friedman et al. 2001; Keck et al. 2011; Lin et al. 2014), leading to the

prediction that fraction 3 is the most highly phosphorylated fraction and that increasing

phosphorylation correlates with increasing γTuRC assembly activity. This implies that

dephosphorylation should cause all three fractions to exhibit the same behavior in the FRET

assay. In contrast to my expectations, dephosphorylating each of the three fractions enhanced

both affinity and average assembly size (Figure 1C). This indicates that stabilization of γTuRC

can be regulated by phosphorylation, but that some other mechanism is also at play.

Given that Spc110 contains a long coiled-coil domain (Kilmartin et al. 1993) and that

overexpression of Spc110 leads to formation of ordered, spheroidal intranuclear assemblies

(Kilmartin and Goh 1996), I used size-exclusion chromatography coupled with multiangle light

scattering (SEC-MALS) to assess the oligomer distributions of the Spc110$^{1-401}$-GST fractions

(Figure 1D-F). The oligomer distributions differed substantially, with fraction 1 (Figure 1D)

predominantly dimeric (predicted monomer molar mass 73.3 kDa), with fractions 2 and 3

containing increasing amounts of tetrameric and higher-order species (Figure 1E-F). When

Spc110$^{1-401}$-GST was dephosphorylated to the level of a non-phosphorylated control protein as

assessed by Pro-Q Diamond gel stain (Figure 1G), no significant change in oligomer distribution

was observed by blue native polyacrylamide gel electrophoresis (Figure 1H-I), indicating that

while a role for phosphorylation in oligomer assembly cannot be excluded, dephosphorylation

is not sufficient to disassemble oligomers.

These observations led directly to the experiments presented in the remainder of this chapter, but were excluded from the published manuscript in favor of experiments using more homogeneous Spc110 preparations which allowed for more straightforward explanation of the relative roles of phosphorylation and oligomerization in stabilizing γTuRC.

Summary

The microtubule (MT) cytoskeleton plays important roles in many cellular processes. *In vivo*, MT nucleation is controlled by the γ-tubulin ring complex (γTuRC), a 2.1 MDa complex composed of γ-tubulin small complex (γTuSC) subunits. The mechanisms underlying the assembly of γTuRC are largely unknown. In yeast the conserved protein Spc110p both stimulates the assembly of the γTuRC and anchors the γTuRC to the spindle pole body (SPB). Using a quantitative *in vitro* FRET assay, we show that γTuRC assembly is critically dependent on the oligomerization state of Spc110p, with higher-order oligomers dramatically enhancing the stability of assembled γTuRCs. Our *in vitro* findings were confirmed with a novel *in vivo* γTuSC recruitment assay. We conclude that precise spatial control over MT nucleation is achieved by coupling localization and higher-order oligomerization of the receptor for γTuRC.

Introduction

The MT cytoskeleton plays important roles in many cellular processes, including signaling, intracellular transport, polarization, motility, and cell division. While the pathways controlling these processes are complex, in general they impinge upon the cytoskeleton to regulate MT nucleation, elongation, and catastrophe. While elongation and catastrophe are largely controlled by soluble proteins, nucleation is regulated by factors anchored in microtubule organizing centers (MTOCs) like the budding yeast SPB and the metazoan centrosome (Kollman et al. 2011). Within the MTOC, the γTuRC nucleates MTs by forming a ring-shaped template from which MTs grow. In all eukaryotes, γTuRCs are built from multiple copies of the conserved core complex known as γTuSC, which in turn is composed of two γ-tubulins bound at the top of a Y-shaped complex formed by Spc97p and Spc98p (Kollman et al. 2008). In budding yeast, seven γTuSCs associate laterally to form a one-start helix with one-half γTuSC overlap after one turn, yielding 13 γ-tubulins presented as a MT template (Kollman et al. 2010; Kollman et al. 2015). In metazoans, canonical γTuSCs are mixed with γTuSC-like structures composed of γ-tubulin complexed with homologs of Spc97p and Spc98p, known as the γTuRC-specific components GCP4, -5, and -6, to form γTuRCs (Guillet et al. 2011; Kollman et al. 2011).

In metazoans, γTuRCs exist predominantly as soluble complexes that are recruited to sites of MT nucleation by a variety of attachment factors (Kollman et al. 2011; Moudjou et al. 1996). In contrast, yeast γTuSC alone does not form γTuRC-like structures (Kollman et al. 2008). However, co-expression of γTuSC with the N-terminal domain of Spc110p, which anchors γTuSCs to the nuclear face of the SPB (Knop and Schiebel 1997; Knop and Schiebel 1998;

Kollman et al. 2010), leads to formation of larger ring-shaped and filamentous assemblies (Kollman et al. 2010). Co-expression with larger Spc110p fragments precludes filament formation (Kollman et al. 2015). Previous reports have implicated Spc110p phosphorylation in stimulating γTuRC assembly (Lin et al. 2014). Additionally, a *Schizosaccharomyces pombe* protein homologous to budding yeast Spc72p, the counterpart of Spc110p on the cytoplasmic face of the SPB, has been shown to oligomerize, which potentially stabilizes the γTuRC (Lynch et al. 2014). While suggestive, a detailed analysis of the processes underlying Spc110p-dependent γTuRC assembly is still lacking. We therefore aimed to describe the γTuRC assembly process using a quantitative biochemical, biophysical, and cell biological approach that would allow assessment of the relative contribution of the various regulatory mechanisms impacting Spc110p and γTuSC.

Using budding yeast γTuSC and a novel FRET assay, we reconstituted γTuRC assembly *in vitro* and dissected the features of Spc110p required for assembly. We find that higher-order oligomerization of Spc110p is the principal driver of γTuRC assembly, with oligomerization state impacting γTuRC assembly much more dramatically than a phosphomimetic mutation previously reported to enhance γTuRC assembly (Lin et al. 2014). In N-terminal deletion studies, deleting up to, but not through, the conserved centrosome motif 1 (CM1) domain of Spc110p preserves the ability to assemble γTuRCs. We use a novel *in vivo* γTuSC recruitment assay to confirm the importance of Spc110p oligomerization in the cellular context. Our results suggest a molecular mechanism by which higher-order Spc110p oligomerization can restrict γTuRC assembly and hence MT nucleating ability to the SPB, ensuring precise spatiotemporal regulation of the MT cytoskeleton.

Results

γTuSC assembly reconstituted in vitro

Spurred by the observation that co-expression of GST-Spc110p[1-220] with γTuSC in baculovirus-infected insect cells led to formation of rings and larger filamentous assemblies (Kollman et al. 2010), we developed a FRET assay to monitor the Spc110p-dependent γTuSC ring assembly process *in vitro* (Figure 2A) (see also Materials and Methods and Supplemental Figure S1). (For clarity we will refer to the process of γTuSC oligomerization as 'γTuSC assembly' and reserve γTuRC for fully formed rings.) The FRET assay is highly quantitative, allowing different forms of Spc110p to be accurately compared, and, importantly, is sensitive enough to allow measurements to be made at physiologically relevant γTuSC concentrations. The FRET analysis measures both

apparent affinity (from the concentration of Spc110p yielding half-maximal signal) and the extent of γTuSC assembly (from the plateau value).
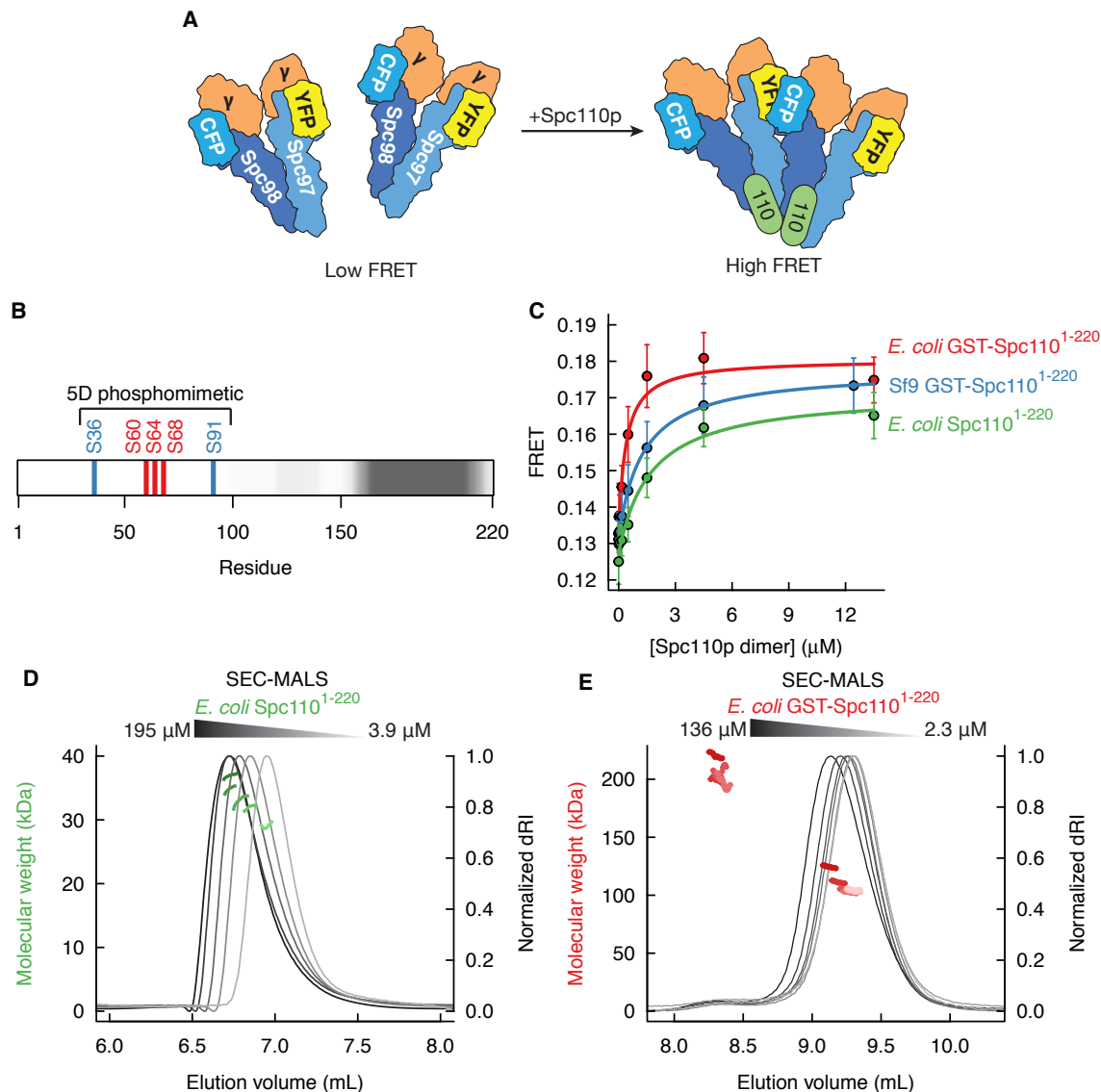
Figure 2. **Reconstitution of γTuRC assembly *in vitro*. A.** Schematic of FRET assay for γTuRC assembly. Spc110p-induced γTuRC assembly increases CFP-YFP FRET. **B.** Diagram of Spc110p residues 1-220. Regions with high coiled-coil probability, calculated with MARCOIL (Delorenzi and Speed 2002), are indicated with darker shades of grey. The residues mutated in the 5D phosphomimetic mutant are highlighted. **C.** γTuRC assembly measured by FRET in the presence of 75 nM γTuSC. Dissociation constants are *E. coli* GST-Spc110p[1-220]: 370 nM; Sf9 GST-Spc110p[1-220]: 1290 nM; *E. coli* Spc110p[1-220]: 1700 nM. **D.** SEC-MALS analysis of untagged *E. coli* Spc110p[1-220] at concentrations ranging from 3.9 μM (light colored trace) to 195 μM (dark colored trace) calculated on a monomer basis. The molecular weights calculated are between the predicted monomer (26 kDa) and predicted dimer (52 kDa), indicating untagged Spc110p[1-220] is in monomer-dimer equilibrium. **E.** SEC-MALS analysis of *E. coli* GST-Spc110p[1-220] at concentrations ranging from 2.3 μM (light colored trace) to 136 μM (dark-colored trace) calculated on a monomer basis. GST-Spc110p[1-220] is at least dimeric (predicted molecular weight 104 kDa) at all concentrations, with small amounts of tetramers present.

20

We expressed and purified γTuSC labeled with CFP and YFP FRET probes on the C-termini of Spc98p and Spc97p, respectively, from baculovirus-infected insect cells (Choy et al. 2009). To decrease sample heterogeneity, we purified γTuSC based on its ability to interact with Spc110p, thereby discarding any protein lacking post-translational modifications or other features required for Spc110p interaction. We estimate ~50% of γTuSC in insect cells is capable of interacting with Spc110p (Supplemental Figure S2). When combined with GST-Spc110p[1-220], which we have previously shown induces γTuSC self-assembly (Kollman et al. 2010), γTuSC oligomers form with an apparent K_d of 1290 nM (Figure 2B). While this confirms the ability of Spc110p[1-220] to stimulate γTuSC assembly, the K_d was surprisingly high given that the *in vivo* concentration of Spc110p dimer has been estimated to be ~80 nM (Ghaemmaghami et al. 2003).

As Spc110p is phosphorylated at numerous positions within residues 1-220 both in yeast and when expressed in insect cells (Friedman et al. 2001; Keck et al. 2011; Lin et al. 2014) (Figure 2C), we considered that phosphorylation of Spc110p may impact the efficiency of the γTuSC assembly process. We therefore compared baculovirus-expressed Spc110p with that expressed in *E. coli*, which lacks the relevant cell-cycle regulatory kinases. To our surprise, *E. coli*-expressed Spc110p induced assembly ~3-fold more efficiently, with an apparent K_d of 370 nM (Figure 2B). This suggests that phosphorylation sites targeted by insect cell kinases have a mild inhibitory effect on γTuSC assembly.

We next considered that the GST fusion protein may perturb the assembly process, as GST itself forms dimers and might shift the oligomeric state of Spc110p. Untagged Spc110p[1-220] was produced via proteolytic cleavage of the hexahistadine purification tag and was nearly 5-

fold less efficient at γTuSC assembly (K_d = 1700 nM) (Figure 2B). To understand this difference,

we analyzed the oligomeric state of Spc110p using size exclusion chromatography coupled with

multiangle light scattering (SEC-MALS) over a range of concentrations (Figure 2D-E). Untagged

Spc110p[1-220] had a calculated molecular weight intermediate between that of a monomer and a

dimer (Figure 2D). As molecular weights calculated by SEC-MALS are a weighted average of the

species present, this indicates that untagged Spc110p[1-220] exists in a monomer-dimer

equilibrium whose species are not resolved by the size exclusion column. In contrast, GST-

Spc110p[1-220] was dimeric under all concentration conditions tested, with a small fraction of

tetrameric species (Figure 2E). Thus, the oligomerization state of Spc110p[1-220] was strongly

perturbed by the GST tag, and the oligomerization state of the Spc110p constructs correlates

with the apparent K_d for γTuSC assembly.

Higher-order Spc110p oligomerization is necessary for γTuSC assembly at physiological

concentrations

      To avoid the confounding effects of the GST tag and phosphorylation state, we

addressed the role of Spc110p oligomerization in a well-defined system utilizing a protein

engineering approach with bacterially-expressed protein. Spc110p[1-220], which is
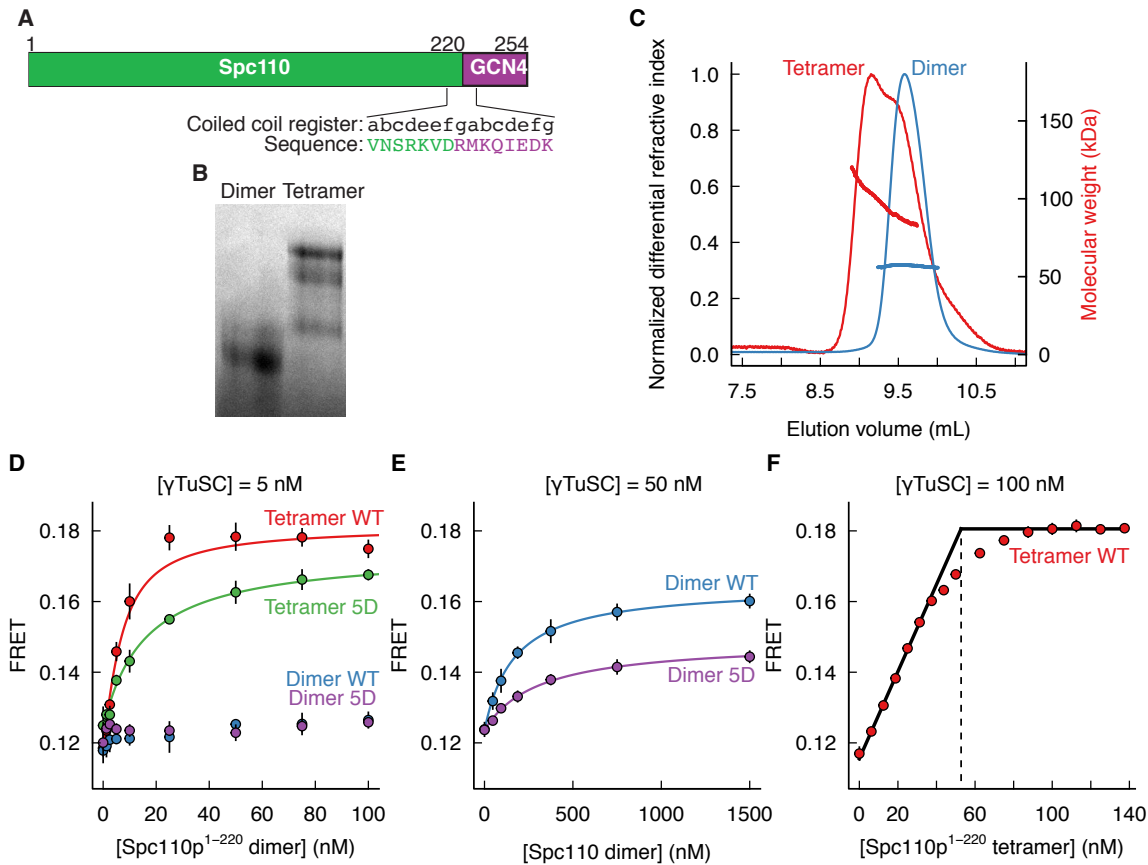
Figure 3. **Spc110p oligomerization is required for γTuRC assembly at physiological concentrations. A.** Diagram of Spc110p[1-220]-GCN4 coiled coil domain fusion constructs. The predicted coiled-coil register of Spc110p[1-220] is fused in frame with the register of GCN4. **B.** Analysis of Spc110p[1-220]-dimer and -tetramer oligomerization state by Blue Native PAGE. **C.** Molecular weights of Spc110p[1-220]-dimer and -tetramer measured by SEC-MALS are consistent with dimers or tetramers of ~29.5 kDa monomers. Samples in HB250 were separated on a Shodex KW-804 column. **D.** Spc110p[1-220]-dimer has no activity in the presence of 5 nM γTuSC, while Spc110p[1-220]-tetramer stimulates robust assembly. The wild-type binding curve was fit to a tight binding model, while the 5D phosphomimetic was fit to a simple binding model. **E.** Spc110p[1-220]-dimer stimulates γTuRC assembly in the presence of 50 nM γTuSC. **F.** Stoichiometry analysis of Spc110p:γTuSC complex. At 100 nM γTuSC, far greater than the apparent K_d, the assembly curve saturates at an Spc110p[1-220]-tetramer concentration of ~50 nM, indicating a stoichiometry of 1 Spc110p[1-220]-tetramer : 2 γTuSC, or 2 Spc110p monomers per γTuSC.

sufficient for assembly of γTuSC filaments (Kollman et al. 2010) but has only a weak tendency to dimerize on its own (Figure 2D), was fused with either the dimeric coiled-coil domain of the transcription factor GCN4, or a mutant version that preferentially forms tetramers (Harbury et al. 1993) (Figure 3A). Analysis of oligomeric state by blue native polyacrylamide gel electrophoresis (Figure 3B) and molecular weight determination by SEC-MALS (Figure 3C) confirmed that engineered Spc110p derivatives formed the expected oligomers.

Engineered Spc110p dimers failed to induce any detectable γTuSC assembly at a γTuSC concentration of 5 nM (Figure 3D). In contrast, under these conditions tetramers promoted robust assembly, with an apparent dissociation constant of 4 nM, determined using a tight binding formalism (Pollard 2010) (Figure 3D). At the higher γTuSC concentration of 50 nM, Spc110p$^{1-220}$-dimer was able to induce assembly, but with a substantially reduced affinity of 170 nM (Figure 3E). This dependence on γTuSC concentration indicates that γTuSC-γTuSC self-association contributes to γTuSC assembly, but must be stabilized by interactions with Spc110p oligomers. The striking difference in assembly efficiency between dimeric and tetrameric Spc110p was also evident in negative stain electron micrographs, where γTuSC assemblies were much less prevalent in the presence of Spc110p$^{1-220}$-dimer than with the tetramer (Figure 4A-F). This confirms that higher-order oligomerization of Spc110p is necessary for γTuSC assembly under physiological concentration regimes, estimated at ~80 nM Spc110p dimer (Ghaemmaghami et al. 2003).
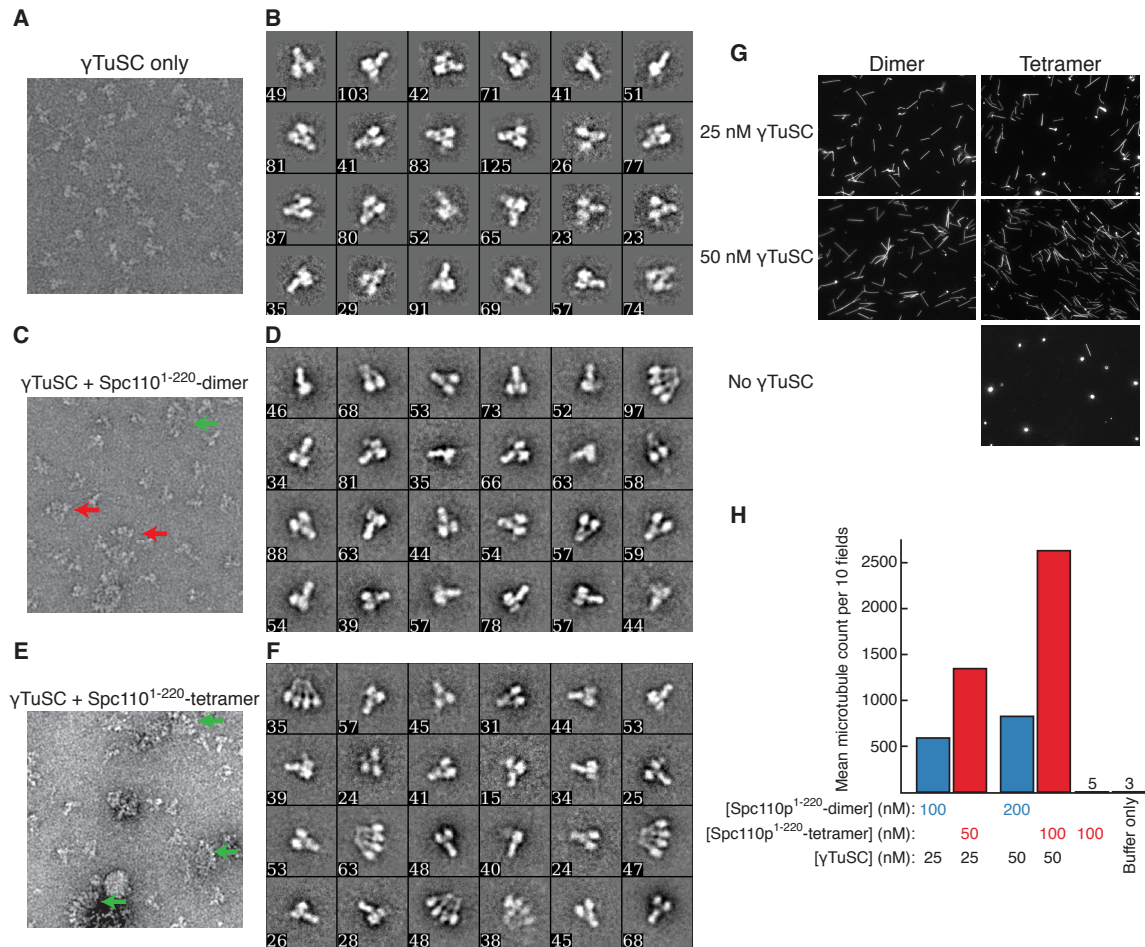
Figure 4. **Structural and functional analysis of γTuSC-Spc110p[1-220]-dimer and – tetramer complexes.** Representative negative stain micrograph and class averages of 75 nM γTuSC (**A-B**), γTuSC + Spc110p[1-220]-dimer (**C-D),** and γTuSC + Spc110p[1-220]-tetramer (**E-F).** Red arrows indicate complexes containing two γTuSCs, while green arrows indicate complexes with larger numbers of γTuSC (**A**, **C**, **E**). Numbers indicate the number of particles represented in each class (**B**, **D**, **F**). γTuSC only class averages (**B**) are shown padded to the same box size as γTuSC-Spc110p classes. **G.** Engineered Spc110p[1-220] oligomers form MT nucleation-competent complexes with γTuSC. γTuSC was incubated with an 4-fold excess of Spc110p[1-220]-dimer or -tetramer, calculated on dimer basis, and 1.5 μM *S. cerevisiae* tubulin. Spc110p[1-220]-tetramer in the absence of γTuSC was included as a negative control. Representative epifluorescence images are shown. **H.** Quantification of G. The mean (n=2) microtubule count from 10 randomly chosen fields is plotted.

We next compared the relative importance of oligomerization and phosphorylation

using phosphomimetic aspartic acid mutations to residues S36, S91 (Cdk1 targets), S60, T64,

and T68 (Mps1 targets). This mutation, denoted 5D (Figure 3C), was shown to enhance

assembly of γTuSCs by dimeric GST-Spc110p$^{1-220}$ (Lin et al. 2014). However, we found that the

5D phosphomimetic mutation had only mild effects, and actually weakened the apparent K_d to

15 nM for the tetrameric Spc110p, and from 170 nM to 310 nM for Spc110p$^{1-220}$-dimer. The 5D

mutation did not affect Spc110p oligomerization state as analyzed by SEC-MALS (Supplemental

Figure S3A). The effects of the 5D phosphomimetic mutation were similar when analyzed with a

size-exclusion chromatography assay for γTuSC assembly similar to that used by Lin et al. 2014

(Supplemental Figure S3B). We also compared the Tris pH 7 buffer used by Lin et al. to our

HEPES pH 7.5 buffer and found that the 5D phosphomimetic was inhibitory in both cases, with

the Tris pH 7 buffer promoting a higher level of Spc110-independent γTuSC assembly

(Supplemental Figure S3C). The enhancement of γTuSC assembly upon higher-order

oligomerization is thus much more robust than this previously examined set of phosphomimetic

mutations.

The more-homogeneous *E. coli* Spc110p$^{1-220}$-tetramer preparation allowed the

Spc110p:γTuSC stoichiometry required for assembly to be determined. When γTuSC is present

at 100 nM, a concentration much greater than the apparent K_d, the FRET signal saturates at ~50

nM Spc110p tetramer. This indicates a stoichiometry of one Spc110p tetramer per γTuSC dimer,

or 2:1 Spc110p monomer:γTuSC (Figure 3F), consistent with previous observations (Erlemann et

al. 2012; Kollman et al. 2015). Taken together, these data indicate that a dimer of dimers is the

minimal Spc110p species sufficient to allow γTuSC assembly, with each γTuSC being bound by a single Spc110p dimer.

To ensure that the engineered Spc110p$^{1-220}$-tetramer assembles γTuSCs into native-like conformations, we assessed their ability to nucleate MTs *in vitro* using *S. cerevisiae* αβ-tubulin, which is much more active for yeast γTuRCs than the typically used porcine brain tubulin (Figure 4G-H) (Kollman et al. 2015). Although complete γTuRCs were not observed by negative stain electron microscopy (EM) due to the relatively low protein concentration used (Figure 4C-F), γTuSC incubated with Spc110p$^{1-220}$-tetramer nucleates 2-3-fold more MTs than does Spc110p$^{1-220}$ dimer. This confirms that the increased FRET elicited by Spc110p$^{1-220}$-tetramer is due to authentic and functional γTuSC assembly interactions.

The γTuSC assembly process quantified by computational simulation

While Spc110p-dependent γTuSC assembly data can be adequately fit by the simple, two-component, single-site binding model (Figures 1B, 2D-E), several observations suggest the assembly process is more complex. We observed large differences in binding curves at varying γTuSC concentration and a reproducible fall-off in FRET with 5 nM γTuSC at high Spc110p$^{1-220}$-tetramer concentration (Figure 5A). Additionally, the formation of microtubules by Spc110$^{1-220}$ tetramer and the presence of larger γTuSC assemblies observed by negative stain EM (Figure 4E) indicates that complexes containing more than two γTuSCs can form, potentially mediated by higher-
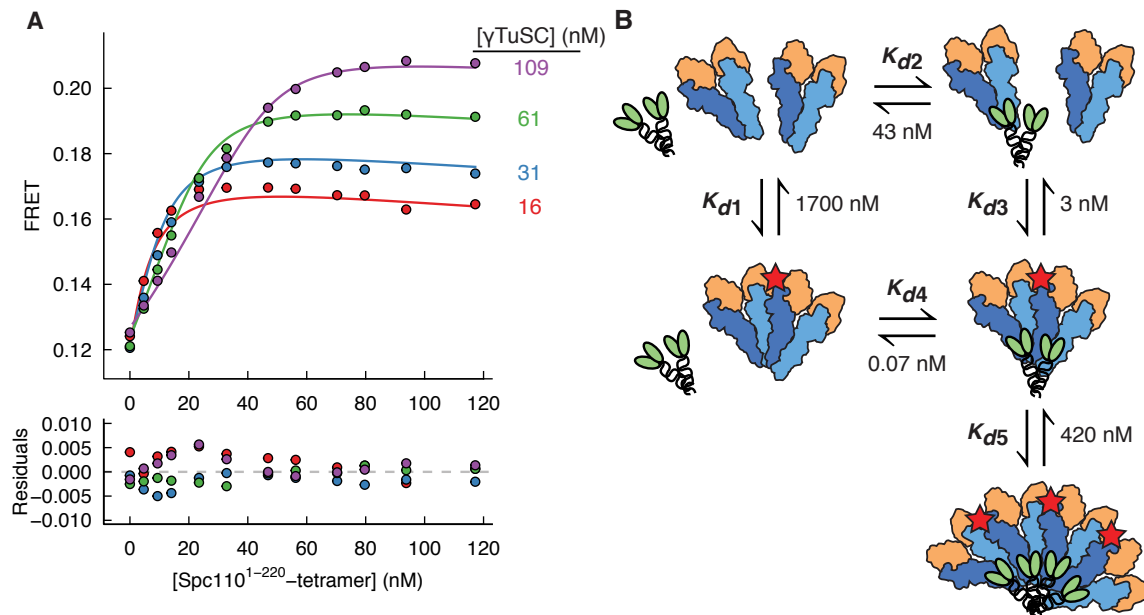
Figure 5. **Quantifying interaction affinities underlying Spc110p-dependent γTuRC assembly. A.**
Spc110p[1-220]-tetramer-induced γTuRC assembly behavior at varying γTuSC concentrations, with
fits derived from computational simulation. Best-fit γTuSC concentrations are indicated. **B.**
Schematic of γTuSC-Spc110p[1-220]-tetramer interactions, with interactions giving rise to FRET
indicated (★). Dissociation constants derived from kinetic modeling are indicated.

order oligomerization of Spc110p. To account for these observations, a more comprehensive

assembly model where γTuSC monomers are bound sequentially by an Spc110p tetramer to

form a dimer, or where γTuSC dimers are captured by an Spc110p tetramer (Figure 5B). The

ability to form γTuSC tetramers was included in the model to account for higher order

assemblies.

To estimate the resulting five dissociation constants, we modeled the γTuSC assembly

process as a system of ordinary differential equations (ODEs) according to the scheme shown in

Figure 5B. For a given set of initial species concentrations and rate constants, equilibrium

concentrations are obtained by numerical integration of the ODE system. Experimental FRET

data was then fit to the model by assuming a fixed on-rate for each reaction and numerically

optimizing the off-rates, thus yielding a dissociation constant for each reaction. As fits using the

nominal initial γTuSC concentrations were unsatisfactory, the lowest initial γTuSC concentration

was included as an additional free parameter in the fit, with the higher γTuSC concentrations

scaled relative to this based on the mean total fluorescence at each concentration (see

Methods and Supplemental Figure S4A). This approach led to robust binding constant estimates

for almost every parameter (Supplemental Figure S4C-I).

While the K_{d1} for γTuSC dimerization in the absence of Spc110p is not well constrained

due to limitations on the maximum practical γTuSC concentration (Supplemental Figure S4C),

the model fits suggest a dissociation constant for γTuSC dimerization (K_{d1}) of approximately 1.7

μM. The affinity of Spc110p-tetramer for a single γTuSC is substantially stronger, with K_{d2} = 43

nM. Binding a second γTuSC to this complex is stabilized by both Spc110p and the γTuSC self-

interaction, with a substantial local concentration effect yielding a very strong K_{d3} = 3 nM. The

formation of γTuSC tetramers from two pre-assembled γTuSC:Spc110p complexes occurs with a

dissociation constant K_{d5} of 420 nM, which is stronger than the γTuSC self-interaction and

indicates that larger γTuSC assemblies are also stabilized through additional Spc110p-mediated

interactions. The dissociation constants account for the lack of full ring assemblies in electron

micrographs (Figure 4C-F), as the 75 nM γTuSC and Spc110p concentrations would limit

abundance of large assemblies given the 420 nM K_{d5}. Taken together, our model provides a

detailed mechanism underlying the observed requirement for Spc110p in γTuRC assembly: in

the absence of stabilization by Spc110p oligomers, the γTuSC self-interaction affinity is simply

too weak to support assembly.

Higher-order Spc110 oligomerization is required for γTuSC assembly in vivo

Our results indicate that Spc110p must oligomerize beyond a dimer in order for γTuSCs to assemble to a MT nucleation-competent state. To assess the relevance of Spc110p oligomerization *in vivo*, we designed an approach that would allow interrogation of γTuSC-Spc110p binding in live cells. Chimeric Spc110p[1-220] constructs bearing the GCN4 dimerization or tetramerization domains, along with GFP and the lacI DNA-binding domain (Figure 6A) were artificially targeted to a chromosomally integrated lacO repeat array (Figure 6B). We then measured colocalization between mCherry-labeled Spc97p and GFP-labeled Spc110p chimeras (Figure 6B-C). In asynchronous cells, no colocalization to either Spc110p-dimer or -tetramer were observed. However, in cells arrested at the spindle assembly checkpoint by nocodazole treatment, 46 ± 1.8% of Spc110p-tetramer foci were colocalized with γTuSC, whereas only 6.7 ± 1.1% co-localization was observed with the Spc110p-dimer. Consistent with the results of the *in vitro* FRET assay, introducing the 5D phosphomimetic mutation to the Spc110p-tetramer mildly reduced γTuSC colocalization to 30 ± 7%. While these results suggest that nocodazole arrest is required to establish a state permitting γTuSC recruitment, it also confirms that an Spc110p tetramer is the minimal species required for cooperative assembly of γTuSC oligomers *in vivo*.
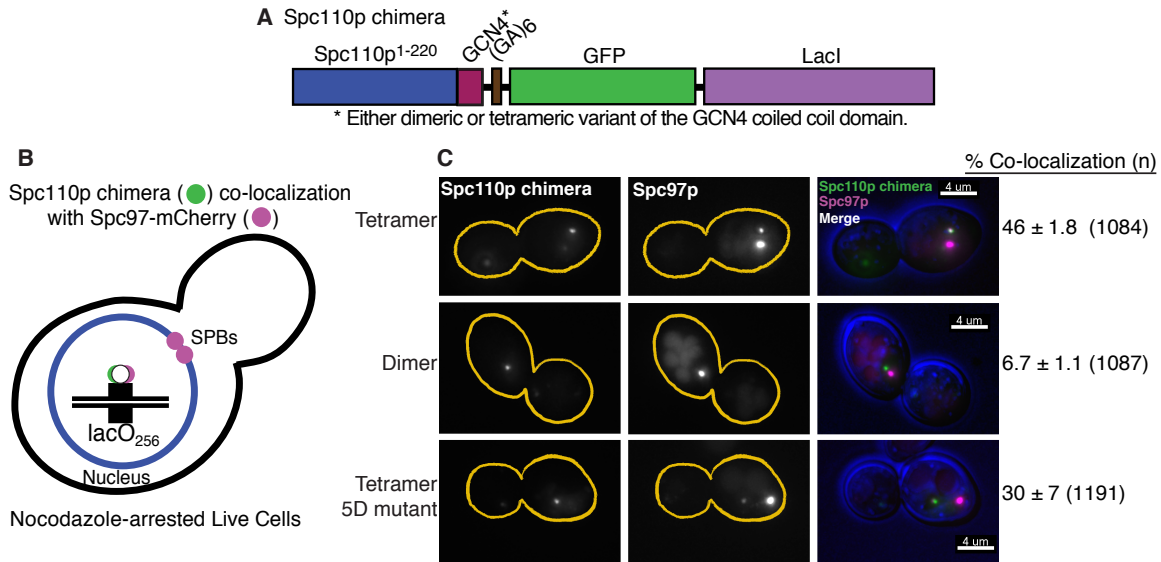
Figure 6. Spc110p oligomerization is required for γTuSC recruitment *in vivo*.
A. Diagram of Spc110p$^{1-220}$-GCN4-GFP-lacI chimeric fusion protein. Width of bars is proportional to molecular weight. **B.** Schematic of *in vivo* recruitment assay. The recruitment of γTuSC by the Spc110p$^{1-220}$ variants was measured by the co-localization of Spc97-mCherry to the GFP puncta formed by the Spc110 chimeras at lacO arrays positioned on the right arm of chromosome 12, 80 Kb from the centromere. Cells were arrested in mitosis with nocodazole. **C.** Representative epifluorescence images and quantification of the co-localization. The top row shows co-localization between Spc97p-mCherry and the tetrameric form of the Spc110p$^{1-220}$ chimera. The middle row shows the predominant lack of co-localization between Spc97-mCherry and dimeric Spc110p chimera. The bottom row shows partial co-localization of the 5D mutant of the tetrameric Spc110p chimera. Note that besides the reduction in the percentage of colocalization, those cells expressing the 5D mutant show a reduced mCherry signal at the lacO array. The colocalization values represent the average of two independent experiments with approximately equal numbers of puncta examined in each experiment.

The conserved centrosomin motif 1 of Spc110p is required for γTuSC binding

Previous studies have characterized the N-terminal 150 residues of Spc110p as the minimal domain required for interaction with γTuSC *in vivo* (Knop and Schiebel 1998; Nguyen et al. 1998). However, the manner in which these residues contribute to γTuRC function is unclear. To more quantitatively interrogate their role, fusion proteins
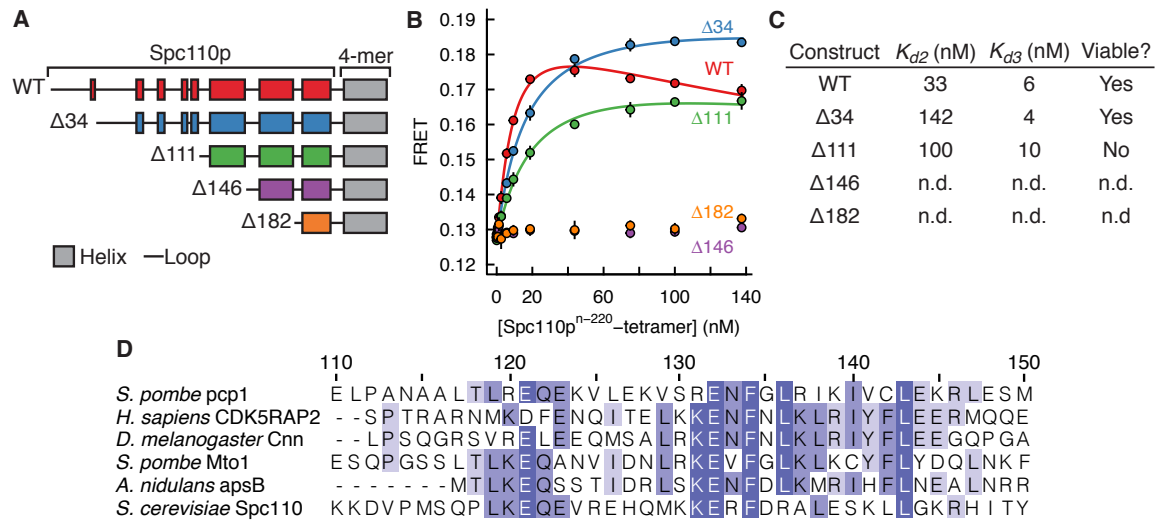
Figure 7. **The centrosome motif 1 domain is required for Spc110p-dependent γTuRC assembly.**
A. Domain diagrams of Spc110p$^{1-220}$-tetramer N-terminal truncation constructs. Predicted alpha helices and loops are shown as colored boxes and lines, respectively. 4-mer indicates the GCN4 tetramerization domain. **B.** γTuRC assembly in the presence of ~20 nM γTuSC and Spc110p$^{1-220}$-tetramer N-terminal truncation mutants. Data were fit using the computational simulation approach described in Figure 5, with K_{d1} and K_{d5} as fixed parameters (Supplemental Figure S5A-I). **C.** Dissociation constants derived from fitting by kinetic simulation. Viability was assessed by red/white plasmid shuffle assay (Supplemental Figure S6). n.d., not determined. **D.** Amino acid sequence conservation of CM1-containing proteins with Spc110p CM1, located within residues 112-146.

of N-terminally truncated Spc110p and the GCN4 tetramerization domain were constructed and

their ability to stimulate γTuSC assembly was measured. The resulting curves were fit as

described (Figure 5). However, K_{d1} and K_{d5} were fixed at the values determined in Figure 5, as

these parameters were poorly constrained (Figure 7A-C and Supplemental Figure S5). Spc110p

lacking the first 34 residues, which includes the Spc110/Pcp1 motif (Lin et al. 2014), supported

robust assembly *in vitro*, with K_{d2} decreased ~4 fold but K_{d3} approximately the same as wild-

type. This Δ34 mutant was viable *in vivo* as assessed by a plasmid shuffle assay (Figure 7B-C and

Supplemental Figure S6B). Surprisingly, Spc110p lacking the first 111 residues supported

assembly *in vitro*, albeit with reduced K_{d2} and K_{d3}. As this truncation eliminates a nuclear

localization sequence (NLS) at residues 24-59 (Adams and Kilmartin 1999) , we assessed

viability with an exogenous NLS fused to the N-terminus. Even with the added NLS, the Δ111

mutant was inviable (Supplemental Figure S6C-D), suggesting the γTuSC interaction affinity is

too low to support γTuRC assembly *in vivo*, or that a domain essential for interacting with other

factors was removed. A further truncation removing the predicted α-helix from residues 112-

147 abolished assembly *in vitro*, indicating the minimal γTuSC interaction domain includes at

least this region. This region contains the CM1 motif, which is found in γTuRC-binding proteins

from diverse organisms (Figure 7D) (Sawin et al. 2004), suggesting that the core γTuSC binding

determinants are broadly conserved.

Discussion

γTuSC assembly in budding yeast requires higher-order oligomerization of Spc110p

We have demonstrated that γTuSC assembly in budding yeast is cooperative and strictly

dependent on Spc110p, as the weak γTuSC self-interaction is dramatically enhanced by

additional interactions with Spc110p (Figure 5). Further, we have shown that higher-order

Spc110p oligomerization is a fundamental requirement for promoting γTuSC assembly both *in*

vitro and, using stable γTuSC recruitment as a proxy, *in vivo*. These observations provide a

mechanistic explanation for how MT nucleation is restricted to the SPB in budding yeast. *In*

vivo, the weak self-interaction of γTuSCs prevents assembly of γTuRCs elsewhere in the cell,

while the high local concentration of Spc110p at the SPB, where ~300 Spc110p molecules are

bound (Erlemann et al. 2012), provides a favorable environment for Spc110p oligomerization,

which in turn stabilizes assembly of γTuRCs. Thus, γTuRC formation represents the first

regulatory step in MT nucleation, after which the processes of ring closure (Kollman et al. 2015), and potentially allosteric conformational activation of γ-tubulin, act in a multi-level regulatory cascade (Figure 8).
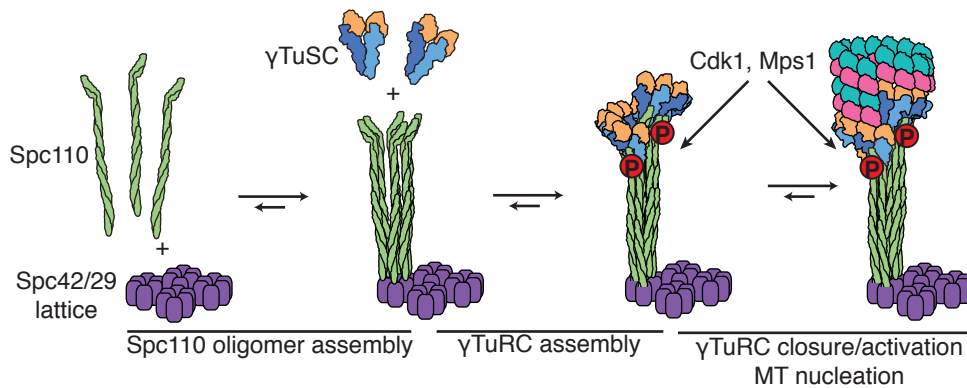
Figure 8. Model for Spc110p-dependent γTuRC assembly. Spc110p coiled-coil dimers assemble into higher-order oligomers, possibly directed by the hexagonal Spc42p lattice (Bullitt et al. 1997). The weak self-interaction of γTuSCs prevents assembly of γTuRCs away from the SPB, while dramatically stronger interactions with Spc110p higher-order oligomers drive γTuRCs to assemble exclusively at SPBs. Spc110p phosphorylation by Cdk1 and Mps1 occur after the onset of S-phase, after γTuRCs have assembled. Once γTuRCs are assembled, they are activated by conformational changes, including ring closure and potentially allosteric activation of γ-tubulin, to allow MT nucleation.

In vivo, Spc110p assembles at the SPB via interactions with Spc29p, calmodulin, and Spc42p, which forms a 2D crystal-like lattice at the central plaque (Bullitt et al. 1997; Elliott et al. 1999; Muller et al. 2005). We propose that Spc110p oligomer assembly is organized by interactions with the Spc42p lattice and is further driven by coiled-coil self-interactions between Spc110p molecules (Figure 8). Spc110p assembles at the SPB dynamically in G1/S phases of mitosis, then becomes stabilized during G2, suggesting that regulation of Spc110p recruitment and/or assembly is coupled to the cell cycle (Yoder et al. 2003).

The potential mismatch between the six-fold symmetric Spc42p lattice and the 6.5-fold symmetry of the γTuRC raises important questions as to how Spc110p assembly at the SPB is coupled to γTuRC assembly. While γTuRCs could contain either 6 γTuSCs, leading to the presentation of 12 γ-tubulins and a gap, or 7 γTuSCs with a half γTuSC overlap (Kollman et al, 2010), cryo-EM tomography of intact SPBs indicates that *in vivo* γTuRCs contain 7 γTuSCs (Kollman et al. 2015). In one possible model, the six-fold symmetry would remain coherent all the way from the central plaque to the γTuRC, with a hexamer of Spc110p dimers the functional unit interacting with γTuSCs to form γTuRCs. An additional factor would then be required to stabilize the seventh γTuSC to complete the γTuRC. Alternatively, the six-fold symmetry of the Spc42p lattice could break down as it propagates through the flexible coiled-coil domain of Spc110p, possibly due to predicted breaks in the coiled-coil register, allowing Spc110p oligomer sizes greater than a hexamer of dimers. This would allow each γTuSC to interact with an Spc110p dimer.

In a higher-resolution cryo-EM map of γTuSC helical filaments we have observed density that appears to connect part of the Spc110p coiled-coil with the γ-tubulin in the ring below (Kollman et al. 2015). This suggests that the seventh γTuSC in a γTuRC is cooperatively stabilized beyond the principal Spc97/98p-Spc110p interactions, thereby favoring formation of heptameric γTuRCs over smaller assemblies.

In vivo, we have shown via an engineered Spc110p targeting system that Spc110p assemblies larger than dimers favor stable association of γTuSC with Spc110p. Given that dimeric Spc110p is able to induce γTuSC assembly, but with substantially weaker K_d (Figure 4D-E), it is not surprising that we observe low-level γTuSC recruitment to dimeric Spc110p *in vivo*.

The role of Spc110p phosphorylation

Overall, our results indicate that Spc110p higher-order oligomerization is the primary driver of γTuRC assembly. While Spc110p phosphorylation does affect γTuRC assembly, our results point to a generally mild effect. (Figure 2C, Figure 3D-E). However, Spc110p is subject to a highly complex mixture of phosphorylation events, with many known phosphorylation sites attributed to at least two kinases: cyclin-Cdk1 and Mps1(Huisman et al. 2007; Keck et al. 2011; Lin et al. 2011). We are unable to account for the effects of all of these modifications in our study, and the relevant combination and sequence of phosphorylation events required for γTuRC assembly and MT nucleation has not yet been systematically explored. However, from our *in vivo* experiments, where both dimeric and tetrameric Spc110p are subject to the same post-translational modifications, it is clear that Spc110p phosphorylation in the absence of higher-order oligomerization is insufficient to support γTuRC assembly under physiological conditions.

Previous observations provide some constraints on which kinases may regulate Spc110p-dependent γTuRC assembly, and at which points in the cell cycle they must act. Mps1p phosphorylates Spc110p after S-phase onset, as *cdc4* mutant cells, which arrest at the G1/S transition, lack the Mps1p-dependent phosphorylated isoform of Spc110p (Friedman et al. 1996). However, nuclear MTs are present at *cdc4* mutant SPBs (Byers and Goetsch 1974). The same is true of *cdc53* mutant cells, which arrest prior to S-phase through the same mechanism as *cdc4* (Mathias et al. 1996). This indicates that Mps1p phosphorylation, represented in the 5D phosphomimetic mutation (Figure 2B), is unlikely to be required for γTuRC assembly, and

instead acts after the formation of γTuRCs to regulate other aspects of γTuRC function. This leaves open the role of cyclin-Cdk1 phosphorylation of Spc110p, though Spc110p shows strong preferential phosphorylation by S-phase Clb5-Cdk1 (Loog and Morgan 2005), suggesting it primarily affects γTuRC function after the onset of S-phase, potentially in tandem with Mps1p.

In our *in vivo* Spc110p targeting assay, we only observed γTuSC association with Spc110p in cells arrested in M phase by treatment with the microtubule depolymerizing agent nocodazole (Figure 6). Activation of the spindle assembly checkpoint under nocodazole arrest may establish a state favoring γTuRC formation, though the precise mechanism responsible requires further investigation.

Implications of Spc110p:γTuSC interactions mediated by the conserved centrosomin motif 1

Using truncation mutants, we have determined that the N-terminal 111 residues of Spc110p are dispensable for γTuSC binding *in vitro*, and that the minimal binding domain contains at least residues 112-147 (Figure 7). *In vivo*, a truncation mutant lacking the first 34 residues was viable (Supplemental Figure S6B). This indicates that the Spc110/Pcp1 motif (Lin et al. 2014) at residues 15-27 is not required for γTuRC assembly and function *in vitro* or *in vivo*. However, the more extensive 111 residue deletion mutant was not viable (Supplemental Figure S6C-D). The binding affinity of this mutant for γTuSC was ~3-fold weaker than the full-length Spc110p (Figure 7B-C), suggesting that the mutant interaction was too weak for normal function *in vivo*. Alternatively, this domain of Spc110p may be required for interaction with additional, essential regulatory factors. Consistent with this, much of the N-terminus lacks clear density in cryo-EM reconstructions of the γTuSC-Spc110p filament (Kollman et al. 2015), suggesting that this domain may not stably associate with γTuSC and instead may serve to

recruit additional factors. As 14 of 31 known phosphorylation sites on Spc110p are located within the 111-residue N-terminal domain (Keck et al. 2011) , with none in residues 112-147, it may be the case that Spc110p contains a core γTuSC binding domain coupled to a regulatory domain that is heavily phosphorylated.

Spc110p residues 112-147 are conserved with γTuRC binding proteins, including human CDK5RAP2 (Choi et al. 2010), *S. pombe* Mto1 and Pcp1 (Flory et al. 2002; Samejima et al. 2008), *A. nidulans* apsB (Zekert et al. 2010), and *D. melanogaster* centrosomin (Terada et al. 2003). This raises the possibility that the interactions between γTuRCs and their binding proteins, as well as localization-dependent assembly, are conserved in metazoans. In *S. pombe*, the Mto1/2 complex has been suggested to play a very similar role to Spc110p in assembling the γTuRC (Lynch et al. 2014). In *D. melanogaster* cells where the γTuRC-specific components Dgrip75, Dgrip128, Dgrip163, and GCP71WD have been depleted by RNAi, localization of γTuSC to centrosomes, but not the spindle, is maintained (Verollet et al. 2006). In this state, which resembles budding yeast in that only γTuSC components are present, soluble γTuRCs are not observed, but MTs are still nucleated from centrosomes. We hypothesize that under these conditions, γTuRC assembly may be facilitated by centrosomin or other centrosome-localized γTuRC binding proteins, similar to the case with Spc110p in budding yeast. The evolution of the γTuRC-specific components may thus have been driven by a need for stable γTuRC self-assembly allowing MT nucleation at sites distinct from centrosome-localized γTuRC assembly factors, relying on attachment factors such as augmin to mediate nucleation within the spindle (Goshima et al. 2008) or AKAP450 and GM-210 at the golgi (Rios et al. 2004; Rivero et al. 2009).

Materials and Methods

Protein Expression Constructs

Baculoviral constructs for γTuSC expression were prepared as described (Choy et al. 2009; Vinh et al. 2002). All *E. coli* expression vectors for Spc110p were prepared by standard PCR and restriction enzyme based cloning methods, except for GCN4 coiled-coil fusion constructs, which were prepared by overlap extension PCR. The Spc110 fragment was prepared by PCR with primers designed to introduce a region of sequence overlap with GCN4-p1 (dimer) or -LI (tetramer). The GCN4-LI and -p1 fragments were constructed from a series of overlapping synthetic oligonucleotides as described (Hoover and Lubkowski 2002). Spc110p$^{1-220}$-5D-dimer and -tetramer constructs were synthesized (Life Technologies) and cloned into either pGEX-6P-2, for expression as a GST fusion, or pET28 with an N-terminal 6His tag and TEV protease cleavage site.

Protein Expression and Purification

All procedures were carried out at 4°C. Buffer HB*n* is 40 mM HEPES, pH 7.5, 1 mM MgCl$_2$, and 1 mM EGTA with *n* mM KCl. For expression in *E. coli*, cultures were grown in terrific broth at 37°C to OD$_{600}$ of approximately 0.4, then cooled to 18 °C prior to induction of expression at OD$_{600}$ 0.6-0.8 with 100 µM isopropyl β-D-thiogalactoside (IPTG) for 16-18 hours. Cells were then harvested by centrifugation and further processed for protein purification, or flash frozen in liquid nitrogen and stored at -80 ˚C. All cells were lysed with an Emulsiflex C3 cooled with a 4 °C water bath (Avestin, Ottawa, ON, Canada).

γTuSC. Sf9 cells were co-infected with baculovirus encoding GST-Spc110[1-220], γ-tubulin[S48C/S153C]

(Kollman et al. 2015), Spc97-YFP, and Spc98-CFP and grown for 48 hours. We opted to use the

γ-tubulin[S48C/S153C] mutation as it allows the use of oxidizing agent as a positive control for γTuRC

assembly, while it behaves like wild-type γTuSC in the presence of reducing agent (5 mM DTT in

our experiments). Cells were harvested by centrifugation and washed with PBS containing 1

mM phenylmethylsulfonyl fluoride before flash freezing in liquid nitrogen. Cells were lysed in

HB100 with 5 mM dithiothreitol (DTT), 0.5% Tween-20, 1X cOmplete protease inhibitor, EDTA-

free, (Roche Diagnostics, Indianapolis, IN), and 0.1% phosphatase inhibitor cocktails 2 and 3

(Sigma-Aldrich, St. Louis, MO) before glutathione affinity purification and anion exchange

chromatography as described (Vinh et al. 2002). γTuSC was buffer exchanged into HB100 with 5

mM DTT and 10% glycerol using a PD10 desalting column (GE Healthcare Life Sciences,

Piscataway, NJ) before flash freezing in liquid nitrogen and storage at -80 °C.

Spc110[1-401]-GST

Spc110[1-401]-GST was expressed via baculovirus in Sf9 insect cells using the Bac-to-Bac system

(Life Technologies). Cells were harvested 48 h post-infection then flash-frozen in liquid nitrogen

prior to purification. Cells were thawed in 40 mM PIPES pH 6.8, 100 mM KCl, 1 mM DTT, 2 mM

EDTA, 2x cOmplete protease inhibitor, EDTA-free (Roche), 0.1% protease inhibitor cocktails 2

and 3 (Sigma-Aldrich), and 0.5% Tween-20, then lysed by Emulsiflex which was precooled with

an ice pack. Lysate was cleared by ultracentrifugation, then applied to glutathione sepharose 4B

and incubated with gentle agitation for 1 h at 4 °C. The resin was then packed into a column

and washed with 5 CV of lysis buffer, then 5 CV of HB100 with protease inhibitors, phosphatase

inhibitors, and DTT. The column was eluted 4x with 1 CV of HB100 with 25 mM reduced

glutathione, incubating with gentle agitation for 10 min prior to each elution. The pooled eluate

was further purified by anion exchange chromatography on a MonoQ 10/100 GL column.

Fractions containing Spc110 were pooled, centrifugally concentrated, then glycerol was added

to 10% final concentration and flash frozen in liquid nitrogen and stored at -80 °C. The

purification procedure must be completed as quickly as possible (typically 10-12 hours from

lysis to freezing) to prevent proteolysis of the Spc110 N-terminal domain.

GST-Spc110$^{1-220}$. Baculovirus-expressed GST-Spc110p$^{1-220}$ was purified along with γTuSC as

described above. Following the anion exchange step, fractions containing GST-Spc110p$^{1-220}$

were further purified by size exclusion chromatography on a Superdex 200 16/60pg (GE

Healthcare Life Sciences). *E. coli*-derived GST-Spc110$^{1-220}$ was expressed in BL21(DE3) Codon

Plus-RIL. Cells were lysed in HB300 lysis buffer (HB300 with 1 mM DTT, 0.5% Tween-20, and 1x

cOmplete protease inhibitor cocktail). Lysate was clarified by ultracentrifugation at 125,000 × g

and the supernatant was bound to Glutathione Sepharose-4B (GE Healthcare Life Sciences) for

3 h with gentle agitation. The resin was packed into a column, washed with 10 CV HB300 lysis

buffer, then 10 CV HB300. Protein was was eluted by suspending the resin in 1 CV elution buffer

(25 mM Tris pH 7.8, 100 mM KCl, 1 mM DTT, 25 mM reduced glutathione) with gentle agitation

for 10 min. The eluate was removed, and then the elution procedure was repeated 3 additional

times. The pooled eluate was further purified by anion exchange chromatography followed by

size exclusion chromatography as shown in Table 1.

Table 1. Spc110p purification procedures.

Construct	Dialysis buffer	Ion exchange	Size exclusion
Baculovirus-expressed GST-Spc110p$^{1-220}$	Not applicable	MonoQ 10/300 GL	Superdex 200 16/60pg
E. coli-expressed GST-Spc110p$^{1-220}$	25 mM Tris, pH 7.8, 250 mM KCl, 1 mM DTT	MonoQ 10/300 GL	Superdex 200 16/60pg
Untagged Spc110p$^{1-220}$	25 mM potassium phosphate, pH 6, 250 mM KCl, 1 mM DTT	MonoS 10/300 GL	Superdex 75 16/60pg
Spc110p$^{1-220}$-dimer	HB250, 1 mM DTT	HiTrap SP	Superdex 200 16/60pg
Spc110p$^{1-220}$-tetramer	HB250, 1 mM DTT	HiTrap SP	Superdex 200 16/60pg
Spc110p$^{35-220}$-tetramer	HB250, 1 mM DTT	HiTrap SP	Superdex 200 16/60pg
Spc110p$^{112-220}$-tetramer	HB250, 1 mM DTT	HiTrap SP	Superdex 75 16/60pg
Spc110p$^{183-220}$-tetramer	50 mM potassium phosphate, pH 8.0, 250 mM KCl, 1 mM DTT	MonoQ 10/300 GL	Superdex 75 16/60pg

Spc110p$^{1-220}$-dimer, -tetramer, and truncation mutants. Proteins were expressed in *E. coli*

BL21(DE3) CodonPlus-RIL. Cells were lysed in NiNTA lysis buffer (50 mM potassium phosphate,

pH 8.0, 500 mM KCl, 10 mM imidazole, 1 mM DTT, cOmplete protease inhibitor cocktail, and

0.5% Tween-20). Lysates were clarified by ultracentrifugation at 125,000 × g and the

supernatants were applied to NiNTA Superflow resin with gentle agitation for 1 hr. The resin

was packed into a column then washed with 10 CV lysis buffer, followed by 10 CV wash buffer

(50 mM potassium phosphate, pH 8.0, 250 mM KCl, 25 mM imidazole, 1 mM DTT, and

cOmplete protease inhibitor cocktail), then eluted with 4 × 1 CV elution buffer (wash buffer

with 250 mM imidazole). Eluate was pooled, TEV protease was added to remove 6His tags, and dialyzed overnight into the buffer indicated in Table 1. Following dialysis, protein was applied to the indicated ion exchange column (Table 1) and eluted with a linear gradient of 0.25-1 M KCl. Fractions containing Spc110p were pooled, concentrated to ~2 mL, and applied to the indicated size exclusion column and eluted with HB250 with 10% glycerol and 1 mM DTT (Table 1). Fractions containing Spc110p were pooled, concentrated, flash frozen in liquid nitrogen, and stored at -80 °C.

Spc110p$^{1-220}$. Untagged Spc110p$^{1-220}$ was expressed as a 6xHis-Maltose Binding Protein-3C protease cleavage site fusion from the vector H-MBP-3C (Alexandrov et al. 2001) in *E. coli* BL21(DE3) CodonPlus-RIL. The purification proceeded as above for Spc110p$^{1-220}$-dimer, except the His-MBP tag was cleaved with 3C protease. Additional chromatography steps are shown in Table 1.

Spc110p$^{147-220}$-tetramer. As we could not obtain Spc110p$^{147-220}$-tetramer in soluble form, we purified it from inclusion bodies under denaturing conditions. Protein was expressed in *E. coli* BL21(DE3) CodonPlus-RIL. After lysis using an Emulsiflex C3 in NiNTA lysis buffer, inclusion bodies were pelleted by ultracentrifugation at 125,000 × g then dissolved in pH 8.0 solubilization buffer (8 M urea, 100 mM potassium phosphate, 10 mM Tris). Solubilized inclusion bodies were incubated with NiNTA superflow resin with gentle agitation for 1 hr, washed with 10 CV pH 6.3 solubilization buffer, and eluted with 4 CV pH 5.9 solubilization buffer, then 4 CV pH 4.5 solubilization buffer. Protein was refolded by dropwise dilution into a

10× volume of refolding buffer (HB250, 10% glycerol, 400 mM L-arginine, 1 mM DTT). Refolded

protein was concentrated by capture on NiNTA Superflow resin, which was then washed with

10 CV wash buffer, and eluted with 4 × 1 CV elution buffer. Eluate was pooled, TEV protease

was added, and dialyzed overnight into HB250, 10% glycerol, 1 mM DTT. Following dialysis,

protein was concentrated to ~2 mL, applied to a Superdex 75 16/60 pg size exclusion column,

and eluted with HB250, 10% glycerol, 1 mM DTT. Fractions containing Spc110p$^{147-220}$-tetramer

were pooled, concentrated, flash frozen in liquid nitrogen, and stored at -80 °C.

Quantifying efficiency of γTuSC purification

Our purification method selects for γTuSC that is competent to interact with Spc110p. To

quantify the fraction of γTuSC within baculovirus-infected insect cells that is capable of

interacting with Spc110p, we performed a series of γTuSC purifications with varying amounts of

glutathione-sepharose resin. The high-speed supernatant and flowthrough fractions were

analyzed by western blotting for each condition. γTuSC$^{CFP/YFP}$ and GST-Spc110p$^{1-220}$ were

detected by α-GFP (1:4000; A-11122, Life Technologies) and α-GST (1:8000; G7781, Sigma-

Aldrich), respectively, imaged by fluorophore-conjugated goat α-rabbit secondary antibody

(1:2000; 926-68021, Licor Biosciences). Blots were scanned using a Licor Odyssey scanner. Band

intensities were quantified using Fiji (Schindelin et al. 2012).

FRET assay

The TB150 buffer (50 mM Tris pH 7.0, 150 mM KCl) used previously (Lin et al. 2014) led to high

levels of Spc110p-independent FRET, so we used a HEPES buffer (40 mM HEPES pH 7.5, 1 mM

MgCl$_2$, 1 mM EGTA, 5 mM DTT) in which γTuSC was better behaved (Supplemental Figure S3C).

Proteins were exchanged into assay buffer (HB*n* with 10% glycerol, 5 mM DTT, and 0.1%

phosphatase inhibitor cocktails 2 and 3) using Zeba desalting spin columns (Pierce). For assays

with Spc110-dimer and -tetramer, γTuSC was in assay buffer with 100 mM KCl and Spc110 was

in assay buffer with 250 mM KCl. Spc110 and γTuSC were combined to give a final KCl

concentration of 150 mM. For other assays, proteins were prepared in assay buffer with 150

mM KCl. Reactions were assembled in black clear-bottom 384-well plates (Corning 3655) in

assay buffer with 0.1 mg/mL BSA using a Mantis liquid dispenser (Formulatrix, Waltham, MA)

and mixed by pipetting. Reactions were sealed and incubated for 15 min at 25 °C. Fluorescence

spectra were recorded with a Spectramax M5 plate reader (Molecular Devices, Sunnyvale, CA)

with excitation at 420 nm and emission recorded from 460-600 nm in 5 nm steps through a 455

nm long-pass filter. Photomultiplier tube sensitivity was set to automatic and 100 readings

were averaged per well.

FRET data analysis

Background spectra from samples containing no fluorophore were subtracted from

experimental spectra, and then spectra were decomposed into CFP and YFP components by

least squares fitting as a linear combination of CFP and YFP basis spectra (Zimmermann 2005)

using scripts written in R (Supplemental Figure S1A-C) (R Core Team 2013). Correction for direct

excitation of the YFP acceptor (i.e. YFP signal not attributable to FRET) was determined by

measuring γTuSC[YFP] emission spectra with excitation at 420 nm in the absence of CFP

(Supplemental Figure S1E). Spectra were recorded at varying γTuSC[YFP] concentrations, then fit

as a linear combination of YFP and buffer blank basis spectra (Supplemental Figure S1D-E). The

YFP fluorescence intensity due to direct excitation was plotted as a function of γTuSC^{YFP}

concentration and fit by linear least squares. This yielded the correction term YFP$_{corr}$ =

0.40[γTuSC]-0.75 (Supplemental Figure S1F). FRET was calculated as:

$$\frac{YFP - YFP_{corr}}{CFP + YFP - YFP_{corr}}$$

Binding curve fitting was performed by non-linear least squares in R using either a

simple binding model:

$$FRET = (FRET_{max} - FRET_{min}) \left(\frac{[Spc110p]}{[Spc110p] + K_d} \right) + FRET_{min} ,$$

or, when γTuSC concentration was very close to the calculated K_d, a tight binding model (Pollard

2010) :

$$FRET = (FRET_{max} - FRET_{min}) \left(\frac{[\gamma TuSC] + [Spc110] + K_d - \sqrt{([\gamma TuSC] + [Spc110] + K_d)^2 - 4[\gamma TuSC][Spc110]}}{2[\gamma TuSC]} \right) + FRET_{min}$$

where the free parameters FRET$_{min}$ and FRET$_{max}$ are the minimal and maximal FRET, K_d is the

dissociation constant.

All FRET data is the average of three technical replicates with error bars indicating

standard deviation.

Computational simulation of γTuRC assembly pathway

With the goal of obtaining K_d values, the γTuRC assembly process up to a γTuSC tetramer

(Figure 5B) in the presence of Spc110p$^{1-220}$-tetramer was modeled as a system of ordinary

differential equations (ODEs) with a fixed k_{on} of 10^5 M^{-1}s^{-1} and variable k_{off}. As we sought to fit

equilibrium FRET data with the ODE model, the absolute magnitudes of k_{on} and k_{off} are not physically meaningful. Only their ratio, $K_d = k_{off} / k_{on}$, is taken into account and is determined by numerical optimization of k_{off}. Subscripts to γTuSC and Spc110p represent their oligomeric state:

$$\frac{d[\gamma\text{TuSC}]}{dt} = \begin{aligned}[t] &-2k_{on}[\gamma\text{TuSC}]^2 + 2k_{off1}[\gamma\text{TuSC}_2] \\ &- k_{on}[\gamma\text{TuSC}][\text{Spc110}_4] + k_{off2}[\gamma\text{TuSC} \cdot \text{Spc110}_4] \\ &- k_{on}[\gamma\text{TuSC} \cdot \text{Spc110}_4][\gamma\text{TuSC}] + k_{off3}[\gamma\text{TuSC}_2 \cdot \text{Spc110}_4] \end{aligned}$$

$$\frac{d[\text{Spc110}_4]}{dt} = \begin{aligned}[t] &-k_{on}[\gamma\text{TuSC}][\text{Spc110}_4] + k_{off2}[\gamma\text{TuSC} \cdot \text{Spc110}_4] \\ &- k_{on}[\gamma\text{TuSC}_2][\text{Spc110}_4] + k_{off4}[\gamma\text{TuSC}_2 \cdot \text{Spc110}_4] \end{aligned}$$

$$\frac{d[\gamma\text{TuSC}_2]}{dt} = \begin{aligned}[t] &k_{on}[\gamma\text{TuSC}]^2 - k_{off1}[\gamma\text{TuSC}_2] \\ &- k_{on}[\gamma\text{TuSC}_2][\text{Spc110}_4] + k_{off4}[\gamma\text{TuSC}_2 \cdot \text{Spc110}_4] \end{aligned}$$

$$\frac{d[\gamma\text{TuSC} \cdot \text{Spc110}_4]}{dt} = \begin{aligned}[t] &k_{on}[\gamma\text{TuSC}][\text{Spc110}_4] + k_{off2}[\gamma\text{TuSC} \cdot \text{Spc110}_4] \\ &- k_{on}[\gamma\text{TuSC} \cdot \text{Spc110}_4][\gamma\text{TuSC}] + k_{off3}[\gamma\text{TuSC}_2 \cdot \text{Spc110}_4] \end{aligned}$$

$$\frac{d[\gamma\text{TuSC}_2 \cdot \text{Spc110}_4]}{dt} = \begin{aligned}[t] &k_{on}[\gamma\text{TuSC} \cdot \text{Spc110}_4][\gamma\text{TuSC}] - k_{off3}[\gamma\text{TuSC}_2 \cdot \text{Spc110}_4] \\ &+ k_{on}[\gamma\text{TuSC}_2][\text{Spc110}_4] - k_{off4}[\gamma\text{TuSC}_2 \cdot \text{Spc110}_4] \\ &- 2k_{on}[\gamma\text{TuSC}_2 \cdot \text{Spc110}_4]^2 + 2k_{off5}[\gamma\text{TuSC}_4 \cdot \text{Spc110}_8] \end{aligned}$$

$$\frac{d[\gamma\text{TuSC}_4 \cdot \text{Spc110}_8]}{dt} = k_{on}[\gamma\text{TuSC}_2 \cdot \text{Spc110}_4]^2 - k_{off5}[\gamma\text{TuSC}_4 \cdot \text{Spc110}_8]$$

The system of ODEs was solved numerically using the deSolve package in R (Soetaert et al. 2010) to obtain equilibrium concentrations of each species. Simulated FRET values were calculated as follows:

$$\text{FRET} = \beta \left(\frac{[\gamma\text{TuSC}_2]_{eq}}{\frac{1}{2}[\gamma\text{TuSC}]_i} + \frac{[\gamma\text{TuSC}_2 \cdot \text{Spc110}_2]_{eq}}{\frac{1}{2}[\gamma\text{TuSC}]_i} + 3\frac{[\gamma\text{TuSC}_4 \cdot \text{Spc110}_2]_{eq}}{\frac{1}{4}[\gamma\text{TuSC}]_i} \right) + \alpha ,$$

where *eq* denotes an equilibrium concentration, *i* denotes initial concentration, β relates

concentrations of FRET-producing species to FRET units, and α is the baseline FRET from γTuSC

in the absence of Spc110p.

To fit the model to experimental FRET data, an objective function giving the sum of

squared residuals between simulated and experimental FRET data was minimized using the L-

BFGS-B algorithm implemented in the R function optim. A lower bound of zero was used for all

parameters. Free parameters include k_{off1}, k_{off2}, k_{off3}, k_{off5}, α, and β. k_{off4} was defined in terms of

k_{on}, k_{off1}, k_{off2}, and k_{off3} based on the thermodynamic cycle shown in Figure 5b as follows:

$$k_{off1} \cdot k_{off4} \cdot k_{on} \cdot k_{on} = k_{off2} \cdot k_{off3} \cdot k_{on} \cdot k_{on}$$
$$k_{off4} = \frac{k_{off2} \cdot k_{off3}}{k_{off1}}$$

Using the nominal γTuSC concentrations in the optimization procedure did not yield satisfactory

fits. We reasoned that the model is extremely sensitive to the initial γTuSC concentration

because of the appearance of terms with second-power dependence on both γTuSC and

$\gamma TuSC_2 \cdot Spc110_4$ concentration in the system of ODEs. Thus, the initial lowest γTuSC

concentration was included as an additional free parameter in the model. The higher γTuSC

concentrations were then scaled according to the mean total fluorescence (i.e., summed across

all wavelengths of a spectrum) at each concentration (Supplemental Figure S4A). The

optimization changed the initial lowest γTuSC concentration from a nominal 10 nM to 16 nM.

After deriving an initial set of parameter estimates by manual parameter adjustment followed

by one round of computational optimization, the initial estimates were randomized 100 times

within bounds 3-fold less or greater than the initial estimate (Supplemental Figure S4B-I). The

parameters from the best fit achieved from this procedure are quoted in Figure 5B. Additional

rounds of parameter randomization did not improve the fit.

Size exclusion chromatography-multi-angle light scattering (SEC-MALS) and analytical size

exclusion

MALS analysis was performed with WTC-050S5 (Wyatt Technology, Santa Barbara, CA) or KW-

804 (Shodex, New York, NY) size exclusion columns on an Ettan liquid chromatography system

(GE Healthcare Life Science) with inline DAWN HELEOS MALS and Optilab rEX differential

refractive index detectors (Wyatt Technology). Data was analyzed using ASTRA VI software

(Wyatt Technology). Size exclusion chromatography was performed with HB150 or HB250 with

5 mM DTT. Analytical size exclusion was performed on the Ettan liquid chromatography system

with Superdex 200 PC 3.2/30 column (GE Healthcare Life Science) with a flow rate of 40 µL/min.

Blue native polyacrylamide gel electrophoresis

Samples in HB150 with 5 mM DTT and 10% glycerol were separated on NativePAGE Novex 3-

12% bis-tris gels in NativePAGE running buffer along with NativeMark size standards (Life

Technologies). The cathode buffer contained 0.02% Coomassie Brilliant Blue G-250.

Electrophoresis was performed at 4 ˚C at 150 V for 1 hour, then 250 V until the dye front

reached the bottom of the gel. Gels were then fixed by microwaving in 40% methanol and 10%

acetic acid then incubating for 15 min, then destained by microwaving in 8% acetic acid and

incubating until bands appeared on a clear background. Gels were then washed in water.

Negative stain electron microscopy

γTuSC or γTuSC-Spc110p complexes at 75 nM in assay buffer were applied to glow discharged carbon-coated 400-mesh copper grids as 2 uL drops and incubated for 30 s. Excess sample was blotted away, the grid was washed quickly with 2 drops of water, then stained with 0.75% uranyl formate for 30 s. After removing excess stain, grids were air dried prior to imaging with a Tecnai 12 (FEI Company, Hillsboro, OR) operating at 120 kV. Images were acquired with ~1.5 μm defocus on a 4k × 4k CCD camera (Gatan Inc., Pleasonton, CA) with a pixel size of 2.21 Å. Particles were picked in 128 ×128 (γTuSC) or 180 × 180 (γTuSC-Spc110p complexes) pixel boxes using e2boxer.py, part of EMAN2 (Tang et al. 2007). Reference-free 2D class averages were generated using e2refine2d.py. Particles belonging to indistinct class averages were discarded using e2evalparticles.py. The final class averages were generated after several cycles of class averaging followed by discarding bad particles.

Microtubule nucleation assay

S. cerevisiae tubulin was over-expressed and purified as described (Johnson et al. 2011). γTuSC and Spc110p[1-220]-dimer or -tetramer, prepared in the same manner as for the FRET assay, were combined at 10× final concentration in a 1:4 molar ratio (calculated on a dimer basis) and incubated at room temperature for 15 min. γTuSC:Spc110p[1-220]-dimer or -tetramer complexes and *S. cerevisiae* tubulin were diluted at the appropriate concentrations into microtubule assembly buffer (80mM K-PIPES pH 6.9, 125mM KCl, 20% glycerol, 1mM EGTA, 1mM MgCl2, 1mM GTP) on ice. Reactions were incubated at 30 °C for 20 min, fixed 3 min in 10 volumes of 1% glutaraldehyde in BRB80 (80mM K-PIPES pH 6.9, 1mM EGTA, 1mM MgCl2), and then diluted

10 times into BRB80 (final volume 1.5ml). 1ml of the resulting fixed reactions was layered onto

20% glycerol/BRB80 cushions and centrifuged for 45 min, 24,000 x g, onto 18 mm round

coverslips. Microtubules were visualized on the coverslips by immunofluorescence with FITC-

mouse-anti-α-tubulin (Sigma F2168) and 5-10 fields of microtubules were counted for each

experiment.

In vivo γTuSC recruitment assay

The *in vivo* recruitment assay (Figure 6) used wide-field fluorescence microscopy to monitor the

binding of γTuSC, tagged with Spc97p-mCherry, to Spc110p$^{1-220}$ that was C-terminally tagged

with GFP and lacI. Spc110p was visualized as GFP puncta localized to a lacO array positioned on

chromosome XII. Co-localization of GFP and mCherry fluorescence was quantified using Imaris

software (Bitplane, South Windsor, CT). Co-localization was measured as the total number of

GFP puncta in the nucleus that were within 0.5 µm of mCherry puncta. Any GFP puncta within

0.5 µm of the SPB were excluded.

The Spc110p$^{1-220}$-dimer and -tetramer regions were derived from the same plasmids

used above for expression in *E. coli*. The GFP-lacI sequence was derived from pGVH60 (Bystricky

et al. 2005). This yeast integrating plasmid also provided the backbone for integration of the

SPC110 chimera at the *ADE2* locus. Expression in *S. cerevisiae* used a β-estradiol inducible

expression system (McIsaac et al. 2013). The Z$_4$EV promoter element was derived from pMN10.

The gene encoding the Z$_4$EV artificial transcription factor (from DBY12395) was PCR amplified

and integrated at the *CAN1* locus into strain KGY315 (Greenland et al. 2010). An array of 256

copies of the lacO sequence was integrated on the right arm of chromosome XII, within the

intergenic region between *TRX1* and *PDC1* using pGM22. pGM22 contains the KpnI-SacI

fragment from pLI831(Muller 1996) cloned into pSB11(gift from Sue Biggins). Spc97p was

tagged with mCherry at the C-terminus using pBS34 and standard protocols

(http://depts.washington.edu/yeastrc/pages/pBS34.html).

Strains used in this study were GMY128 (*ade2-1oc/ade2-1*::Z$_4$EVpr-SPC110$^{1-220}$-GCN4-

p1-GA-GFP-LacI-ADE2; *ADE3/ADE3*; *can1-100/can1-100*::NatMX-ACT1pr-Z4EV; *his3-

11,15/his3-11,15*; *leu2-3,112/leu2-3,112*; *trp1-1/trp1-1*; *ura3-1/ura3-1*; ChrXII-R/ChrXII-

R::lacO-TRP1; *SPC97*-mCherry::HphMX/*SPC97*-mCherry::hphMX), GMY129 (same as GMY128

except *ade2-1oc/ade2-1*::Z$_4$EVpr-SPC110$^{1-220}$-GCN4-LI-GA-GFP-LacI-ADE2) and KYY90 (same as

GMY128 except *ade2-1oc/ade2-1*::Z$_4$EVpr-SPC110$^{1-220}$5D-GCN4-LI-GA-GFP-LacI-ADE2).

Cells grown at 30°C to mid-log phase in YPD were incubated for 30 min with 100 nM β-

estradiol, then nocodazole (15 µg/ml) was added and incubation continued for 1 hr. Cells were

washed, resuspended in YPD with 15 µg/ml nocodazole without estradiol and incubated for

another 1.5 hours. Cells were washed to remove YPD, resuspended in SD media and mounted

on a 1% SeaKem LE agarose in SD pad. Fluorescence microscopy images were taken using a

DeltaVision system (Applied Precision) with an IX70 inverted microscope (Olympus), a Uplan

Apo 100× oil objective (1.35 NA), and a CoolSnap HQ digital camera (Photometrics) as

previously described(Muller et al. 2005).

Red/white plasmid shuffle assay

To evaluate whether N-terminal truncations of Spc110 were functional we employed a

red/white plasmid shuffle system as described previously (Tien et al. 2013). Strain HSY2-12C

(*MATα ade2-1oc ade3Δ can1-100 his3-11,15 leu2-3,112 lys2Δ::HIS3 spc110Δ::TRP1 trp1-1 ura3-1*) harboring 2-micron plasmid pHS26 (*ADE3 LYS2 SPC110*) (Sundberg et al. 1996) was transformed with mutant derivatives of plasmid pHS29 (*CEN6 ARSH4 URA3 SPC110*) (Sundberg et al. 1996) . These plasmids, pKY20-21, carried N-terminal deletions of Spc110p that removed up to amino acid residue V34 and K111, respectively. They were constructed using the QuikChange Multi Site-Directed Mutagenesis Kit (Agilent) with pHS29 as a DNA template and primers that spanned the region to be deleted. pKY176 bearing Spc110Δ111 with an added N-terminal nuclear localization sequence was constructed by QuikChange using an oligonucleotide encoding the nuclear localization sequence from pBS41 (Genbank accession KF177452). The plasmids were transformed into HSY2-12C and selected for growth on SD-ura low ade plates. Deletions that rendered SPC110 nonfunctional were dependent on pHS26 for viability and grew as solid red colonies. If the pKY plasmids encoded a functional SPC110 then cells would lose pHS26 and the colonies would sector white.

References

Adams IR and Kilmartin JV. 1999. Localization of core spindle pole body (SPB) components during SPB duplication in saccharomyces cerevisiae. *J Cell Biol* **145**:809-23. doi:10.1083/jcb.145.4.809.

Alexandrov A, Dutta K, Pascal SM. 2001. MBP fusion protein with a viral protease cleavage site: One-step cleavage/purification of insoluble proteins. *BioTechniques* **30**:1194. .

Bullitt E, Rout MP, Kilmartin JV, Akey CW. 1997. The yeast spindle pole body is assembled around a central crystal of Spc42p. *Cell* **89**:1077-86. doi:10.1016/S0092-8674(00)80295-0.

Byers B and Goetsch L. 1974. Duplication of spindle plaques and integration of the yeast cell cycle. *Cold Spring Harb Symp Quant Biol* **38**:123-31. doi:10.1101/SQB.1974.038.01.016.

Bystricky K, Laroche T, van Houwe G, Blaszczyk M, Gasser SM. 2005. Chromosome looping in yeast: Telomere pairing and coordinated movement reflect anchoring efficiency and territorial organization. *J Cell Biol* **168**:375-87. doi:10.1083/jcb.200409091.

Choi Y-, Liu P, Sze SK, Dai C, Qi RZ. 2010. CDK5RAP2 stimulates microtubule nucleation by the γ-tubulin ring complex. *J Cell Biol* **191**:1089-95. doi:10.1083/jcb.201007030.

Choy RM, Kollman JM, Zelter A, Davis TN, Agard DA. 2009. Localization and orientation of the gamma-tubulin small complex components using protein tags as labels for single particle EM. *J Struct Biol* **168**:571-4. doi:10.1016/j.jsb.2009.08.012.

Elliott S, Knop M, Schlenstedt G, Schiebel E. 1999. Spc29p is a component of the Spc110p subcomplex and is essential for spindle pole body duplication. *Proc Natl Acad Sci U S A* **96**:6205-10. doi:10.1073/pnas.96.11.6205.

Erlemann S, Neuner A, Gombos L, Gibeaux R, Antony C, Schiebel E. 2012. An extended gamma-tubulin ring functions as a stable platform in microtubule nucleation. *J Cell Biol* **197**:59-74. doi:10.1083/jcb.201111123.

Flory MR, Morphew M, Joseph JD, Means AR, Davis TN. 2002. Pcp1p, an Spc110p-related calmodulin target at the centrosome of the fission yeast schizosaccharomyces pombe. *Cell Growth Differ* **13**:47-58. .

Friedman DB, Sundberg HA, Huang EY, Davis TN. 1996. The 110-kD spindle pole body component of saccharomyces cerevisiae is a phosphoprotein that is modified in a cell cycle-dependent manner. *J Cell Biol* **132**:903-14. doi:10.1083/jcb.132.5.903.

Friedman DB, Kern JW, Huneycutt BJ, Vinh DB, Crawford DK, Steiner E, Scheiltz D, Yates J,3rd, Resing KA, Ahn NG, et al. 2001. Yeast Mps1p phosphorylates the spindle pole component Spc110p in the N-terminal domain. *J Biol Chem* **276**:17958-67. doi:10.1074/jbc.M010461200.

Ghaemmaghami S, Huh WK, Bower K, Howson RW, Belle A, Dephoure N, O'Shea EK, Weissman JS. 2003. Global analysis of protein expression in yeast. *Nature* **425**:737-41. doi:10.1038/nature02046.

Goshima G, Mayer M, Zhang N, Stuurman N, Vale RD. 2008. Augmin: A protein complex required for centrosome-independent microtubule generation within the spindle. *J Cell Biol* **181**:421-9. doi:10.1083/jcb.200711053.

Greenland KB, Ding H, Costanzo M, Boone C, Davis TN. 2010. Identification of saccharomyces cerevisiae spindle pole body remodeling factors. *PLoS One* **5**:e15426. doi:10.1371/journal.pone.0015426.

Guillet V, Knibiehler M, Gregory-Pauron L, Remy M, Chemin C, Raynaud-Messina B, Bon C, Kollman JM, Agard DA, Merdes A, et al. 2011. Crystal structure of γ-tubulin complex protein GCP4 provides insight into microtubule nucleation. *Nature Structural & Molecular Biology* **18**:915-9. doi:10.1038/nsmb.2083.

Harbury PB, Zhang T, Kim PS, Alber T. 1993. A switch between two-, three-, and four-stranded coiled coils in GCN4 leucine zipper mutants. *Science* **262**:1401-7. doi:10.1126/science.8248779.

Hoover DM and Lubkowski J. 2002. DNAWorks: An automated method for designing oligonucleotides for PCR-based gene synthesis. *Nucleic Acids Res* **30**:e43. doi:10.1093/nar/30.10.e43.

Huisman SM, Smeets MFMA, Segal M. 2007. Phosphorylation of Spc110p by Cdc28p-Clb5p kinase contributes to correct spindle morphogenesis in *S. cerevisiae*. *J Cell Sci* **120**:435-46. doi:10.1242/jcs.03342.

Johnson V, Ayaz P, Huddleston P, Rice LM. 2011. Design, overexpression, and purification of polymerization-blocked yeast alphabeta-tubulin mutants. *Biochemistry* **50**:8636-44. doi:10.1021/bi2005174.

Keck JM, Jones MH, Wong CCL, Binkley J, Chen D, Jaspersen SL, Holinger EP, Xu T, Niepel M, Rout MP, et al. 2011. A cell cycle phosphoproteome of the yeast centrosome. *Science* **332**:1557-61. doi:10.1126/science.1205193.

Kilmartin JV, Dyos SL, Kershaw D, Finch JT. 1993. A Space Protein in the *Saccharomyces cerevisiae* Spindle Pole Body Whose Transcript Is Cell Cycle-Regulated. *J Cell Biol* **123**: 1175-1184. doi: 10.1083/jcb.123.5.1175

Kilmartin JV, Goh P-Y. 1996. Spc110p: assembly properties and role in the connection of nuclear microtubules to the yeast spindle pole body. *EMBO J* **15**: 4592-4602.

Knop M and Schiebel E. 1998. Receptors determine the cellular localization of a gamma-tubulin complex and thereby the site of microtubule formation. *EMBO J* **17**:3952-67. doi:10.1093/emboj/17.14.3952.

Knop M and Schiebel E. 1997. Spc98p and Spc97p of the yeast gamma -tubulin complex mediate binding to the spindle pole body via their interaction with Spc110p. *EMBO J* **16**:6985-95. doi:10.1093/emboj/16.23.6985.

Kollman JM, Merdes A, Mourey L, Agard DA. 2011. Microtubule nucleation by gamma-tubulin complexes. *Nat Rev Mol Cell Biol* **12**:709-21. doi:10.1038/nrm3209.

Kollman JM, Zelter A, Muller EG, Fox B, Rice LM, Davis TN, Agard DA. 2008. The structure of the gamma-tubulin small complex: Implications of its architecture and flexibility for microtubule nucleation. *Mol Biol Cell* **19**:207-15. doi:10.1091/mbc.E07-09-0879.

Kollman JM, Polka JK, Zelter A, Davis TN, Agard DA. 2010. Microtubule nucleating γ-TuSC assembles structures with 13-fold microtubule-like symmetry. *Nature* **466**:879-82. doi:10.1038/nature09207.

Kollman JM, Greenberg CH, Li S, Moritz M, Zelter A, Fong KK, Fernandez J, Sali A, Kilmartin J, Davis TN, et al. 2015. Ring closure activates yeast γTuRC for species-specific microtubule nucleation. *Nat Struct Mol Biol* **22**:132-7. doi:10.1038/nsmb.2953.

Lin TC, Neuner A, Schlosser YT, Scharf AN, Weber L, Schiebel E. 2014. Cell-cycle dependent phosphorylation of yeast pericentrin regulates gamma-TuSC-mediated microtubule nucleation. *Elife* **3**:e02208. doi:10.7554/eLife.02208.

Lin TC, Gombos L, Neuner A, Sebastian D, Olsen JV, Hrle A, Benda C, Schiebel E. 2011. Phosphorylation of the yeast gamma-tubulin Tub4 regulates microtubule function. *PLoS One* **6**:e19700. doi:10.1371/journal.pone.0019700.

Loog M and Morgan DO. 2005. Cyclin specificity in the phosphorylation of cyclin-dependent kinase substrates. *Nature* **434**:104-8. doi:nature03329.

Lynch EM, Groocock LM, Borek WE, Sawin KE. 2014. Activation of the gamma-tubulin complex by the Mto1/2 complex. *Curr Biol* **24**:896-903. doi:10.1016/j.cub.2014.03.006.

Mathias N, Johnson SL, Winey M, Adams AE, Goetsch L, Pringle JR, Byers B, Goebl MG. 1996. Cdc53p acts in concert with Cdc4p and Cdc34p to control the G1-to-S-phase transition and identifies a conserved family of proteins. *Mol Cell Biol* **16**:6634-43. .

McIsaac RS, Oakes BL, Wang X, Dummit KA, Botstein D, Noyes MB. 2013. Synthetic gene expression perturbation systems with rapid, tunable, single-gene specificity in yeast. *Nucleic Acids Res* **41**:e57. doi:10.1093/nar/gks1313.

Moudjou M, Bordes N, Paintrand M, Bornens M. 1996. Γ-tubulin in mammalian cells: The centrosomal and the cytosolic forms. *J Cell Sci* **109 (Pt 4)**:875-87. .

Muller EG. 1996. A glutathione reductase mutant of yeast accumulates high levels of oxidized glutathione and requires thioredoxin for growth. *Mol Biol Cell* **7**:1805-13. doi:10.1091/mbc.7.11.1805.

Muller EG, Snydsman BE, Novik I, Hailey DW, Gestaut DR, Niemann CA, O'Toole ET, Giddings TH,Jr, Sundin BA, Davis TN. 2005. The organization of the core proteins of the yeast spindle pole body. *Mol Biol Cell* **16**:3341-52. doi:10.1091/mbc.E05-03-0214.

Nguyen T, Vinh DB, Crawford DK, Davis TN. 1998. A genetic analysis of interactions with Spc110p reveals distinct functions of Spc97p and Spc98p, components of the yeast gamma-tubulin complex. *Mol Biol Cell* **9**:2201-16. doi:10.1091/mbc.9.8.2201.

Pollard TD. 2010. A guide to simple and informative binding assays. *Mol Biol Cell* **21**:4061-7. doi:10.1091/mbc.E10-08-0683.

R Core Team. 2013. R: A language and environment for statistical computing. R foundation for statistical computing. http://Www.R-project.org/. .

Rios RM, Sanchis A, Tassin AM, Fedriani C, Bornens M. 2004. GMAP-210 recruits gamma-tubulin complexes to cis-golgi membranes and is required for golgi ribbon formation. *Cell* **118**:323-35. doi:10.1016/j.cell.2004.07.012.

Rivero S, Cardenas J, Bornens M, Rios RM. 2009. Microtubule nucleation at the cis-side of the golgi apparatus requires AKAP450 and GM130. *EMBO J* **28**:1016-28. doi:10.1038/emboj.2009.47.

Samejima I, Miller VJ, Groocock LM, Sawin KE. 2008. Two distinct regions of Mto1 are required for normal microtubule nucleation and efficient association with the gamma-tubulin complex in vivo. *J Cell Sci* **121**:3971-80. doi:10.1242/jcs.038414; 10.1242/jcs.038414.

Sawin KE, Lourenco PC, Snaith HA. 2004. Microtubule nucleation at non-spindle pole body microtubule-organizing centers requires fission yeast centrosomin-related protein mod20p. *Curr Biol* **14**:763-75. doi:10.1016/j.cub.2004.03.042.

Schindelin J, Arganda-Carreras I, Frise E, Kaynig V, Longair M, Pietzsch T, Preibisch S, Rueden C, Saalfeld S, Schmid B, et al. 2012. Fiji: An open-source platform for biological-image analysis. *Nat Methods* **9**:676-82. doi:10.1038/nmeth.2019 [doi].

Soetaert K, Petzoldt T, Setzer WR. 2010. Solving differential equations in R: Package deSolve. *Journal of Statistical Software* **33**:1-25. .

Sundberg HA, Goetsch L, Byers B, Davis TN. 1996. Role of calmodulin and Spc110p interaction in the proper assembly of spindle pole body compenents. *J Cell Biol* **133**:111-24. .

Tang G, Peng L, Baldwin PR, Mann DS, Jiang W, Rees I, Ludtke SJ. 2007. EMAN2: An extensible image processing suite for electron microscopy. *J Struct Biol* **157**:38-46. doi:10.1016/j.jsb.2006.05.009.

Terada Y, Uetake Y, Kuriyama R. 2003. Interaction of aurora-A and centrosomin at the microtubule-nucleating site in drosophila and mammalian cells. *J Cell Biol* **162**:757-63. doi:10.1083/jcb.200305048.

Tien JF, Fong KK, Umbreit NT, Payen C, Zelter A, Asbury CL, Dunham MJ, Davis TN. 2013. Coupling unbiased mutagenesis to high-throughput DNA sequencing uncovers functional domains in the Ndc80 kinetochore protein of saccharomyces cerevisiae. *Genetics* **195**:159-70. doi:10.1534/genetics.113.152728.

Verollet C, Colombie N, Daubon T, Bourbon HM, Wright M, Raynaud-Messina B. 2006. Drosophila melanogaster gamma-TuRC is dispensable for targeting gamma-tubulin to the centrosome and microtubule nucleation. *J Cell Biol* **172**:517-28. doi:10.1083/jcb.200511071.

Vinh DB, Kern JW, Hancock WO, Howard J, Davis TN. 2002. Reconstitution and characterization of budding yeast gamma-tubulin complex. *Mol Biol Cell* **13**:1144-57. doi:10.1091/mbc.02-01-0607.

Yoder TJ, Pearson CG, Bloom K, Davis TN. 2003. The saccharomyces cerevisiae spindle pole body is a dynamic structure. *Mol Biol Cell* **14**:3494-505. doi:10.1091/mbc.E02-10-0655.

Zekert N, Veith D, Fischer R. 2010. Interaction of the aspergillus nidulans microtubule-organizing center (MTOC) component ApsB with gamma-tubulin and evidence for a role of a subclass of peroxisomes in the formation of septal MTOCs. *Eukaryotic Cell* **9**:795-805. doi:10.1128/EC.00058-10.

Zimmermann T. 2005. Spectral imaging and linear unmixing in light microscopy. In: Rietdorf J, editor. Berlin: Springer. p. 245-65.
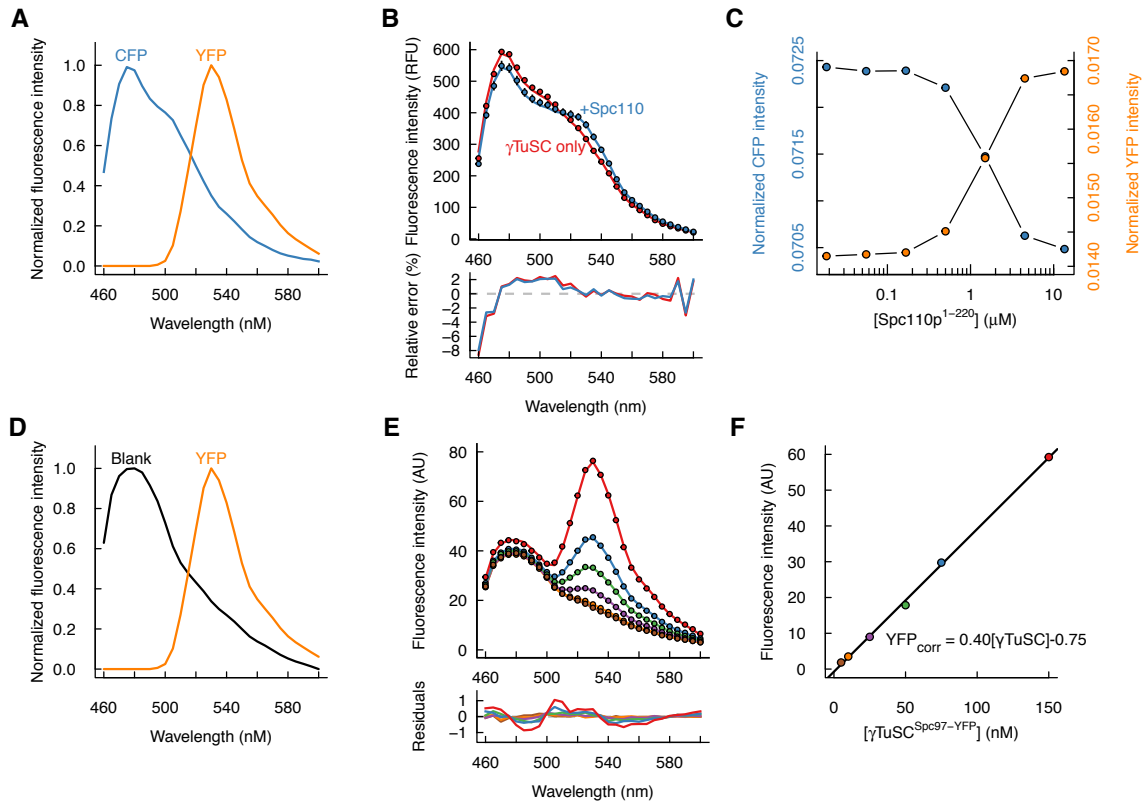
Supplemental Figure S1. FRET data analysis. A. γTuSC[Spc98-CFP] and γTuSC[Spc97-YFP] basis spectra used for fitting experimental CFP/YFP FRET spectra. **B.** γTuSC[CFP/YFP] (70 nM) spectra in the presence or absence of 120 nM Spc110[1-220]-tetramer, showing increase in intensity at 530 nm due to FRET in the presence of Spc110p. Lines represent fits as linear combinations of basis spectra shown in A. Residuals from fits are shown as relative error: (Measured intensity – Fit intensity)/(Measured intensity) × 100%.
C. Example of anticorrelation between CFP intensity and YFP intensity as Spc110p[1-220] concentration increases, indicating authentic FRET. Spectra from γTuRC assembly assay in the presence of varying Spc110p[1-220] concentrations (Figure 2C) were scaled so that the total intensity of each spectrum summed to one. The CFP and YFP components from linear combination fits of each spectra are shown. **D.** Basis spectra of buffer blank and γTuSC[Spc97-YFP] used for fitting spectra (**E**) of γTuSC[Spc97-YFP] excited at 420 nm in the absence of CFP donor fluorophore. **F.** Derivation of correction for direct excitation of YFP acceptor fluorophore in the absence of FRET. YFP intensities from fits to spectra shown in **E** are linear with respect to [γTuSC], allowing introduction of a correction term YFP$_{corr}$ to account for direct excitation of the YFP acceptor fluorophore by the donor excitation wavelength.
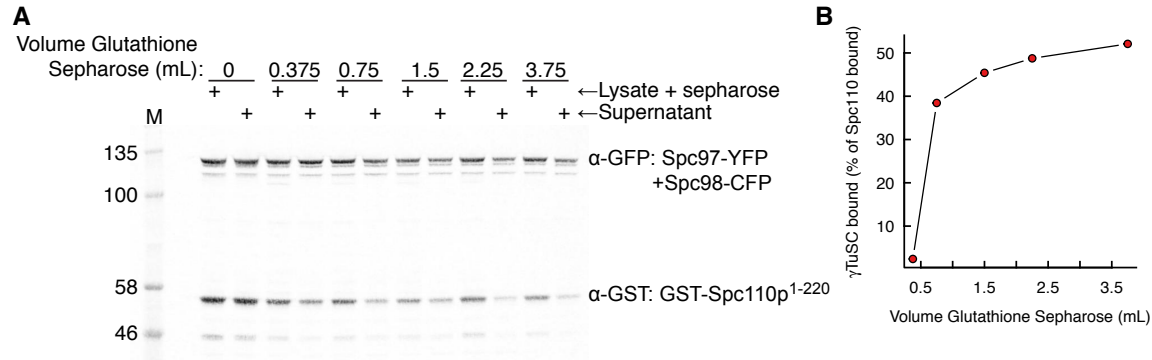
Supplemental Figure S2. **Quantification of γTuSC purification. A.** Western blot of γTuSC[CFP/YFP] and GST-Spc110p[1-220] showing the amount of γTuSC co-purified with Spc110p. After incubating lysate from Sf9 cells expressing γTuSC and GST-Spc110p[1-220] with the indicated volume of glutathione sepharose, equal volumes of the lysate + glutathione sepharose mixture or the supernatant after pelleting the glutathione sepharose were analyzed by western blotting for γTuSC[CFP/YFP] (anti-GFP) or GST-Spc110p[1-220] (anti-GST). **B.** Quantification of western blot in **A**. As γTuSC is purified via its interaction with Spc110p, the fraction γTuSC bound is normalized to the fraction Spc110p bound such that the percent bound is calculated as [1 - (Supernatant$_{\gamma TuSC}$ /Lysate+sepharose$_{\gamma TuSC}$)] / [1 - (Supernatant$_{Spc110p}$ / Lysate+sepharose$_{Spc110p}$)] × 100%. Approximately 50% of γTuSC is competent to interact with Spc110p.
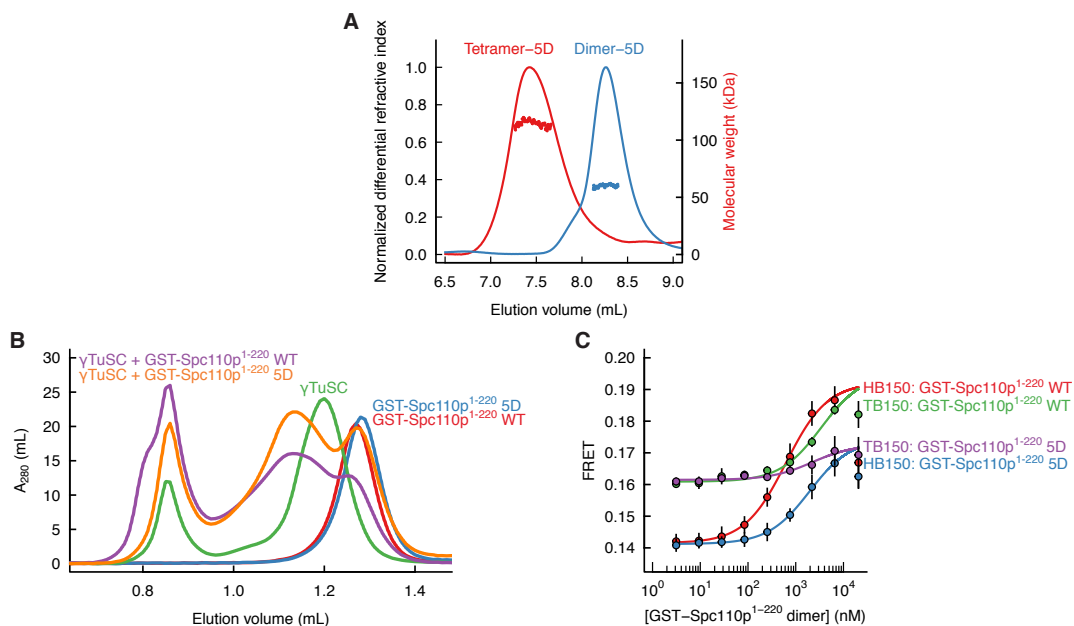
Supplemental figure S3. **Characterization of 5D phosphomimetic mutant to Spc110[1-220]-tetramer. A.** The 5D phosphomimetic mutation does not affect the oligomerization state of Spc110p[1-220]-dimer or -tetramer as analyzed by SEC-MALS. **B.** Size exclusion chromatography analysis of γTuRC assembly in the presence GST-Spc110p[1-220] performed as in Lin et al. (2014). γTuSC (2.3 μM), GST-Spc110p[1-220] (9.3 μM), and combinations thereof in TB150 (50 mM Tris pH 7.0, 150 mM KCl, 1 mM DTT) were incubated for 1 hr then 25 μL was separated on a Superdex 200 PC 3.2/30 column. **C.** Comparison of assembly of 100 nM γTuSC in TB150 buffer used by Lin et al. (2014) and HB150 used in this work. Spc110p-independent assembly is enhanced in TB150 relative to HB150.
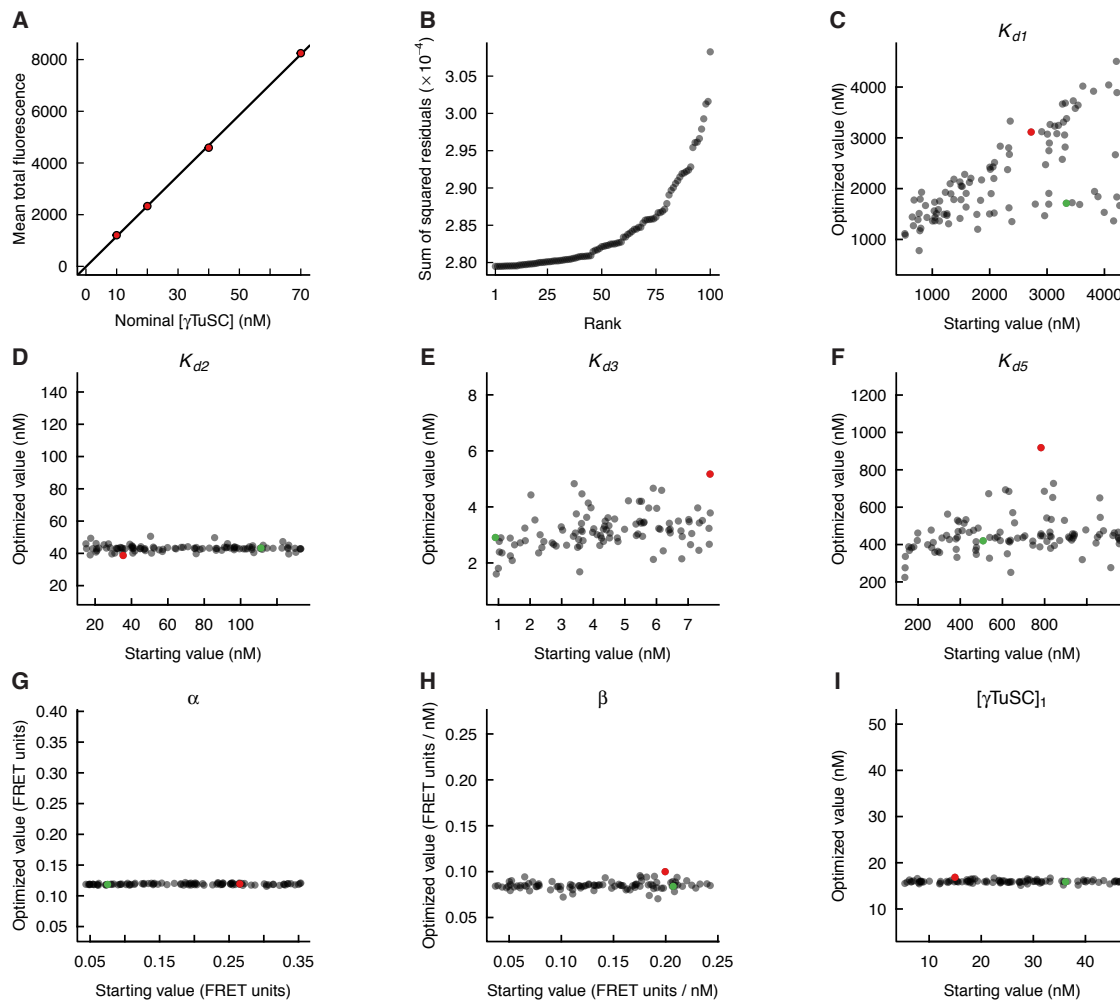
Supplemental Figure S4. **Characterizing the performance of the fitting procedure used to derive dissociation constants for interactions underlying γTuRC assembly. A.** Mean total fluorescence from data shown in Figure 5A plotted as a function of nominal γTuSC concentration, with linear fit. Error bars are smaller than points. To optimize γTuSC concentrations as part of the modeling procedure, the lowest initial γTuSC concentration is included as a parameter in the model and the additional concentrations are scaled relative to this based on the mean total fluorescence. **B.** Sum of squared residuals resulting from optimization procedure. After deriving an initial set of parameter estimates by manual parameter adjustment followed by one round of computational optimization, the initial estimates were randomized 100 times within bounds 3-fold less or greater than the initial estimate. **C-I.** Optimized parameter estimates are stable over a broad range of starting values. The optimized parameter estimates resulting from 100 randomizations of initial values are shown, with the best-fit value shown in green and the worst in red.
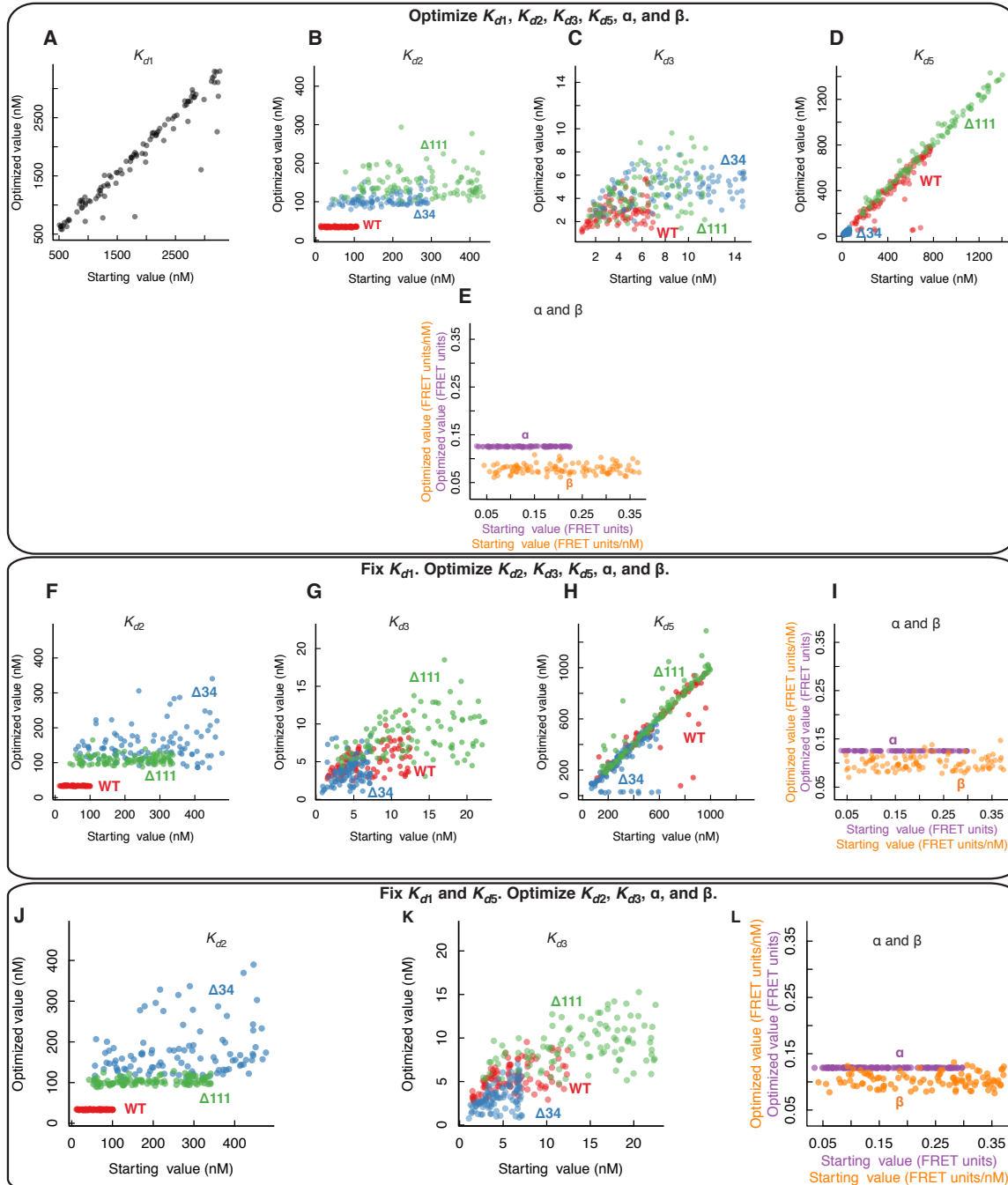
Supplemental Figure S5. **Characterizing the performance of the fitting procedure used to derive dissociation constants for interactions underlying γTuRC assembly in the presence of Spc110p N-terminal truncation mutants. A-E.** Correlation between starting values and optimized values for a model with K_{d1}, K_{d2}, K_{d3}, K_{d5}, α, and β as free parameters. Optimized values K_{d1} and K_{d5} strongly correlate with starting values (**A**, **D**), indicating these parameters are not constrained by the data set. **F-I.** Staring value-optimized value correlations for a model with K_{d1} fixed with the value determined in Figure 5 and all others as free parameters. K_{d5} (**H**) is not constrained by the data set. **J-L.** No strong starting-optimized value correlations exist in a model with K_{d1} and K_{d5} fixed at the values obtained in Figure 5 with all others as free parameters.
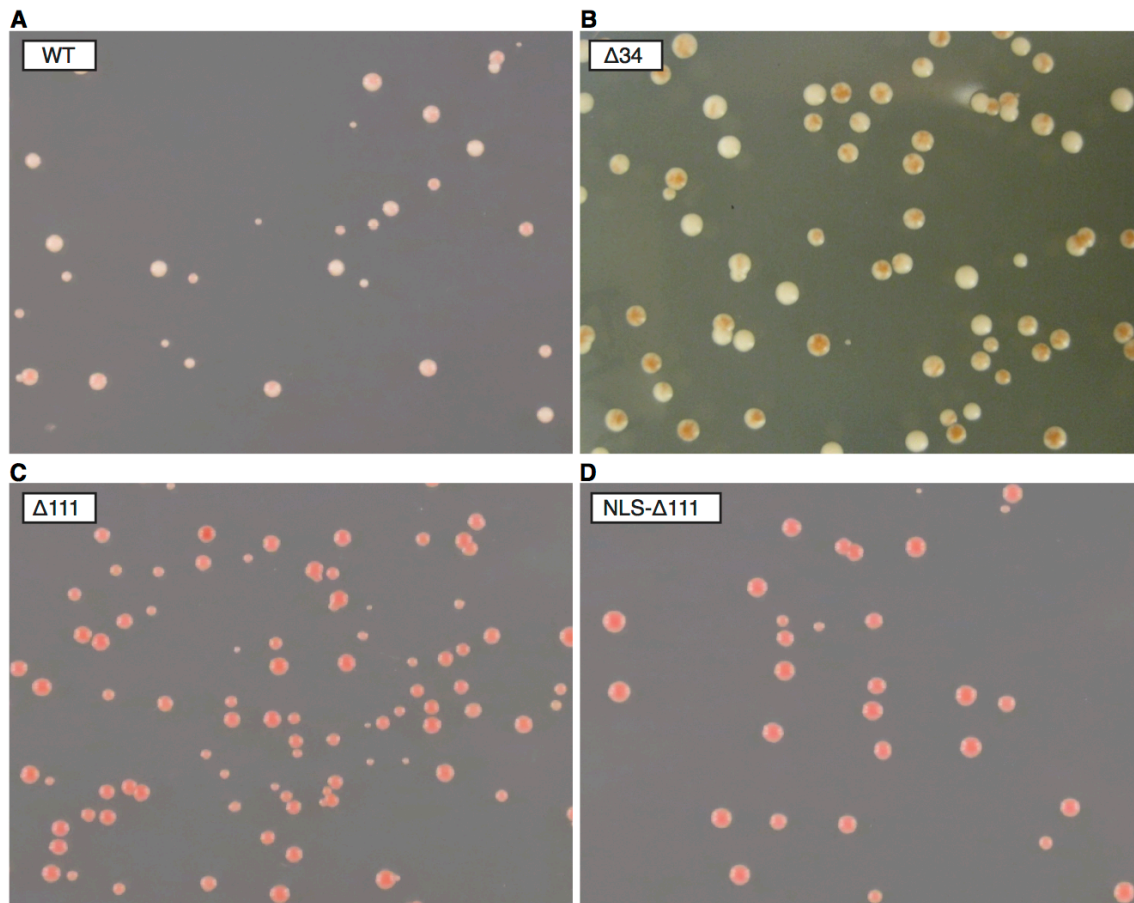
Supplemental Figure S6. Red/white plasmid shuffle assay for viability when N-terminal truncation mutants are expressed as the sole source of Spc110p. **A-B.** White-sectoring colonies indicate that wild-type (**A**) and the N-terminal 34 residue deletion (**B**) can support growth. **C-D.** No white sectors are observed for N-terminal 111 residue deletion (**C**), even when an additional nuclear localization sequence is fused to the N-terminus (**D**), indicating residues between 35 and 111 are essential for Spc110p function in vivo.

Chapter 3

Spc110 N-Terminal Domains Act Independently to Mediate Stable γ-Tubulin Small Complex Binding and γ-Tubulin Ring Complex Assembly

Contributing Authors

Alex Zelter (University of Washington), Shruthi Viswanath (UCSF), Alison Maxwell (UCSF), Richard Johnson (University of Washington), King Clyde B. Yabut (University of Washington), Michael MacCoss (University of Washington), Trisha N. Davis (University of Washington), Eric Muller (University of Washington), Andrej Sali (UCSF), David A. Agard (UCSF).

Introduction

Spc110 plays a dual role in the budding yeast *Saccharomyces cerevisiae*, both connecting the γ-tubulin small complex (γTuSC) with the nuclear face of the spindle pole body (SPB) (Kilmartin, et al., 1993; Knop & Schiebel, 1997; Knop & Schiebel, 1998) and regulating assembly of γTuSC subassemblies into the microtubule-nucleating γ-tubulin ring complex (γTuRC) (Kollman, et al., 2010; Lin, et al., 2015). Our previous work has demonstrated that γTuSC self assembles via relatively low-affinity interactions which must be cooperatively stabilized by higher-order oligomers of Spc110 for efficient γTuRC assembly to occur both in vitro and in vivo (Lyon, et al., 2016). This higher-order assembly is thought to occur via coiled-coil mediated oligomerization which would be highly favorable due to very high local concentration of Spc110 at the SPB.

While higher-order oligomerization is clearly a crucial determinant of Spc110-mediated γTuRC stabilization, several observations indicated the importance of the 163-residue N-terminal domain (hereafter NTD). First, at higher γTuSC concentration a

dimeric Spc110 construct induces γTuRC assembly, albeit with reduced average

assembly size and weaker affinity (Chapter 2, Figure 3E). This indicates that

oligomerization via the C-terminal coiled-coil domain is not the only determinant of

γTuRC stabilization. Further, while a 34-residue N-terminal deletion mutant is viable in

vivo, a 111-residue deletion is not, either due to reduced affinity or due to loss of a

binding site for an additional, as yet unidentified factor. Complicating this, however, is

the lack of density consistent with the Spc110 NTD in cryo-EM reconstructions of closed,

disulfide stabilized γTuSC filaments (Kollman, et al., 2015).

In this work, we refine the understanding of the Spc110 NTD in γTuRC assembly

via structural and biochemical approaches. We use chemical crosslinking coupled with

mass spectrometry (XL-MS) to define interactions between Spc110 and γTuSC. This

allowed assignment of the Spc110 N-terminal coiled-coil domain as the density

previously observed in a cryo-EM reconstruction (Kollman, et al., 2015). Integrated

structural modeling using the XL-MS dataset revealed that only a single Spc110 NTD is

sufficient to satisfy the crosslink distance restraints. Using our FRET assay for γTuRC

assembly (Lyon, et al., 2016) and covalently linked Spc110 heterodimers, we present

data indicating the Spc110 NTDs act independently to stabilize γTuRC assembly, one

associating with a γTuSC, while the other stablizing interactions with an adjacent

laterally associated γTuSC.

Results

Defining Spc110-γTuSC interaction by crosslink-mass spectrometry

The 6.9 Å cryo-EM reconstruction of Spc110-bound γTuSC filaments in a closed conformation revealed density consistent with approximately 40 residues of coiled-coil derived from Spc110. The Spc110$^{1-220}$ construct used in the reconstruction contains a 45-residue high-probability coiled-coil domain at positions 164-208 (hereafter referred to as the N-terminal coiled-coil, or NCC, domain), as well as a lower-probability coiled-coil domain co-extensive with the centrosomin motif 1 (CM1) domain (Figure 1). Given the limited resolution of the cryo-EM map, it was not possible to unambiguously assign the coiled-coil density to any portion of Spc110. Biochemical assays for γTuRC assembly indicate the N-terminal domain of Spc110 contributes significantly to the stabilization of γTuRC, and cells expressing Spc110 lacking this domain are unviable (Lyon, et al., 2016). However, the cryo-EM map lacked any apparent density consistent with this domain.
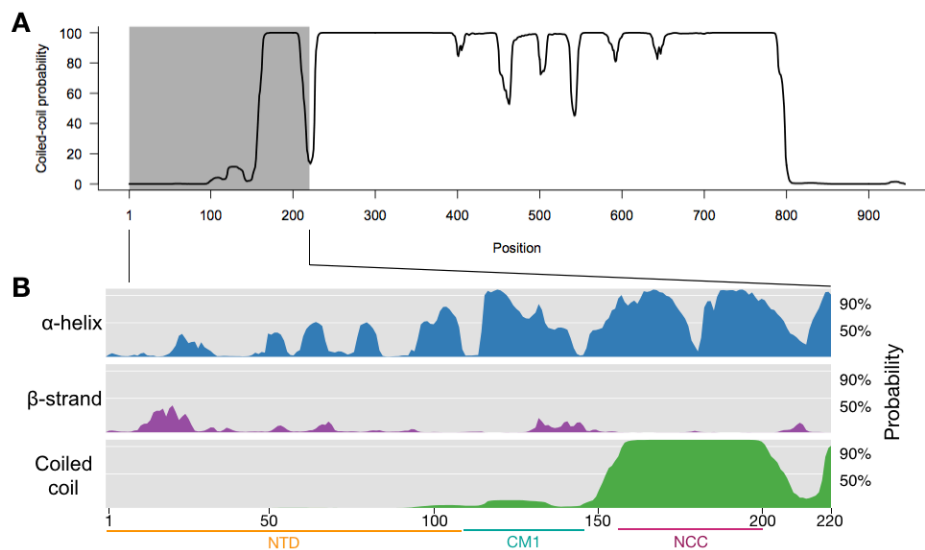
Figure 1. Spc110 domains and secondary structure. A. Spc110 coiled-coil prediction using MARCOIL. **B.** Spc110 N-terminal region secondary structure prediction, showing

lack of secondary structure for the first 111 residues (NTD). Also shown are the CM1 domain and the NCC domain.

To define these important interaction interfaces between Spc110 and γTuSC, we utilized chemical crosslinking coupled with mass spectrometry (XL-MS). We performed XL-MS using two Spc110 constructs. The Spc110$^{1-220}$-GCN4 dimer construct stabilizes γTuRC assembly in vitro and in vivo, but relatively weakly compared with higher-order oligomers (Chapter 2, figure 3E). The Spc110$^{1-401}$-GST construct purified from baculovirus-infected insect cells forms large oligomers and stabilizes γTuRC assembly very efficiently (Chapter 2, figure 1; Kollman et al. 2015). We used two chemical crosslinking reagents with different reactivities and linker lengths: disuccinimidyl suberate (DSS), a homo-bifunctional amine reactive reagent with an 11.4 Å aliphatic spacer, and N-hydroxysuccinimide-1-ethyl-3-(3-dimethylaminopropyl)carbodiimide (NHS-EDC), a so-called "zero-length" amine-carboxyl crosslinker. We identified with high confidence a large number of crosslinked peptides with both crosslinking reagents and Spc110 constructs.

We first focused on crosslinks between the N-terminal portions of Spc97 and Spc98 and Spc110 that would inform on the interaction between the coiled-coil and γTuSC observed in the cryo-EM map. We observed a series of EDC crosslinks between the NCC domain and the N-terminal portions of Spc97 consistent with the coiled-coil-γTuSC interaction apparent in the cryo-EM map (Figure 2, red asterisks).
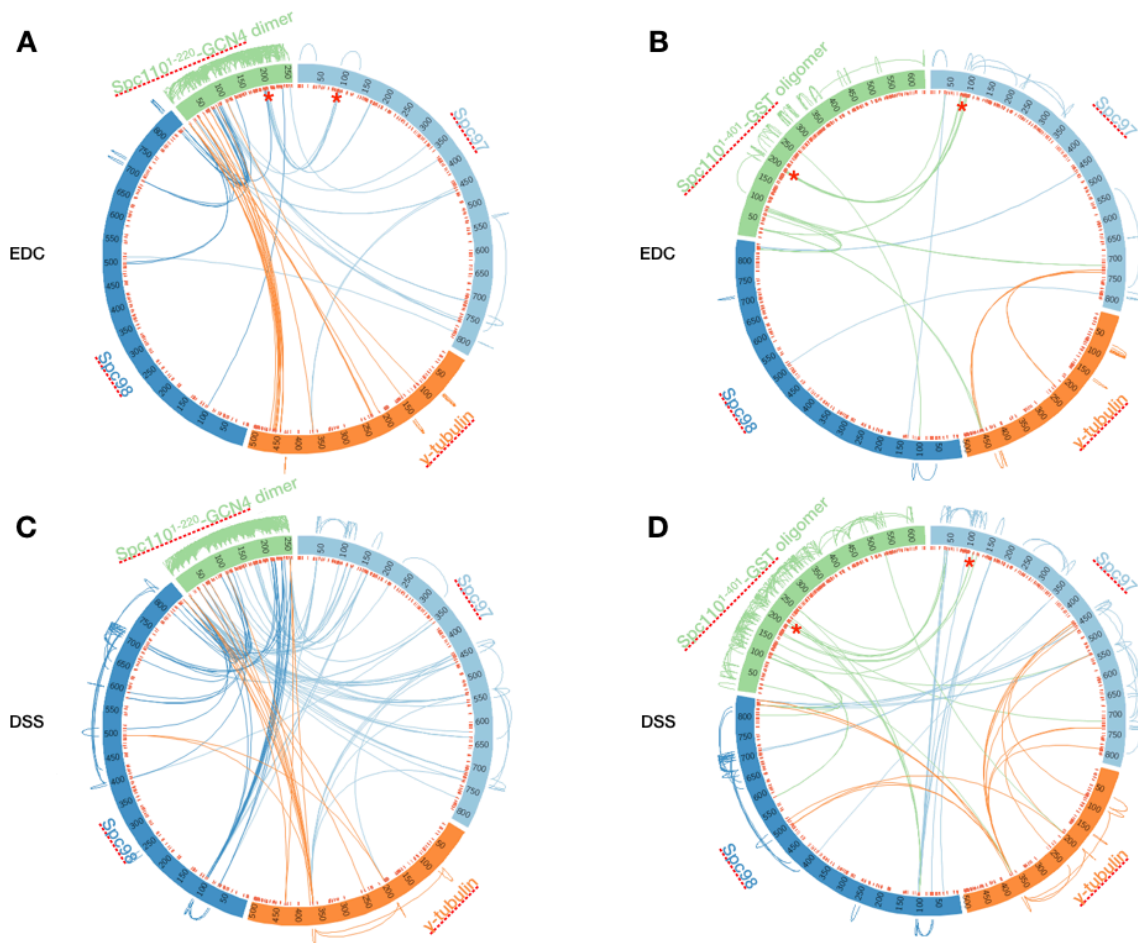
Figure 2. Overview of XL-MS datasets. XL-MS datasets derived from EDC crosslinked (**A-B**) and DSS (**C-D**) crosslinked samples containing γTuSC plus Spc110$^{1-220}$-GCN4 dimer (**A, C**) or Spc110$^{1-401}$-GST (**B, D**). Intermolecular crosslinks are shown within the circle, while intramolecular crosslinks are shown outside the circle. Red ticks inside the circle represent positions that are reactive to the respective crosslinking reagents. The red asterisks show crosslinks between the Spc110 NCC and the N-terminus of Spc97.

The Spc110 NCC binds to γTuSC at the N-terminal regions of Spc97 and Spc98

Due to the limited resolution of the cryo-EM reconstruction, the derived atomic

contains only the peptide backbone. Given the contacts between the NCC and γTuSC

observed by XL-MS, we sought a higher-resolution structure of the NCC via x-ray

crystallography. Our previous size exclusion chromatography-multi-angle light scattering

results indicate that Spc110$^{1-220}$ is only weakly dimeric (Chapter 2, figure 2D). We thus

screened several coiled-coil "stopper" domain fusion constructs of the Spc110 NCC

(Figure 3A). These stopper domains have been shown to aid crystallization of coiled-coil

proteins (Frye, et al., 2010; Klenchin, et al., 2011). N-terminal fusions with Xrcc4 and

Gp7 produced high yields of soluble protein. We elected to move on with the Xrcc4

fusion as it contained a longer portion of the NCC (residues 164-207). The Xrcc4-

Spc110$^{164-207}$ construct crystallized in a variety of conditions. Crystals yielded diffraction

data to 2.1 Å phases were obtained by molecular replacement using the Xrcc4 structure

as a search model. As expected, the model revealed a coiled-coil with observable

density for Spc110 residues 164-203.

When docked into the cryo-EM map, the x-ray model occupies most of the

coiled-coil cryo-EM density. We then mapped the crosslinking data onto the combined

γTuSC-Spc110 NCC atomic model. The majority of both DSS and EDC crosslinks are

within expected C_α-C_α distances (<17 Å for EDC, < 30 Å for DSS). From the crosslinking

data and the fact that the NCC is resolved in the cryo-EM map, we conclude that the

Spc110 NCC domain forms a stable contact with γTuSC.
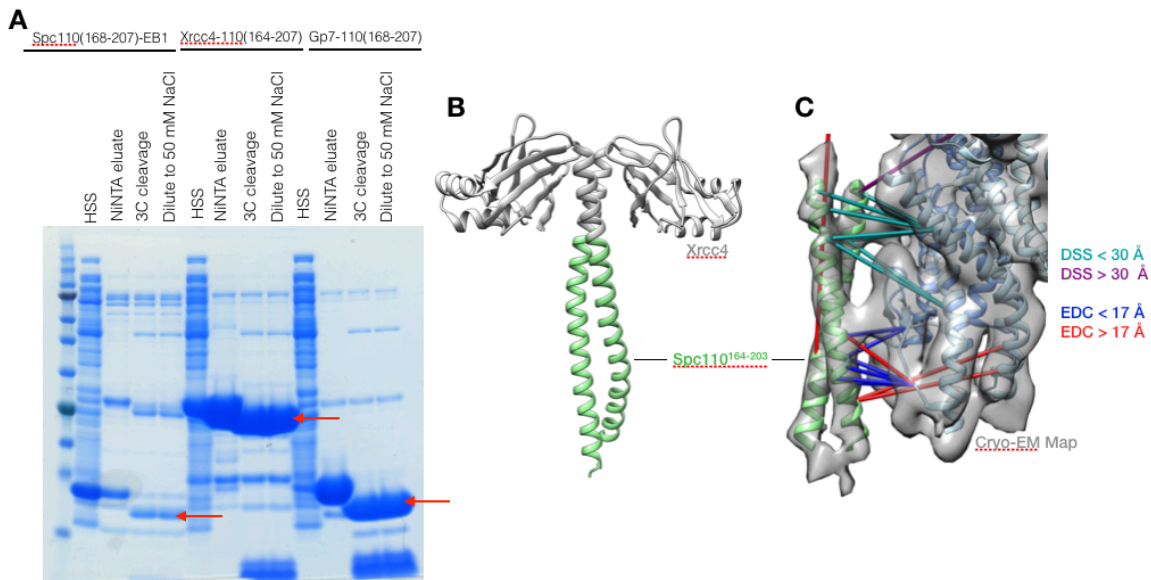
Figure 3. Spc110 NCC structure determination. A. Screening Spc110 NCC coiled-coil "stopper" domain fusion constructs. Constructs were expressed with N-terminal 6His affinity tags in *E. coli* then lysed, centrifuged to produce a high-speed supernatant (HSS), then purified by nickel affinity chromatography. Eluates from nickel affinity columns were incubated with 3C protease to cleave the 6His tag, then diluted with NaCl-free buffer to 50 mM NaCl before further purification. **B**. Structure of Xrcc4-Spc110$^{164-207}$, where Spc110 NCC residues 164-203 are resolved. **C.** Spc110 NCC structure fit into γTuSC cryo-EM density map (Kollman, et al., 2015). The majority of XL-MS distance restraints are satisfied by this model.

Integrated structural model of γTuSC-Spc110 based on cryo-EM, x-ray crystallography, and XL-MS

Given the large number of distance restraints in our XL-MS dataset and the availability of structural models for the Spc110 NCC and γTuSC, we next sought to generate a structural model of the γTuSC-Spc110 complex using Bayesian integrative modeling (Russel, et al., 2012). The experimental data for the model includes the pseudo-atomic model of γTuSC derived from the closed, disulfide-stabilized γTuSC

72
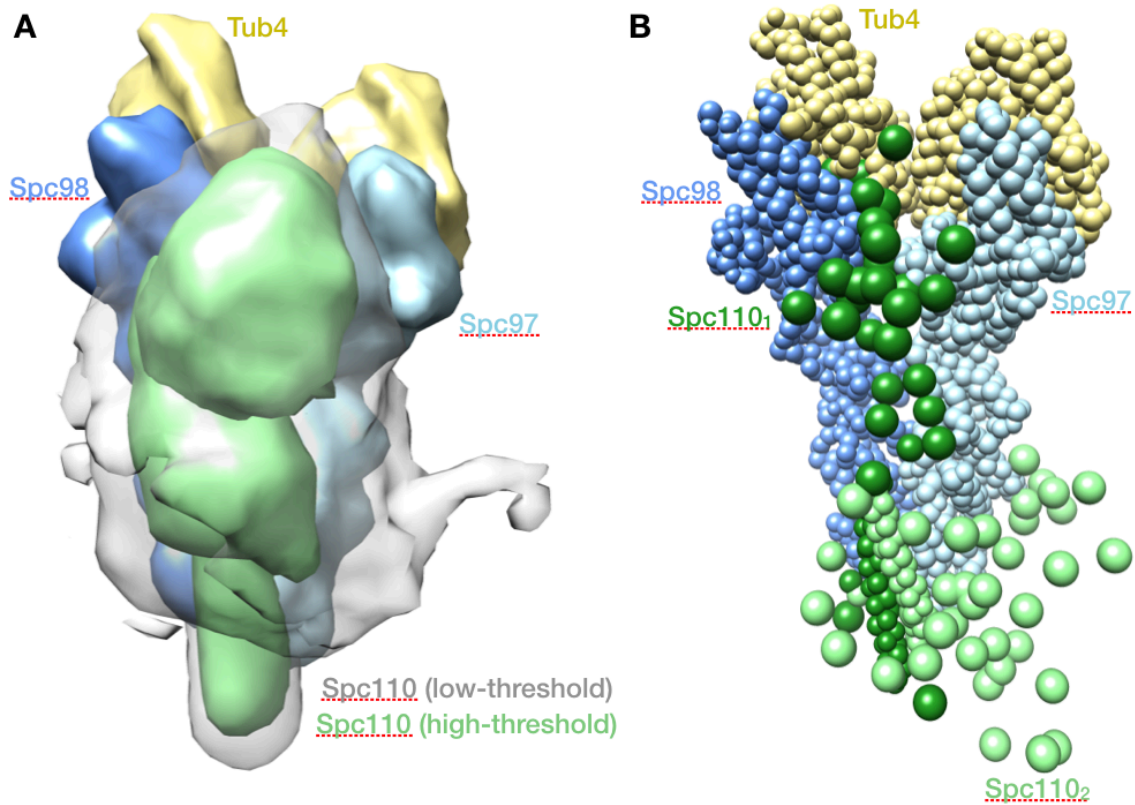
Figure 4. Integrative structural model of γTuSC-Spc110 complex. A. Localization density map. Spc110 is shown divided into three domains (residues 1-163, 164-203, and 204-220) and shown at two contour levels. The light green surface shows the localization density contour at 25% of the maximum voxel value, while the transparent grey surface shows the contour at 10% of the maximum voxel value. **B**. Top-scoring model in bead representation, showing one Spc110 NTD not associated with γTuSC.

filament structure (Kollman, et al., 2015; Greenberg, et al., 2016) and the Spc110 NCC crystal structure (Figure 3B). We used the Spc110[1-401]-GST crosslinks as there were fewer intra-Spc110 crosslinks than with Spc110[1-220]-GCN4 dimer (Figure 2), which may reflect overly aggressive crosslinking conditions that could lead to non-native structural perturbations and spurious results. The NCC domain was docked into the cryo-EM density map by cross-correlation based fitting in Chimera (Pettersen, et al., 2004) and its position was not optimized as part of the integrative modeling process.

The ensemble of models generated in the Bayesian sampling process clustered predominantly in one class (80.5% of models) with an overall localization precision of 46.4 Å RMSD. All crosslinks between Spc110 and γTuSC are satisfied in the top-scoring model in the cluster. In the localization density map for the entire cluster, the position of the Spc110 NTDs appears blurred out, especially at higher contour levels (Figure 4A). In the top scoring-model in the cluster, only one Spc110 NTD is closely associated with γTuSC (Figure 4B, dark green) while the other appears to have an unconstrained localization in the solvent away from γTuSC (Figure 4B, light green). This indicates that all crosslink distance restraints can be satisfied by a single Spc110 NTD, and likely explains the relatively large localization uncertainty when measured over the entire cluster.

Spc110 NTDs act independently to stabilize γTuRC

While our integrative structural model does not conclusively prove that only a single Spc110 NTD is required to bind γTuSC, it suggests the possibility that the two NTDs within a dimer may serve separate purposes. In particular, the close association of one of the NTDs with γTuSC suggests that acts along with the γTuSC-NCC interaction to stabilize Spc110-γTuSC binding (Figure 4B, dark green). The unassociated NTD could then be free to stabilize interactions between γTuSCs, potentially explaining the decrease in average γTuSC assembly size observed with the Spc110-Δ111 truncation mutant (Chapter 2, Figure 7A-B).

To address test these possibilities, we turned to the SpyCatcher-SpyTag system, which has proven useful in understanding asymmetric behavior by homodimeric

proteins (Zakeri, et al., 2012; Elnatan, et al., 2017). As we observed crosslinks between

Spc110 residues further down in the coiled-coil than in the Spc110$^{1-220}$-GCN4 dimer

construct (Figure 2B, D), we generated fusions between Spc110 residues 1-276 and

SpyCatcher or SpyTag domains with short serine/glycine linkers designed to prevent

disruption of the coiled-coil domain by geometric mismatch with between the domains.
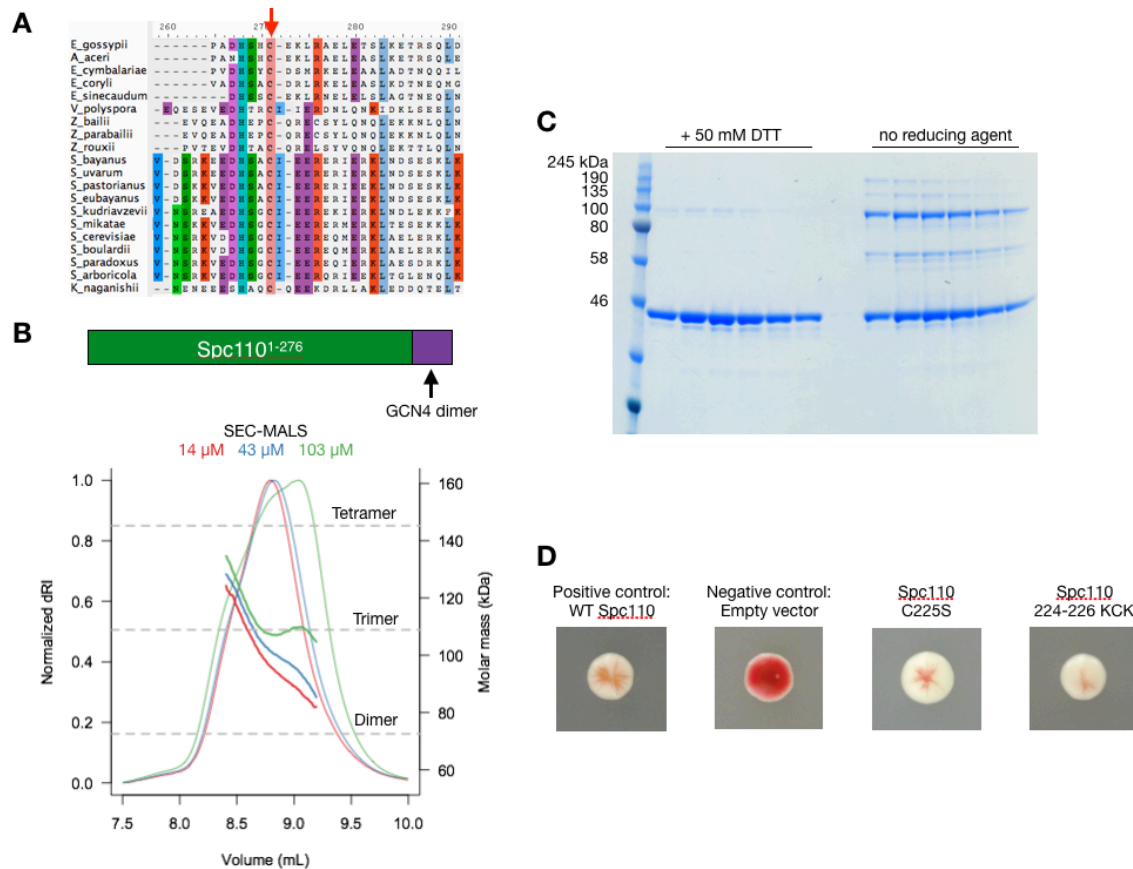
Figure 5. Spc110 contains a non-essential cysteine that forms disulfides in vitro. A.
Alignment of a variety of fungal Spc110 sequences showing conservation of the cysteine
at *S. cerevisiae* position 225. **B.** SEC-MALS analysis of Spc110$^{1-276}$-GCN4 dimer showing
formation of species beyond a dimer. **C.** Non-reducing SDS-PAGE shows Spc110$^{1-276}$-
GCN4 dimer forms disulfide bonds mediated by cysteine 225, the only cysteine in the
construct. **D.** Red-white sectoring plasmid shuffle assay for Spc110 cysteine mutant
viability. Strains bearing functional plasmid-encoded Spc110 sector white, indicating
both the C225S and the hyper-reactive 224-226 KCK variant are both viable mutants.

These constructs required mutating a conserved cysteine at Spc110 position 225 (Figure 5A), as we found that disulfides formed between the cysteines leading to undesired higher-order oligomerization (Figure 5B-C). This is one of two cysteine residues in Spc110, the other being in the calmodulin binding site near the C-terminus, and has been shown to form disulfides in vivo (Knop & Schiebel, 1997). The Spc110 C225S mutant was viable in vivo as assessed by a plasmid shuffle assay, as was a mutation of residues 224 and 226 to lysine, which should generate a hyper-reactive KCK motif, indicating that disulfide formation between Spc110 molecules does not play a crucial role in Spc110 function in vivo (Figure 5D).

SpyCatcher-SpyTag covalent adducts of Spc110$^{1-276}$-C225S formed readily, allowing comparison of full-length/Δ111 heterodimers with the full-length/full-length or Δ111/Δ111 covalent dimers (Figure 6A). At 50 nM γTuSC-CFP/YFP, the full-length/Δ111 heterodimer reduced the apparent affinity for γTuSC assembly as well as the average assembly size compared with the full-length/full-length control (Figure 6C). γTuRC assembly stabilized by the Δ111/Δ111 covalent dimer was severely impaired. The fact that the amplitude of the full-length/Δ111 binding curve was reduced compared with the control implies that the average size of γTuSC assemblies is smaller, and thus that wild-type γTuSC assembly size depends on the presence of two Spc110 NTDs.
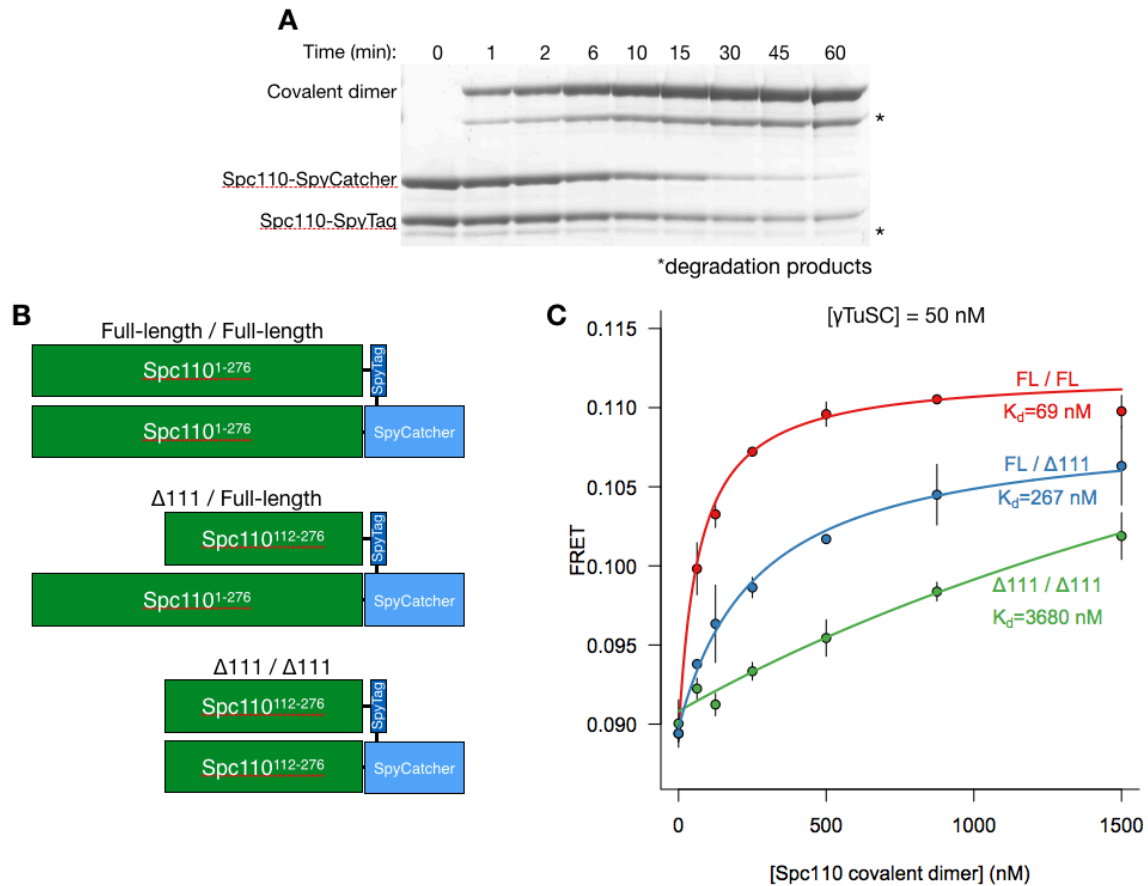
Figure 6. Full-length/Δ111 Spc110 heterodimers show impaired affinity and average assembly size in γTuRC assembly assay. A. Time-course of covalent SpyCatcher-SpyTag adduct formation assayed by SDS-PAGE. The asterisk marks a degradation product which is subsequently removed by anion exchange and size exclusion chromatography. **B.** Diagrams of Spc110 covalent dimers. **C.** FRET assay for γTuRC assembly in the presence of Spc110 covalent heterodimers.

Discussion

Spc110 NTDs serve different roles in γTuRC assembly

We interpret these results as implying two possible binding modes for Spc110 NTDs on γTuSC (Figure 7). In a full-length/full-length Spc110 dimer, both NTDs are equivalent prior to γTuSC binding (Figure 7A). Upon γTuSC binding, this symmetry is broken and one Spc110 NTD makes contacts with the same γTuSC bound by the Spc110 NCC, while the other NTD is poised to make contacts with another γTuSC (Figure 7B).

77

Then, γTuSC self-interaction and the second Spc110 NTD cooperate to stabilize assembly of γTuRC (Figure 7C).

In the case of the full-length/Δ111 heterodimer, the NTDs are not equivalent prior to γTuSC binding (Figure 7D). Thus, Spc110 can bind γTuSC in two configurations (Figure 7E). Only one configuration has an Spc110 NTD posed to contact another γTuSC (Figure 7E, red arrow), leading to γTuRC assemblies where some interfaces are strong due to cooperative stabilization by both γTuSC self-interaction and Spc110, and some are weak due to the absence of additional stabization by Spc110 (Figure 7F).
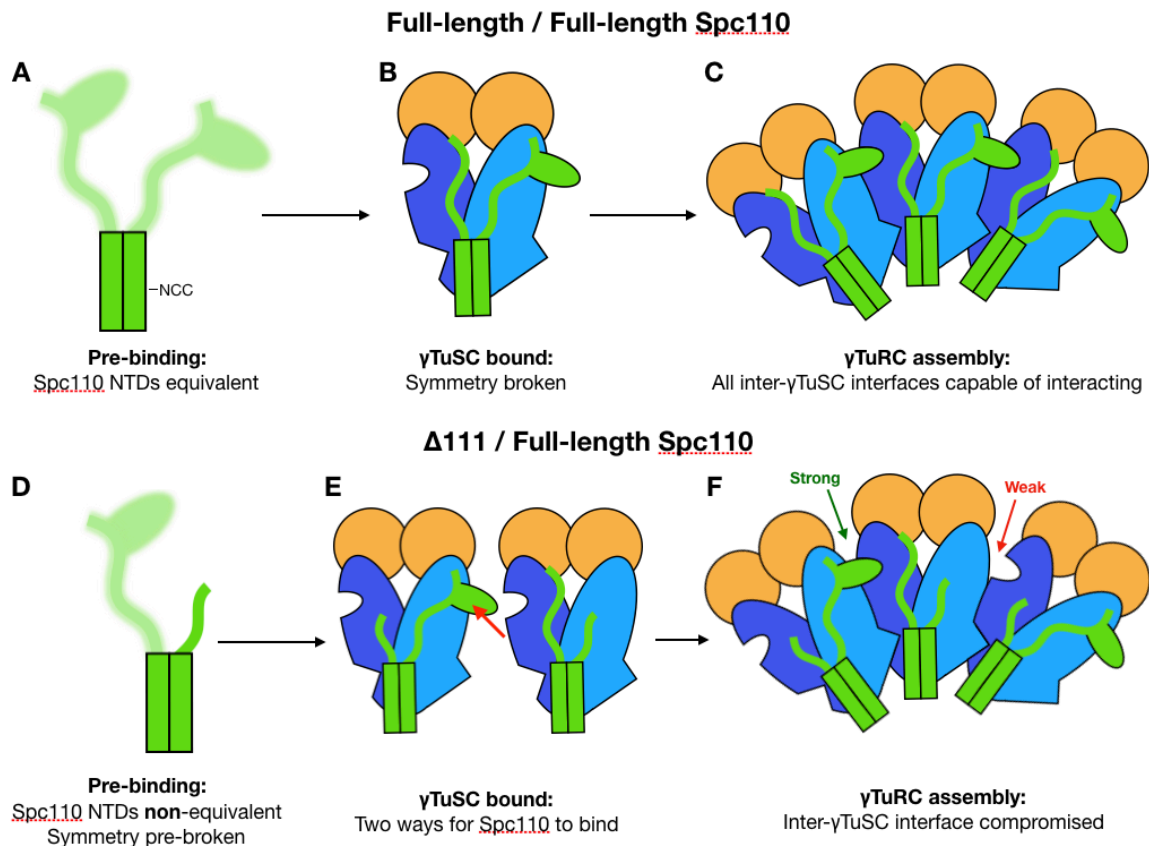
Figure 7. Model for independent action of Spc110 NTDs in stabilizing γTuRC.

While this model is consistent with our data, it is important to recognize that the linked equilibria between Spc110 binding and γTuSC self-assembly can make it difficult to intuitively interpret γTuRC assembly curves. γTuRC assembly data collected at a variety of γTuSC concentrations, similar to Chapter 2, figure 5, would allow for fitting a more complete binding model with parameters that could inform on the relative affinities of the interactions proposed in Figure 7. Additional truncation mutants, or alanine scanning mutants, in the heterodimeric context could also be helpful in clarifying which portions of Spc110 serve either of the two proposed roles in stabilizing γTuRC assembly. More sophisticated XL-MS experiments will also be informative. In particular, we are currently developing methods to allow isotope-labeled crosslinked peptide identification by mass spectrometry. Isotopically labelled ^{14}N/^{15}N Spc110 heterodimers could reveal which domains of Spc110 and γTuSC interact in the context of the proposed assembly mechanism. The five intensively studied Spc110 phosphorylation sites are all present in the Spc110 NTD at positions 36, 60, 64, 68, and 91 (Lin, et al., 2015; Lyon, et al., 2016). It will be very important to understand the role of these sites in the context of the structural model we propose, particularly to understand the conflicting results about these sites.

The Spc110 NCC is a major γTuSC-interacting motif

Our XL-MS dataset revealed the identity of the coiled-coil density previously observed in contact with the N-terminal regions of γTuSC (Figure 3C; Kollman et al. 2015). Unlike the CM1 domain, which we previously proposed to be an important γTuSC interaction motif, the NCC contains several mitosis-specific phosphorylation sites (Davis

Lab, unpublished data), so it will be important to characterize the role of phosphorylation in γTuSC-NCC binding. It will also be necessary to confirm this interaction by mutational analysis in vitro and/or in vivo.

We previously observed that an N-terminal 146-residue truncation completely abolished γTuRC assembly in the context of a GCN4 tetrameric coiled-coil fusion (Chapter 2, figure 7). If the NCC is an important interaction motif, it is unclear why so little activity was observed in the Δ146 mutant. The γTuSC concentration in that experiment was relatively low at 10 nM, so a likely explanation is that the truncation reduces Spc110-γTuSC affinity to the point that very little assembly occurs. If this is the case, increasing the γTuSC concentration should lead to increased assembly. Another possibility is that γTuSC is bound to the Spc110-Δ146 tetramer, but in the absence of the Spc110 NTD γTuSC self-interaction is too weak to allow interactions giving rise to FRET. This could be confirmed via an orthogonal assay for Spc110-γTuSC interaction, such as size-exclusion chromatography.

Implications for γTuRC assembly and the MT cytoskeleton

The results presented in this chapter add another dimension to the role Spc110 plays in γTuRC assembly. In Chapter 2, the focus was on the role of Spc110 oligomerization, which we believe is mediated solely by the coiled-coil domain. We have been unable to detect any self-interaction between the Spc110 NTDs, though the extremely high local concentration at the SPB and especially within γTuRC implies that even very low-affinity interactions may be important. Instead, we propose that the Spc110 NTDs are responsible for high-affinity binding between Spc110 and γTuSC, and

also for stabilizing interactions between adjacent γTuSCs. It remains possible that the NTDs are required to bind additional factors important for MT nucleation, either directly or indirectly. Given recent attention to non-γTuRC-mediated mechanisms of MT nucleation, any cooperation between Spc110, γTuRC, and factors such as Stu2 will be very informative (Roostalu & Surrey, 2017). The cross-γTuSC interactions that we propose are made by Spc110 could also be important to the mechanisms that lead to γTuRC closure, which we have shown activates the MT nucleating activity of γTuRC (Kollman, et al., 2015). Further study of these questions is necessary and likely to be fruitful.

Materials and Methods

Protein expression constructs

Constructs for expression of γTuSC, Spc110$^{1-220}$-GCN4 dimer, and Spc110$^{1-401}$-GST were previously described (Chapter 2, Materials and Methods; Vinh et al. 2002; Lyon et al. 2016). Spc110$^{1-276}$-GCN4 dimer was synthesized by GeneArt (Life Technologies). Spc110$^{1-276}$-SpyTag and SpyCatcher fusion constructs were synthesized with the BioXp instrument (SGI-DNA). These constructs were then cloned into pET28 using Gibson Assembly. Point mutations were constructed by site-directed mutagenesis (Zheng, et al., 2004). Truncation mutants were constructed using the Q5 Site-Directed Mutagenesis kit (New England BioLabs).

Protein Expression and Purification

Purifications for γTuSC, Spc110$^{1-220}$-GCN4 dimer, and Spc110$^{1-401}$-GST were previously described (Chapter 2, Materials and Methods; Vinh et al. 2002; Lyon et al. 2016).

Spc110$^{1-276}$-GCN4 dimer was purified as for Spc110$^{1-220}$-GCN4 dimer. Spc110$^{1-276}$-SpyCatcher and SpyTag were transformed into BL21(DE3) CodonPlus RIL (Agilent). For each construct, 3 L of culture in Terrific Broth was grown at 30 °C until reaching OD$_{600}$ 0.3-0.4. The temperature was then decreased to 18 °C. Once the culture had reached OD$_{600}$ 0.6-0.8, expression was induced with 0.6 mM IPTG for 16-18 h. Cells were harvested by centrifugation then resuspended in lysis buffer (50 mM potassium phosphate pH 8, 300 mM NaCl, 5 mM EDTA, 1 mM DTT, 0.3% Tween-20, 1x cOmplete protease inhibitor, EDTA-free (Roche)). Cells were lyse by Emulsiflex C3 (Avestin). Lysate was cleared by ultracentrifugation at 40,000 x g for 30 min in a Type 45Ti roto (Beckman-Coulter). Cleared lysate was applied to cOmplete His-Tag purification resin (Roche) and incubated for 1 h at 4 °C with gentle agitation. The column was then washed with 10 CV lysis buffer followed by 10 CV lysis buffer without Tween-20. Spc110 was then eluted with 4 CV of elution buffer (25 mM Tris pH 8.3, 75 mM NaCl, 5 mM EDTA, 1 mM DTT, 1x cOmplete protease inhibitor, EDTA-free (Roche), and 250 mM imidazole). Eluates were then diluted to < 5 mS/cm conductivity with MonoQ buffer A (25 mM Tris pH 8.3, 1 mM DTT). The diluted eluates were then applied separately to a MonoQ 10/100 GL pre-equilibrated in 2.5% MonoQ buffer B (25 mM Tris pH 8.3, 1 M NaCl, 1 mM DTT) in MonoQ buffer A. The column was then washed with 2 CV of 2.5% MonoQ buffer B, then eluted with a linear gradient from 2.5-50% MonoQ buffer B. Spc110$^{1-276}$ SpyCatcher and SpyTag typically elute at approximately 17 mS/cm and 9 mS/cm conductivity, respectively. The concentration of the pooled fractions containing Spc110$^{1-276}$-SpyCatcher or SpyTag were measured by using Bradford protein assay

reagent (Bio-Rad), then combined in a 1:1 molar ratio with the addition of TEV protease

to cleave the His-tags. After 1 h, the Spc110 covalent adduct was further purified by size

exclusion chromatography on S200 16/60 pg equilibrated in HB150 + 10% glycerol.

Fractions containing undegraded Spc110 covalent adducts were then pooled,

centrifugally concentrated, flash frozen in liquid nitrogen, and stored at -80 °C. Spc110

coiled-coil "stopper" constructs were purified in essentially the same manner via NiNTA

affinity, anion exchange, and size exclusion chromatography.

XL-MS

Spc110 and γTuSC were combined in a 1:1 molar ratio and crosslinked with DSS for 3

min or NHS-EDC for 30 min as described (Greenberg, et al., 2016; Zelter, et al., 2015).

Protein digestion and mass spectrometry were performed as described (Zelter, et al.,

2015). Crosslinked peptides were identified using Kojak version 1.4.3 (Hoopmann, et al.,

2015) and statistically validated at a 1% false discovery rate using Percolator version

2.08 (Käll, et al., 2007). All crosslinking data will be made available at proxl.yeastrc.org

upon publication of this chapter in a journal.

Crystallography

Crystals of Xrcc4-Spc110[164-207] were obtained with by hanging drop vapor diffusion with

8 mg/mL protein and a well solution containing 13% PEG3350 and 0.2 M magnesium

formate. Crystals were cryo-protected by rapid transfer to well solution with 30%

PEG3350. Diffraction data was collected under cryogenic conditions at Advanced Light

Source beamline 8.3.1. Diffraction data was processed with XDS (Kabsch, 2010) and

indexed in space group P1. Phases were obtained by molecular replacement using

Phaser within the Phenix package (Adams, et al., 2010; McCoy, et al., 2007). The search

model was the PDB ID 1FU1 residues 1-150, with the coiled-coil residues 133-150

mutated to alanine. The S-(dimethylarsenic)cysteine at position 130 in 1FU1 was

modified to cysteine. The majority of the structure was built with phenix.autobuild

(Terwilliger, et al., 2008) with the remainder built manually in Coot (Emsley, et al., 2010)

and refined with phenix.refine (Afonine, et al., 2012). The final structure contains

Spc110 residues 164-203, along with the Xrcc4 fusion domain.

Integrative structural modeling

Modeling was performed using the Integrated Modeling Platform (Russel, et al.,

2012).The system being modeled consists of one copy of the closed-state γTuSC pseudo-

atomic model (PDB ID 5FLZ) derived from the closed, disulfide-stabilized γTuSC filament

cryo-EM map (Greenberg, et al., 2016; Kollman, et al., 2015) and an Spc110 dimer. The

Spc110 NCC (residues 164-203) was then fit into the cryo-EM density map using the Fit

in Map tool in Chimera version 1.12.0 (Pettersen, et al., 2004). Residues present in the

pseudoatomic model and the Spc110 NCC crystal structure are represent with 1 bead

per residue. Missing segments in the γTuSC model are omitted, while the Spc110 NTD

(residues 1-163) and residues C-terminal to the NCC are represented with 1 bead per 5

residues. γTuSC was modeled as a single rigid body. Excluded volume and connectivity

restraints were applied. Crosslink distance restraints were applied with 45 Å and 25 Å

cutoffs for DSS and EDC crosslinks, respectively. The Spc110 NCC was not allowed to

move during the sampling process. Monte Carlo sampling proceeded for 50,000 steps,

after which 1000 randomly selected models were clustered into two classes. The

majority (80.5%) of models clustered in one class which satisfied all Spc110-γTuSC crosslinks.

SEC-MALS

SEC-MALS was performed as described using a Shodex Protein KW-804 column and DAWN HELEOS II and OptiLab t-Rex instruments (Wyatt Technology) (Lyon, et al., 2016). The mobile phase was HB150 with 1 mM DTT.

Sequence alignments

Spc110 sequences were obtained by reciprocal best BLAST (Camacho, et al., 2009) searches with *S. cerevisiae* Spc110 protein sequence. Sequences were aligned using MAFFT version 7.222 (Katoh & Standley, 2013).

Red-White Sectoring Plasmid Shuffle Assay

Viability of Spc110 mutants was performed with a red-white colony sectoring assay as described (Tien, et al., 2013; Lyon, et al., 2016).

Author Contributions

ASL and DAA conceived the study. ASL and AM created expression constructs and purified proteins. AZ perfomed protein crosslinking and mass spectrometry with RJ. SV performed integrative modeling. KCBY performed the red/white plasmid shuffle assay. TND, EM, MM, AS, and DAA supervised research.

References

Adams, P. D. et al., 2010. PHENIX: A comprehensive Python-based system for macromolecular structure solution. *Acta Crystallographica Section D* **66**: 213–21.

Afonine, P. V. et al., 2012. Towards automated crystallographic structure refinement with phenix.refine. *Acta Crystallographica Section D* **68**: 352-367.

Camacho, C. et al., 2009. BLAST+: architecture and applications. *BMC Bioinformatics* **10**: 421-421.

Elnatan, D. et al., 2017. Symmetry broken and rebroken during the ATP hydrolysis cycle of the mitochondrial Hsp90 TRAP1. *eLife* **6**: e25235

Emsley, P., Lohkamp, B., Scott, W. & Cowtan, K., 2010. Features and Development of Coot. *Acta Crystallographica D* **66**: 486-501.

Frye, J. J., Klenchin, V. A. & Rayment, I., 2010. Structure of the tropomyosin overlap complex from chicken smooth muscle: insight into the diversity of N-terminal recognition. *Biochemistry* **49**: 4908-4920.

Greenberg, C. H. et al., 2016. Structure of γ-tubulin small complex based on a cryo-EM map, chemical cross-links, and a remotely related structure.. *Journal of Structural Biology* **194**: 303-310.

Hoopmann, M. R. et al., 2015. Kojak: efficient analysis of chemically cross-linked protein complexes.. *Journal of Proteome Research* **14**: 2190-2198.

Käll, L. et al., 2007. Semi-supervised learning for peptide identification from shotgun proteomics datasets. *Nature Methods* **4**: 923-925.

Kabsch, W., 2010. XDS. *Acta Crystollographica D* **66**: 125-132.

Katoh, K. & Standley, D. M., 2013. MAFFT Multiple Sequence Alignment Software Version 7: Improvements in Performance and Usability. *Molecular Biology and Evolution* **30**: 772-780.

Kilmartin, J. V., Dyos, S. L., Kershaw, D. & Finch, J. T., 1993. A spacer protein in the Saccharomyces cerevisiae spindle poly body whose transcript is cell cycle-regulated. *Journal of Cell Biology* **123**: 1175-1184.

Klenchin, V. A. et al., 2011. Structure-Function Analysis of the C-terminal Domain of CNM67, a Core Component of the Saccharomyces cerevisiae Spindle Pole Body. *Journal of Biological Chemistry* **286**: 18240-18250.

Knop, M. et al., 1997. The spindle pole body component Spc97p interacts with the gamma-tubulin of Saccharomyces cerevisiae and functions in microtubule organization and spindle pole body duplication.. *The EMBO Journal* **16**: 1550-1564.

Knop, M. & Schiebel, E., 1997. Spc98p and Spc97p of the yeast γ-tubulin complex mediate binding to the spindle pole body via their interaction with Spc110p.. *EMBO Journal* **16**: 6985-6995.

Knop, M. & Schiebel, E., 1998. Receptors determine the cellular localization of a γ-tubulin complex and thereby the site of microtubule formation. *The EMBO Journal* **17**: 3952-3967.

Kollman, J. M. et al., 2015. Ring closure activates yeast γTuRC for species-specific microtubule nucleation. *Nature Structural & Molecular Biology* **22**: 132-137.

Lin, T.-c., Neuner, A. & Schiebel, E., 2015. Targeting of γ-tubulin complexes to microtubule organizing centers: conservation and divergence. *Trends in Cell Biology* **25**: 296-307.

Lyon, A. S. et al., 2016. Higher-order oligomerization of Spc110p drives γ-tubulin ring complex assembly. *Molecular Biology of the Cell* **27**: 2245-2258.

McCoy, A. J. et al., 2007. Phaser crystallographic software. *Journal of Applied Crystallography* **40**: 658–674.

Pettersen, E. et al., 2004. UCSF Chimera--a visualization system for exploratory research and analysis. *J Comput Chem* **25**: 1605–12.

Roostalu, J. & Surrey, T., 2017. Microtubule nucleation: beyond the template. *Nature Reviews Molecular Cell Biology* **18**: 702-710.

Russel, D. et al., 2012. Putting the Pieces Together: Integrative Modeling Platform Software for Structure Determination of Macromolecular Assemblies. *PLOS Biology* **10**: e1001244.

Terwilliger, T. C. et al., 2008. Iterative model building, structure refinement and density modification with the PHENIX AutoBuild wizard. *Acta Crystallographica Section D-biological Crystallography* **64**: 61-69.

Tien, J. F. et al., 2013. Coupling Unbiased Mutagenesis to High-throughput DNA Sequencing Uncovers Functional Domains in the Ndc80 Kinetochore Protein of Saccharomyces cerevisiae. *Genetics* **195**: 159-170.

Vinh, D. et al., 2002. Reconstitution and Characterization of Budding Yeast γ-Tubulin Complex. *Molecular Biology of the Cell* **13**: 1144-1157.

Zakeri, B. et al., 2012. Peptide tag forming a rapid covalent bond to a protein, through engineering a bacterial adhesin. *Proceedings of the National Academy of Sciences of the United States of America* **109**: 4347-4348.

Zelter, A. et al., 2015. The molecular architecture of the Dam1 kinetochore complex is defined by cross-linking based structural modelling. *Nature Communications* **6**: 8673-8673.

Zheng, L., Baumann, U. & Reymond, J.-L., 2004. An efficient one-step site-directed and site-saturation mutagenesis protocol. *Nucleic Acids Research* **32**: e115.

Appendix

Analyzing FRET Data with R Package ASLutils

This is a tutorial on how to use the ASLutils R package to analyze FRET data from start to finish.

The first thing to do is install R version 3.4.2 or greater by going to cran.r-project.org. Then you

can install this package as follows:

```r
install.packages("devtools")
devtools::install_github("aslyon/ASLutils")
```

Then load the package:

```r
library(ASLutils)
```

Import Spectral Data

The first step is to import spectral data into R. The file format exported directly by the plate

reader software will almost certainly be incompatible with this function. A simple Python script

is available on GitHub for converting files exported by Molecular Devices SoftMax Pro software.

If you don't want to use the Python script, the data should be a tab-delimted text file with each

column containing one spectrum. The columns must have a header (typically an alphanumeric

well identifier from a microplate) and the first column must identify the wavelengths contained

in each row. Once you have a spectra file in this format, import it into R like this:

```r
mySpectra <- openSpectraFile(file = "/path/to/spectra/file")
```

Get Spectra Corresponding to Different Experimental Conditions

An experiment will most likely have several wells containing only buffer, along with one or

more sets of wells containing fluorophores. The example data included in the matrix

TuSC_Spc110_spectra has "blank" buffer-only spectra in wells A7-B9 and γTuSC-CFP/YFP with

a concentration series of Spc110 in wells C7-I9. We want to manipulate the two sets of spectra separately, so we need to create two different objects, one for the blank spectra and one for the fluorophore-containing spectra:

```
blanks <- getSpectra(TuSC_Spc110_spectra, nRows = c("A", "I"), nCols = 3, sta
rtRow = "A",
    endRow = "B", startColumn = 1, endColumn = 3)
cfpYfp <- getSpectra(TuSC_Spc110_spectra, nRows = c("A", "I"), nCols = 3, sta
rtRow = "C",
    endRow = "I", startColumn = 1, endColumn = 3)
```

Note that rather than specifying the letter codes for the rows of the microplate you can use the ordinal number (A=1, B=2, C=3, etc.):

```
blanks <- getSpectra(TuSC_Spc110_spectra, nRows = 9, nCols = 3, startRow = 1,
    endRow = 2, startColumn = 1, endColumn = 3)
cfpYfp <- getSpectra(TuSC_Spc110_spectra, nRows = 9, nCols = 3, startRow = 3,
    endRow = 9, startColumn = 1, endColumn = 3)
```

Subtract Blank Spectra

Often buffer alone will have some fluorescence signal which must be subtracted from the fluorophore-containing spectra. This is the case here. First plot the blank spectra to make sure nothing untoward has happened (contamination with fluorescent material, for instance):

```
plotSpectra(blanks, wl = seq(from = 460, to = 600, by = 5))
```
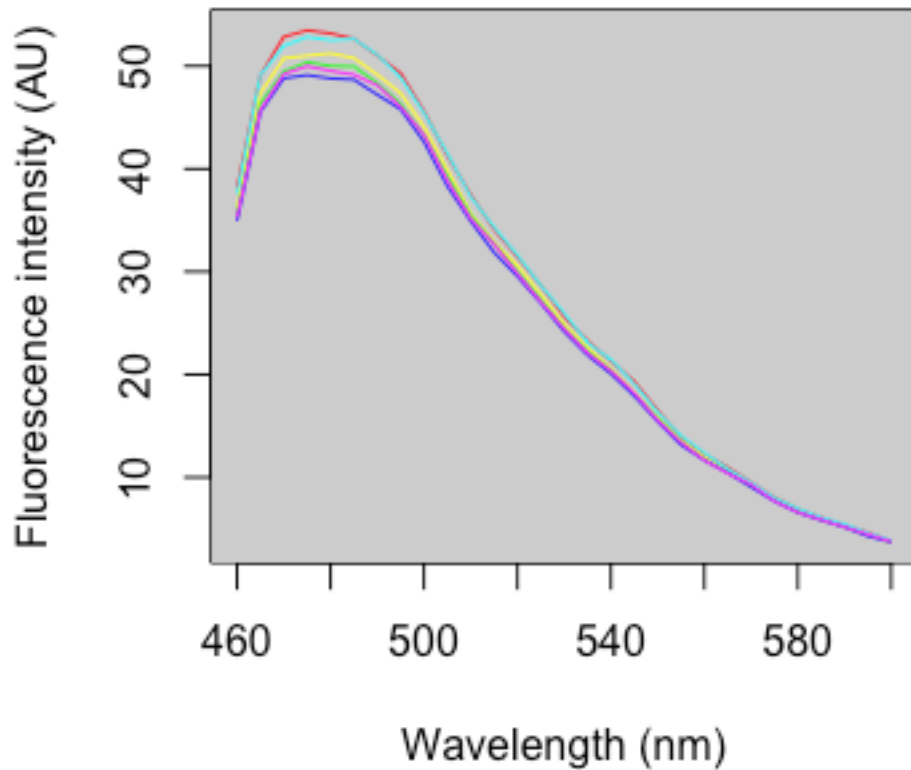
Figure 1. Blank spectra.

These spectra all look acceptable - there are no significant outliers - so we'll calculate the

average, then subtract the average from the fluorophore-containing spectra:

```
blanksAvg <- rowMeans(blanks)
cfpYfpBgSub <- bgSub(spectra = cfpYfp, bgSpectrum = blanksAvg)
```

This is a good point to take a look at the fluorophore-containing spectra and make sure there

are no significant outliers:

```
plotSpectra(cfpYfpBgSub, wl = seq(from = 460, to = 600, by = 5))
```
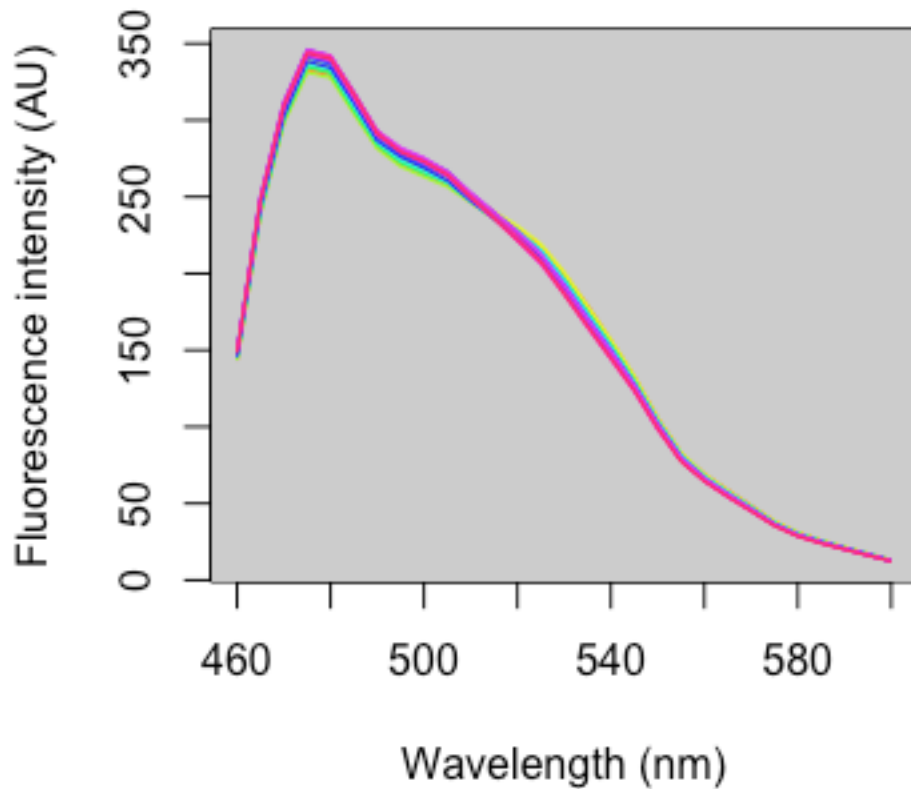
Figure 2. γTuSC-CFP/YFP spectra.

These all look acceptable, so we'll move on to calculting FRET.

Least-Squares Fitting of Fluorescence Spectra

First, let's take a look at the basis spectra we'll use to fit our experimental spectra. These are

included in the package as the matrix `cfp_yfp_ref`.

```
wl <- seq(from = 460, to = 600, by = 5)   #Wavelengths in nm
plot(wl, cfp_yfp_ref[, 1], col = "cyan", type = "l", lwd = 2, xlab = "Wavelen
gth (nm)",
    ylab = "Fluorescence intensity (arbitrary units)")   #CFP
lines(wl, cfp_yfp_ref[, 2], col = "gold", lwd = 2)   #YFP
```
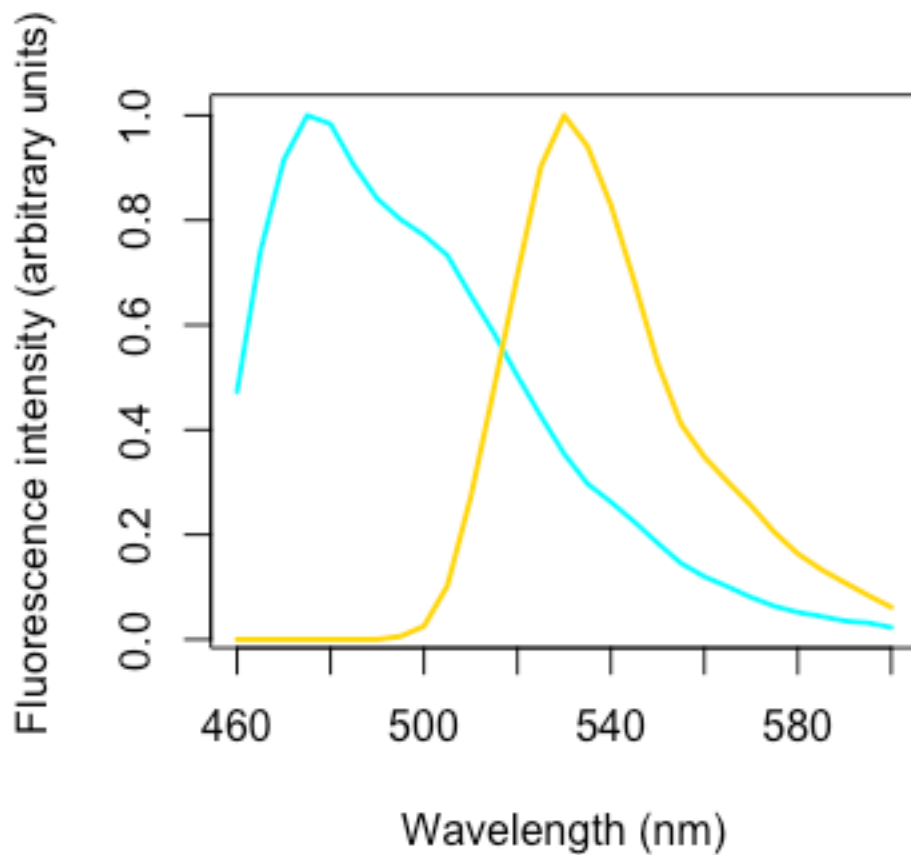
Figure 3. CFP and YFP basis spectra.

For each experimental spectrum, we need to calculate three values: two multiplicative

coefficients that scale each of the two basis spectra and an additive global baseline offset such

that the residual sum of squares between the experimental spectrum and the sum of the scaled

basis spectra is minimized. This is illustrated for synthetic data below:

```
# Make a synthetic experimental spectrum with contributions from CFP and YFP
set.seed(333)
synthData <- runif(1, min = 10, max = 100) * cfp_yfp_ref[, 1] + runif(1, min
= 10,
    max = 100) * cfp_yfp_ref[, 2] + rnorm(29, sd = 0.5)
# Plot it
plot(wl, synthData, xlab = "Wavelength (nm)", main = "Synthetic spectral data
```

```
",
    ylab = "Fluorescence intensity (arbitrary units)")
```

Synthetic spectral data
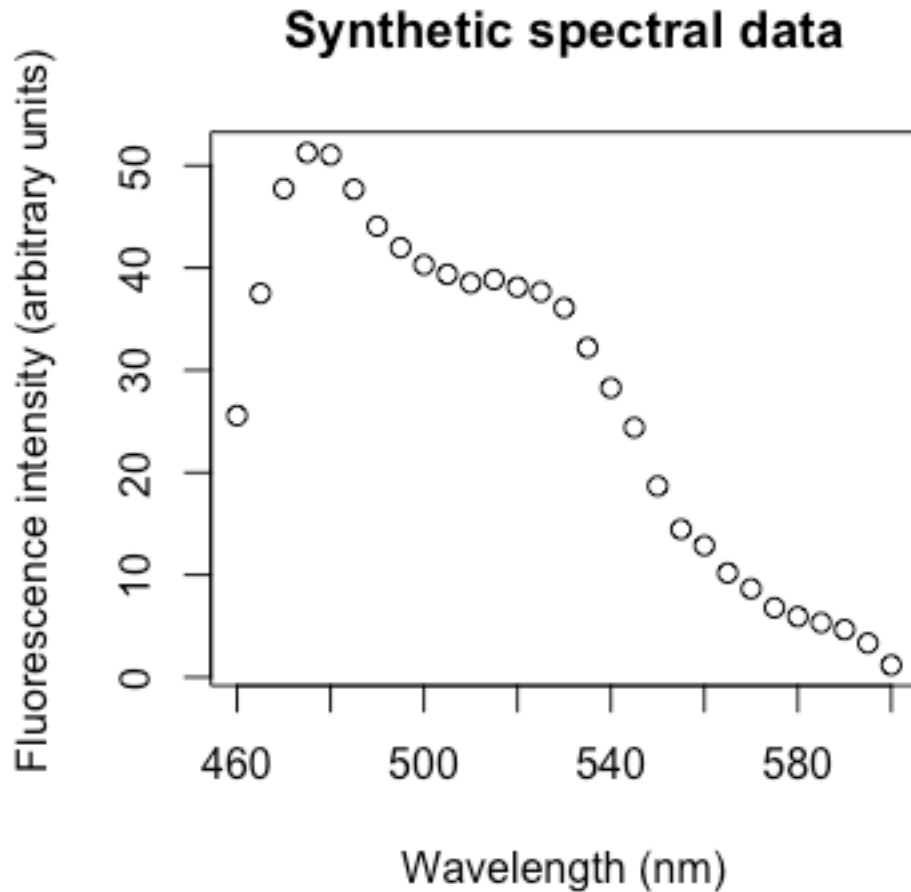
Figure 4. Synthetic spectral data.

Under the hood, the function `fretFit` calculates a least squares fit for many spectra

simultaneously using standard linear algebra techniques as follows. We have a matrix of

observations **Y** with one row per wavelength, and one spectrum per column. We have a matrix

containing the basis spectra **X** and a column of ones. We are looking for the matrix **β** whose

columns contain the coefficeints and baseline offset term described above. This is calculated as

$$\boldsymbol{\beta} = [\mathbf{X}^\top\mathbf{X}]^{-1}[\mathbf{X}^\top\mathbf{Y}]$$

Now we calculate the fit and plot it on our synthetic data:

```
Y <- matrix(synthData, ncol = 1)
X <- cbind(cfp_yfp_ref, rep(1, 29))
beta <- solve((t(X) %*% X)) %*% (t(X) %*% Y)
plot(wl, synthData, xlab = "Wavelength (nm)", main = "Synthetic spectral data
with fit",
    ylab = "Fluorescence intensity (arbitrary units)")
lines(wl, beta[1] * cfp_yfp_ref[, 1], col = "cyan", lwd = 2)
lines(wl, beta[2] * cfp_yfp_ref[, 2], col = "gold", lwd = 2)
lines(wl, X %*% beta, col = "forestgreen", lwd = 2)
legend("topright", legend = c("Data", "Fit", "CFP", "YFP"), pch = c(1, NA, NA
,
    NA), col = c("black", "forestgreen", "cyan", "gold"), lwd = c(NA, 2, 2,
    2))
```


Figure 5. Synthetic spectral data with fit.

As you can see, the basis spectra were scaled so that their sum nicely fits the synthetic

experimental data. Now we'll try this with our background-subtracted spectra `cfpYfpBgSub`

from above. The function `fretFit` does the same calculations as above, but is designed for
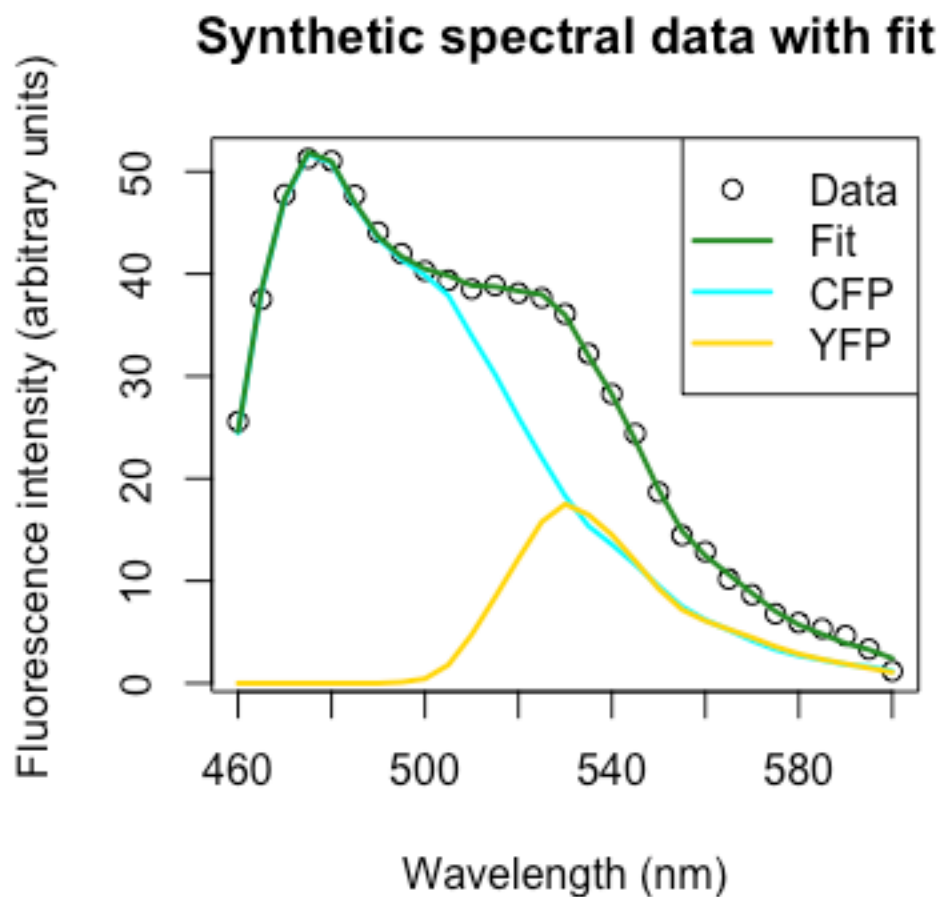
experiments where FRET is measured as a function of some experimental variable, in this case a

concentration series of Spc110 incubated with γTuSC to induce assembly of γTuRC. By default it

will calculate summary statistics (mean and standard deviation) for each value of the

experimental variable.

```
# Concentrations of Spc110 in nM
conc <- sort(rep(c(1500, 750, 375, 187.5, 93.75, 46.875, 0), 3), decreasing =
TRUE)
TuSCSpc110FRET <- fretFit(spectra = cfpYfpBgSub, concentrations = conc, accCo
nc = 50)
```

The most important parameters are `spectra` and `concentrations`. Elements of

`concentrations` must match the columns of `spectra`. The parameter `accConc` is the

concentration of the acceptor fluorophore in the FRET experiment. If you know the linear

relationship between the concentration of acceptor fluorophore and its fluorescence intensity

when excited in the absence of donor fluorophore at the donor excitation wavelength, you can

use this parameter to correct for direct excitation of the acceptor (that is, the acceptor

fluorescence intensity that is not due to FRET). The slope and intercept of this linear relation

are specified in the parameter `accCorr`. The default values are valid for γTuSC-CFP/YFP as

measured in Lyon et al. (2016) and should be remeasured for different experimental situations.

Other potentially useful options include `fitted=TRUE` which causes `fretFit` to return the

fitted spectra rather than FRET values. The option `average=FALSE` can be useful for identifying

outliers when experimental replicates are included (by default, replicate concentrations are

averaged). See `?fretFit` for other capabilities, including the ability to specify basis spectra

other than `cfp_yfp_ref`.

Plotting binding curves

Now that we've fit our spectra, let's take a look at the FRET values:

Table 1. FRET data.

Concentration	FRET	SD	N
0	0.1249	0.001919	3
46.88	0.133	0.002249	3
93.75	0.1388	0.003173	3
187.5	0.1468	0.001544	3
375	0.153	0.003155	3
750	0.1584	0.002179	3
1500	0.1615	0.001862	3

We see an increase in FRET as Spc110 concentration increases. For our $N = 3$ replicates, we

have quite small standard deviations, so everything looks good. Let's plot the data and fit a

binding curve.

```
# Fit a simple binding model
bindingModel <- fitBinding(TuSCSpc110FRET, model = "s")
# Plot the data
plotBinding(TuSCSpc110FRET, errFeet = TRUE, bg = "red")
# Plot the binding model
plotFit(bindingModel, col = "red")
```
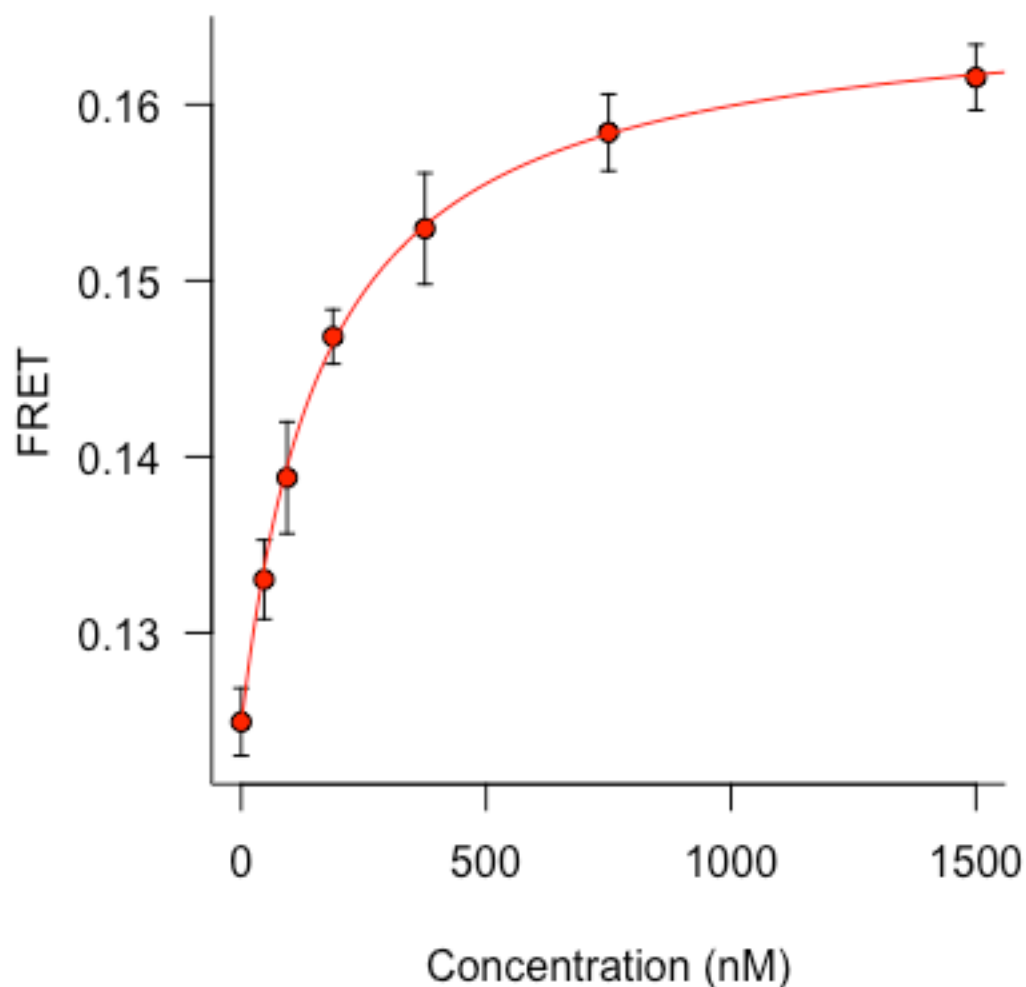
Figure 6. γTuSC-CFP/YFP FRET data as a function of Spc110 concentration.

If we had another binding curve to plot on the same set of axes (for instance, a mutant to compare with wild-type), we could use `pointsBinding`. We'll generate a synthetic dataset, then add it to the example plot above. This example also shows some useful options for how data is shown, specifically coloring the error bars to match to points.

```
# Make synthetic FRET data
synthBinding <- (0.155 - 0.125) * unique(conc)/(unique(conc) + 50) + 0.125
# Make synthetic uncertainty values
synthSD <- abs(rnorm(n = length(synthBinding), mean = mean(TuSCSpc110FRET$SD)
,
    sd = 0.001))
# Combine into a dataframe
synthBindingDF <- data.frame(Concentration = unique(conc), FRET = synthBindin
```

```
g,
    SD = synthSD)
# Fit a binding model to the synthetic data
synthBindingModel <- fitBinding(synthBindingDF, model = "s")
# Plot it
plotBinding(TuSCSpc110FRET, errFeet = TRUE, bg = "red", errCol = "red")
pointsBinding(synthBindingDF, errFeet = TRUE, bg = "blue", errCol = "blue")
plotFit(bindingModel, col = "red")
plotFit(synthBindingModel, col = "blue")
```


Figure 7. Example of adding an additional binding curve to a plot.

Conclusion

We've seen how to fit spectral data as a linear combination of basis spectra, and how to analyze

and plot the resulting binding curves. Most of the functions described have additional

parameters that may be useful in other situations. See the documentation for more details.

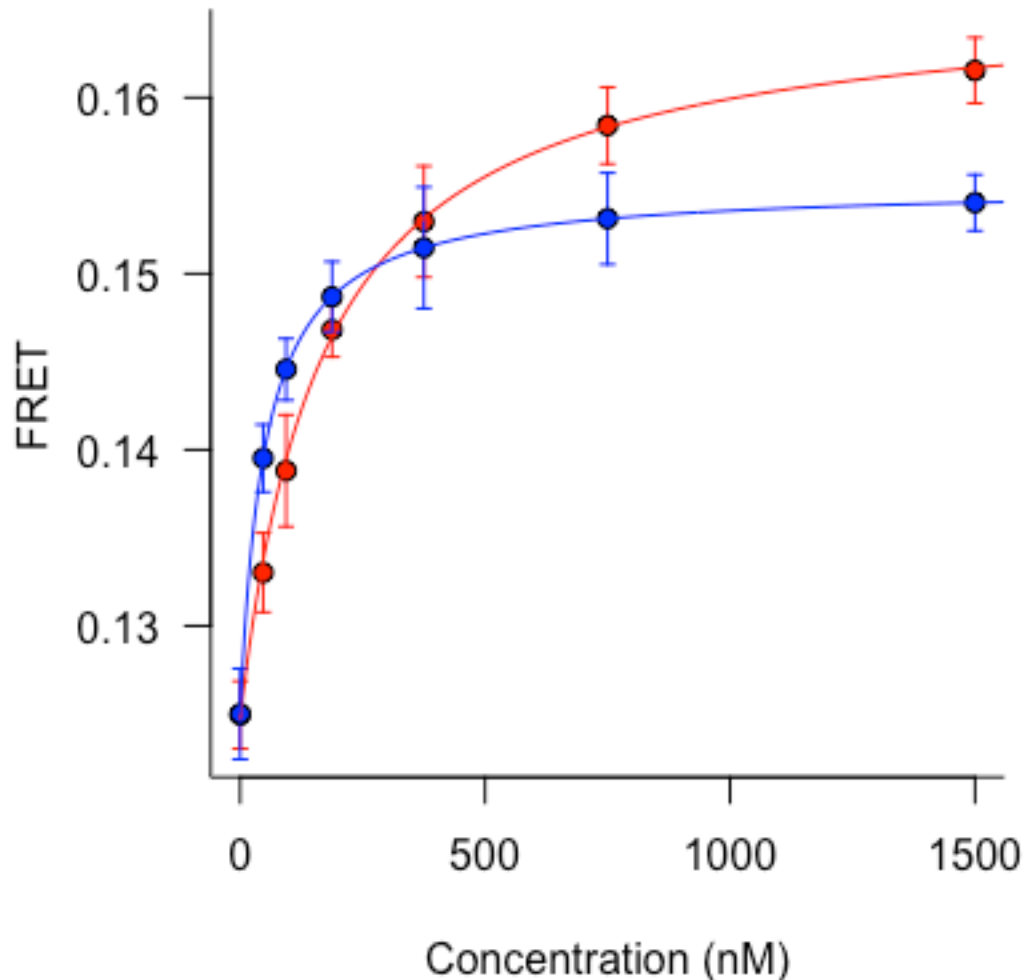# ASLutils Function Documentation

---

bgSub   *Subtract a background spectrum*

Description

Given a matrix containing spectral data and a vector containing a background spectrum, subtract the background spectrum from each spectrum in the matrix.

Usage

```
bgSub(spectra, bgSpectrum)
```

Arguments

spectra   Matrix containing spectral data, typically returned by openSpectraFile or getSpectra.

bgSpectrum   Numeric vector where length(bgSpectrum) == nrow(spectra).

Value

Matrix of same dimensions as spectra containing background-subtracted spectra.

Examples

```
blanks <- getSpectra(TuSC_Spc110_spectra, nRows=9, nCols=3, startRow=1, endRow=2,
startColumn=1, endColumn=3)
spectra <- getSpectra(TuSC_Spc110_Spectra, nRows=9, nCols=3, startRow=3, endRow=9,
startColumn=1, endColumn=3)
spectra_bgsub <- bgSub(spectra=spectra, bgSpectrum=rowMeans(blanks))
```

---

cfp_yfp_ref   *Basis spectra for linear unmixing of CFP/YFP spectra*

Description

Fluorescence spectra from gamma-tubulin small complex (gTuSC) containing Spc97-YFP or Spc98-CFP were recorded on a Molecular Devices SpectraMax M5 plate reader. For gTuSC-CFP, the excitation wavelength was 420 nm with emission recorded through a 455 nm longpass filter in 5 nm increments from 460 to 600 nm. Spectra were recorded in the same manner for gTuSC-YFP, but with excitation at 475 nm, a 495 nm longpass filter, and spectra recorded from 495 to 600 nm. YFP emission from 460 to 490 nm is set to zero. Multiple spectra were recorded, background subtracted, and averaged. The spectra were then scaled so that the maximum intensity is one.

Usage

```
cfp_yfp_ref
```

Format

A matrix with 29 rows and 2 columns. The dimnames attributes indicate CFP or YFP and the wavelengths at which the spectra were recorded in the columns and rows, respectively.

Source

Lyon et al. 2016. Molecular Biology of the Cell 27: 2245, figure S1A.

---

fitBinding   *Fit a binding model to data*

Description

Given a dataframe with an independent variable (typically concentration) and observed values (typically FRET or fluorescence intensity) with optional uncertanties, this function fits one of three binding models using the Levenberg-Marquardt non-linear least squares optimizer. The three available models are

- `"s"` for simple, single-site saturable binding
- `"t"` for tight single-site saturable binding where total and unbound concentrations of the titrated component cannot be assumed equal (i.e. when the non-titrated component concentration is similar to the dissociation constant)
- `"c"` for cooperative binding

Usage

```
fitBinding(data, kdGuess = "auto", probeConcentration, hillCoefficient = 2,
  model = c("s", "t", "c"), weight = TRUE, xCol = 1, yCol = 2,
  uncCol = 3)
```

Arguments

data	Dataframe with at least two columns, typically the output of `fretFit`. Columns must contain an independent variable, observed values. An optional column may contain uncertainties for the observed values.
kdGuess	Either `"auto"` or numeric. If `"auto"`, an initial estimate for the dissociation constant is determined from the data. Alternatively, users may specify an initial estimate as a numeric value.
probeConcentration	
	Numeric. For `model="t"`, the concentration of the non-titrated component in the binding experiment in the same units as the independent variable in `data`.
hillCoefficient	
	Numeric. Initial estimate of the Hill coefficient for `model="c"`.
model	One of `"s"`, `"t"`, or `"c"`. The binding model to fit: `"s"` for simple, `"t"` for tight, `"c"` for cooperative.
weight	Logical. Perform weighted non-linear least squares fit using user-provided uncertainties?
xCol	Integer. The column in `data` containing the independent variable.
yCol	Integer. The column in `data` containing observed values.
uncCol	Integer. The column in `data` containing uncertainties for the observed values. Required if `weight=TRUE`.

Details

Binding model definitions are as follows, where B_{max} is the theoretical observed value as the independent variable approaches infinity, B_{min} is the observed value when the independent variable is zero, K_d is the equilibrium dissociation constant, c is the concentration of the non-titrated component, and n is the Hill coefficient.

Simple:

$$y = (B_{max} - B_{min})\frac{x}{x + K_d} + B_{min}$$

Tight:

$$y = (B_{max} - B_{min})\frac{(x + c + K_d) - \sqrt{(x + c + K_d)^2 - 4xc}}{2c} + B_{min}$$

Cooperative:

$$y = (B_{max} - B_{min})\frac{x^n}{x^n + K_d^n} + B_{min}$$

The kdGuess = "auto" option finds two data points close to the half-maximal observed value, fits a line to them, then interpolates to find the x-axis value corresponding to the half-maximum point on the binding curve. It is likely to have problems with noisy data, data with outliers, or binding curves where saturation has not been reached.

Weighted least-squares is performed with weights $1/\sigma^2$, so the user should supply uncertainties as standard deviations.

Value

Object of class "nls" with optimized binding model parameters.

Examples

```
fitBinding(data=TuSC_Spc110_binding, model="s")
```

---

fretFit   *Fit spectra as a linear combination of basis spectra*

Description

A spectrum recorded from a sample containing more than one fluorophore (or chromophore) is the linear combination of the fluorophores in isolation. Spectra from samples containing unknown contributions from multiple fluorophores can be "unmixed" by least-squares fitting as the sum of multiple basis spectra. This is particularly useful for Forster resonance energy transfer (FRET) experiments. This function performs the least-squares fit and provides several tools useful in FRET applications.

Usage

```
fretFit(spectra, concentrations, accConc, accCorrect = TRUE,
  normalize = TRUE, fitted = FALSE, average = TRUE, basis = cfp_yfp_ref,
  donorCol = 1, accCol = 2, accCorr = c(slope = 0.3986, intercept =
  -0.7486))
```

Arguments

spectra	Matrix with spectral data arranged so that each column contains one spectrum.
concentrations	Numeric vector of concentrations, for instance the concentrations of a titrated component in a binding experiment. The order of concentrations must correspond to the ordering of columns in the spectra matrix. Required if fitted = FALSE.
accConc	Numeric. The concentration of the acceptor fluorophore. Required if accCorrect = TRUE to allow for correction for direct excitation of the acceptor fluorophore in FRET experiments.
accCorrect	Logical. If TRUE, the contribution of the acceptor signal due to direct excitation (i.e., not FRET) is subtracted before further analysis.
normalize	Logical. If TRUE FRET is calculated as Acceptor/(Donor + Acceptor). Otherwise FRET is simply Acceptor/Donor.
fitted	Logical. If TRUE, this function returns a list with components Fitted, a matrix with fitted spectral values, and Coefs, containing the coefficients from the least-squares fit.
average	Logical. If TRUE calculates mean FRET values and standard deviations. Otherwise unaveraged FRET values are returned.
basis	Matrix where nrow(basis) == nrow{spectra}. Basis spectra for the least-squares fit. The default cfp_yfp_ref is basis spectra for CFP-YFP FRET experiments. See ?cfp_yfp_ref.
donorCol	Numeric integer. The column of basis corresponding to the donor fluorophore in FRET experiments.
accCol	Numeric integer. The column of basis corresponding to the acceptor fluorophore in FRET experiments.
accCorr	Numeric vector with components slope and intercept. Values for linear correction term for subtracting acceptor fluorophore signal due to direct excitation of the acceptor (i.e., not FRET). See details.

Value

A dataframe with FRET values, unless fitted=TRUE in which a list with components Fitted, a matrix with fitted spectral values, and Coefs, containing the coefficients from the least-squares fit.

Examples

```
#Get the background spectrum
background_spectrum <- rowMeans(getSpectra(TuSC_Spc110_spectra, nRows=9, nCols=3, startRow=1,
endRow=2, startColumn=1, endColumn=3))
#Subtract background from experimental spectra
TuSC_Spc110_spectra_bgsub <- bgSub(getSpectra(TuSC_Spc110_spectra, nRows=9, nCols=3,
startRow=3, endRow=9, startColumn=1, endColumn=3), background_spectrum)
#Fit the spectra and get FRET values with statistics
TuSC_Spc110_binding <- fretFit(TuSC_Spc110_spectra_bgsub, concentrations=sort(rep(c(1500,
750, 375, 187.5, 93.75, 46.875, 0), 3)), accConc=50, average=TRUE)
#Fit the spectra and get the fitted spectra
TuSC_Spc110_binding <- fretFit(TuSC_Spc110_spectra_bgsub, concentrations=sort(rep(c(1500,
750, 375, 187.5, 93.75, 46.875, 0), 3)), accConc=50, fitted=TRUE)
#Fit the spectra and get unaveraged FRET values
TuSC_Spc110_binding <- fretFit(TuSC_Spc110_spectra_bgsub, concentrations=sort(rep(c(1500,
750, 375, 187.5, 93.75, 46.875, 0), 3)), accConc=50, average=FALSE)
```

getSpectra	*Get a set of spectra corresponding to a group of wells from a microplate*

Description

Microplate experiments often have a set of control samples and a set of experimental samples (for example) where it might be convenient to separate the spectra into different objects for processing and analysis. Given an input matrix containing spectral data from a microplate experiment, this function returns the spectra from a rectangular block of wells.

Usage

```
getSpectra(spectra, nRows, nCols, startRow, endRow = startRow, startColumn,
    endColumn = startColumn)
```

Arguments

spectra
: Matrix, typically returned by openSpectraFile. See details for required features of this matrix.

nRows
: Numeric or length 2 character vector. If numberic, the number of rows containing samples in the microplate. If character vector, the letter codes for the first and last rows containing sample.

nCols
: Numeric. The number of columns containing samples in the microplate.

startRow
: Numeric or character. The first row containing samples of interest. Can be specified as the ordinal number for the row of interest or the letter code.

endRow
: Numeric or character. The last row containing samples of interest. Can be specified as the ordinal number for the row of interest or the letter code.

startColumn
: Numeric. The first column containing samples of interest.

endRow
: Numeric. The last column containing samples of interest.

Details

The spectra matrix must be arranged so that the groups of adjacent columns correspond to wells within a row of a microplate. That is, for a microplate with rows labeled A, B, C, etc., and columns labeled 1, 2, 3, 4, etc., the columns of the spectra matrix correspond to wells A1, A2, A3, A4, B1, B2, B3, B4, C1, C2, C3, C4, etc., in that order.

Value

A matrix where each column is a spectrum.

Examples

```
#The matrix TuSC_110_spectra was recorded in wells A7-I9 of a microplate,
with buffer-only controls in wells A7-B9.
#Get the spectra for the buffer only controls
getSpectra(TuSC_110_spectra, nRows=9, nCols=3, startRow=1, endRow=2, startColumn=1,
endColumn=3)
#Get the experimental spectra using row numbers
```

```
getSpectra(TuSC_Spc110_spectra, nRows=9, nCols=3, startRow=3, endRow=9, startColumn=1,
endColumn=3)
#Get the experimental spectra using row letters
getSpectra(TuSC_Spc110_spectra, nRows=c("A", "I"), ncols=3, startRow="C", endRow="I",
startColumn=1, endColumn=3)
```

---

openSpectraFile   *Open a file containing spectral data*

Description

Simple wrapper around `read.table` for opening tab-delimited spectral data files.

Usage

```
openSpectraFile(file = "")
```

Arguments

file   Character string giving absolute or relative path to a tab-delimited data file.

Value

A matrix where each column is a spectrum.

---

plotBinding   *Plot binding data*

Description

Plot binding data as scatter plot with error bars.

Usage

```
plotBinding(data, xlab = "Concentration (nM)", ylab = "FRET", ylim = NULL,
  xlim = NULL, pch = 21, cex = 1, xlog = F, logBase = 10,
  col = "black", bg = 1, errCol = "black", errLwd = 1,
  errFeet = FALSE, main = NULL, xCol = 1, yCol = 2, uncCol = 3, ...)
```

Arguments

data   Dataframe with at least two columns, typically returned by `fretFit`. The two
                    required columns must contain independent variable and one observations. Un-
                    certainties in the observed values may be included as an optional third column.

xlab   Character. X-axis label.

ylab   Character. Y-axis label.

ylim   Length two numeric vector. The lower and upper boundaries of the vertical axis
                    of the plot.

xlim	Length two numeric vector. The left and right boundaries of the horizontal axis of the plot.
pch	Any valid plot character (numeric or character).
cex	Plot character magnification relative to default size (e.g. cex=2 will make the plot character two times larger than default).
xlog	Logical. Should the x-axis values be logarithmically transformed?
logBase	Numeric. If xlog=TRUE, the base of the logarithmic transform of the x-axis values.
col	Any valid color specification. The foreground color of the plot characters.
bg	Any valid color specification. The background color of the plot characters.
errCol	Any valid color specification. The color of the error bars.
errLwd	Numeric. The line weight of the error bars. errLwd = 1 is a line 1/96 inch thick, errLwd = 0.75 is a line 1 point thick.
errFeet	Logical. Should horizontal lines ("feet") be drawn on the error bars? Default FALSE will draw vertical lines only.
main	Character. Title for plot.
xCol	Integer. The column of data containing the independent variable.
yCol	Integer. The column of data containing observed values.
uncCol	Integer. Optional. The column of data containing uncertainties in observed values.
...	Additional arguments to plot or points

Value

No return value, changes state of graphics device.

Examples

```
#Plot with linear x-axis scale
plotBinding(TuSC_Spc110_binding)
#Plot with "feet" on the error bars the same color as the plot symbols
plotBinding(TuSC_Spc110_binding, errFeet=TRUE, pch=19, col='red', errCol='red')
#Plot with log-10 x-axis scale
plotBinding(TuSC_Spc110_binding, xlog=T)
```

| plotFit | *Plot a binding model* |

Description

Given a fit model (typically returned by fitBinding), plot a curve showing the fit evaluated over a range of x-axis values.

Usage

```
plotFit(model, xRange = NULL, xlog = FALSE, logBase = 10, add = TRUE,
  col = 1, lwd = 1, lty = 1, xlab = "Concentration (nM)",
  ylab = "FRET", xlim = NULL, ylim = NULL, main = NULL, ...)
```

Arguments

model	The model object for which to plot a curve. Typically returned by fitBinding, though models returned by lm, nls are likely to work as well as long as the fitting function was run with model=TRUE.
xRange	Length-two numeric vector. The x-axis values between which the fit model will be evaluated and a curve plotted.
xlog	Logical. Should the curve be drawn with a logarithmic x-axis scale?
logBase	Numeric. The base of the logarithmic transform used if xlog=TRUE.
add	Logical. Should the curve be added to an existing graphics device? If FALSE, the curve is drawn in a new graphics device.
col	Any valid R color specification. The color of the curve.
lwd	Numeric. The line width. lwd=1 is 1/96 of an inch. lwd=0.75 is one point.
lty	Integer. The type of line to draw. 1 is solid, 2 is dashed, 3 is dotted. See lty under ?par for more details.
xlab.	Character. The x-axis label.
ylab.	Character. The y-axis label.
xlim.	Length-two numeric vector. The x-axis limits of the plot window for add=FALSE.
ylim.	Length-two numeric vector. The y-axis limits of the plot window for add=FALSE.
main.	Character. The title of the plot.

Value

No return value, changes state of graphics device.

Examples

```
#Fit a model to some data
fit <- fitBinding(TuSC_Spc110_binding)
#Plot the binding data
plotBinding(TuSC_Spc110_binding)
#Plot the model curve
plotFit(fit)
```

---

plotSpectra	*Plot a set of spectra*

Description

Given a matrix containing spectral data, plot each spectrum on the same set of axes.

Usage

```
plotSpectra(spectra, wl = seq(460, 600, by = 5), xlab = "Wavelength (nm)",
  ylab = "Fluorescence intensity (AU)", bg = "grey80", ...)
```

Arguments

spectra	Matrix containing spectral data, typically returned by `openSpectraFile` or `getSpectra`.
wl	Numeric vector of wavelengths.
xlab	Character. X-axis label.
ylab	Character. Y-axis label.
bg	Any valid R color specification. Background color of plot.
...	Further arguments to `plot`.

Value

No return value, changes state of graphics device.

Examples

```
blanks <- getSpectra(TuSC_Spc110_spectra, nRows=9, nCols=3, startRow=1, endRow=2,
startColumn=1, endColumn=3)
plotSpectra(blanks)
```

---

pointsBinding	*Add binding data to an existing plot*

Description

Given an existing graphics device, adds points and error bars.

Usage

```
pointsBinding(data, pch = 21, cex = 1, xlog = F, logBase = 10,
  col = "black", bg = 1, errCol = "black", errLwd = 1,
  errFeet = FALSE, xCol = 1, yCol = 2, uncCol = 3, ...)
```

Arguments

data	Dataframe with at least two columns, typically returned by `fretFit`. The two required columns must contain independent variable and one observations. Uncertainties in the observed values may be included as an optional third column.
pch	Any valid plot character (numeric or character).
cex	Plot character magnification relative to default size (e.g. `cex=2` will make the plot character two times larger than default).
xlog	Logical. Should the x-axis values be logarithmically transformed?
logBase	Numeric. If `xlog=TRUE`, the base of the logarithmic transform of the x-axis values.
col	Any valid color specification. The foreground color of the plot characters.
bg	Any valid color specification. The background color of the plot characters.
errCol	Any valid color specification. The color of the error bars.
errLwd	Numeric. The line weight of the error bars. `errLwd = 1` is a line 1/96 inch thick, `errLwd = 0.75` is a line 1 point thick.

errFeet	Logical. Should horizontal lines ("feet") be drawn on the error bars? Default `FALSE` will draw vertical lines only.
xCol	Integer. The column of `data` containing the independent variable.
yCol	Integer. The column of `data` containing observed values.
uncCol	Integer. Optional. The column of `data` containing uncertainties in observed values.
...	Additional arguments to `points`

Value

No return value, changes state of graphics device.

TuSC_Spc110_binding   *Spc110-induced gTuRC assembly curve*

Description

FRET data for gTuSC-CFP/YFP in the presence of varying concentrations of Spc110.

Usage

```
TuSC_Spc110_binding
```

Format

7 x 4 dataframe with columns Concentration, FRET, SD, and N.

Source

Lyon et al. 2016. Molecular Biology of the Cell 27: 2245, figure 2E (Dimer WT curve). http://www.molbiolcell.org/content/27/14/2245.long

Examples

```
#TuSC_Spc110_binding was prepared as follows:
background_spectrum <- rowMeans(getSpectra(TuSC_Spc110_spectra, nRows=9, nCols=3, startRow=1,
endRow=2, startColumn=1, endColumn=3))
TuSC_Spc110_spectra_bgsub <- bgSub(getSpectra(TuSC_Spc110_spectra, nRows=9, nCols=3,
startRow=3, endRow=9, startColumn=1, endColumn=3), background_spectrum)
TuSC_Spc110_binding <- fretFit(TuSC_Spc110_spectra_bgsub, concentrations=sort(rep(c(1500, 750,
375, 187.5, 93.75, 46.875, 0), 3)), accConc=50)
```

TuSC_Spc110_spectra	*Fluorescence spectra of gamma-TuSC-CFP/YFP recorded at a variety of Spc110 concentrations*

Description

50 nm gTuSC-CFP/YFP and varying concentration so Spc110 were mixed to allow assembly of gTuRCs, then fluorescence spectra were recorded on a Molecular Devices SpectraMax M5 platereader. Columns 1-6 (wells A7-B9) are blank spectra recorded from buffer alone. Columns 7-27 are gTuSC+Spc110 spectra. The Spc110 concentrations are `sort(rep(c(1500, 750, 375, 187.5,93.75, 46.875, 0), 3),` in nanomolar. These are raw spectra so background spectra from buffer-only controls must be subtracted before further processing.

Usage

`TuSC_Spc110_spectra`

Format

29 x 27 matrix.

Source

Lyon et al. 2016. Molecular Biology of the Cell 27: 2245, figure 2E (Dimer WT curve). `http://www.molbiolcell.org/content/27/14/2245.long`

Publishing Agreement

It is the policy of the University to encourage the distribution of all theses, dissertations, and manuscripts. Copies of all UCSF theses, dissertations, and manuscripts will be routed to the library via the Graduate Division. The library will make all theses, dissertations, and manuscripts accessible to the public and will preserve these to the best of their abilities, in perpetuity.

Please sign the following statement:

I hereby grant permission to the Graduate Division of the University of California, San Francisco to release copies of my thesis, dissertation, or manuscript to the Campus Library to provide access and preservation, in whole or in part, in perpetuity.

_____
Author Signature

12/19/17
Date